CONTRACTOR REPORT

SAND85—7101
Unlimited Release
UC—814

Yucca Mountain Site Characterization Project

A Thermomechanical Far-Field Model of Yucca Mountain

Terje Brandshaug
RE/SPEC Inc.
PO Box 14984
Albuquerque, NM 87191

Prepared by Sandia National Laboratories Albuquerque, New Mexico 87185 and Livermore, California 94550 for the United States Department of Energy under Contract DE-AC04-76DP00789

Printed March 1991

"Prepared by Yucca Mountain Site Characterization Project (YMSCP) participants as part of the Civilian Radioactive Waste Management Program (CRWM). The YMSCP is managed by the Yucca Mountain Project Office of the U.S. Department of Energy, Nevada Operations Office (DOE/NV). YMSCP work is sponsored by the Office of Geologic Repositories (OGR) of the DOE Office of Civilian Radioactive Waste Management (OCRWM)."

Issued by Sandia National Laboratories, operated for the United States Department of Energy by Sandia Corporation.

Available to DOE and DOE contractors from
Office of Scientific and Technical Information
PO Box 62
Oak Ridge, TN 37831

Prices available from (615) 576-8401, FTS 626-8401

Available to the public from
National Technical Information Service
US Department of Commerce
5285 Port Royal Rd
Springfield, VA 22161

NTIS price codes
Printed copy: A06
Microfiche copy: A01

SAND--85-7101

DE91 012134

SAND85-7101
Unlimited Release
Printed April 1991

A THERMOMECHANICAL FAR-FIELD MODEL OF YUCCA MOUNTAIN

by

Terje Brandshaug
RE/SPEC Inc.
4775 Indian School Rd NE, Suite 300
Albuquerque, New Mexico 87110

prepared for*

Sandia National Laboratories
P.O. Box 5800
Albuquerque, New Mexico 87185

Abstract

Thermal and mechanical finite element far-field models have been constructed for a potential repository site in the Topopah Spring Thermal/mechanical Unit at Yucca Mountain on the Nevada Test Site. The models reflect site-specific information that was available at the time of the study on the material properties and structural character of Yucca Mountain. The thermal model simulates transient heat transfer resulting from the emplacement of heat-generating nuclear waste in the repository. Simulation of boiling of the pore water is included in the model. The mechanical model simulates the tuff at Yucca Mountain as being an elastic/plastic, isotropic, heterogeneous continuum with one ubiquitous vertical joint set. The initial conditions of the mechanical model are based on a gravitational stress field. The model uses the temperatures predicted by the thermal finite element model as input to predict thermal stresses and displacements induced by the presence of the repository. Plasticity is incorporated in shear (fracture slip) and tension (fracture opening) by using a Mohr-Coulomb failure criterion.

*This report was prepared by RE/SPEC Inc. under Subcontract Nos. 37-8656 and 57-0881 with Sandia Corporation. The contract was administered by Sandia National Laboratories, Albuquerque, New Mexico, as operated by the Sandia Corporation.

The work described in this report was performed during 1984 and 1985; at that time no QA control structure was in effect. The work was subsequently included in WBS 1.2.4.6.2 which has become WBS 1.2.1.4.3.1 under the fiscal year 1990 WBS structure.

As a result of the SNL Preparedness Review of WBS No. 1.2.1.4.3.1 regarding the initiation of quality affecting work, it was determined that the procedures used during this study were not sufficient to assume compliance with the current SNL QAPP (Rev. E). Therefore, the work reported should be considered as non-quality affecting (NQ).

ACKNOWLEDGMENTS

The Yucca Mountain Project, managed by the Nevada Operations Office of the U.S. Department of Energy, is examining the feasibility of siting a nuclear waste repository at Yucca Mountain on and adjacent to the Nevada Test Site. This work, which was performed as part of the repository design effort, was funded by the Yucca Mountain Project. This report was prepared by RE/SPEC Inc. under Subcontract No. 37-8656 and revised under Subcontract No. 57-0881 with the Sandia Corporation. The subcontract was administered by Sandia National Laboratories, Albuquerque, New Mexico, as operated by the Sandia Corporation.

The author wishes to acknowledge the cooperation and assistance of Samuel W. Key throughout the project and for his constructive technical review. Appreciation is also extended to Joe L. Ratigan for his technical review and comments and to Julie S. Annicchiarico for her editorial comments. The patient and skillful participation by Mary L. Wall in preparing the original manuscript is greatly appreciated. The final manuscript was prepared by Carol K. Corley and Deanna R. Schwalm under the careful direction of Sharon V. Petney who addressed the technical comments formulated by the Sandia National Laboratories reviewers, Stephen J. Bauer and Brian Ehgartner. The author wishes to extend his appreciation to Arthur J. Mansure and Eugene S. Hertel of Sandia National Laboratories for their continued support and cooperation as technical monitors of the contract.

TABLE OF CONTENTS

LIST OF FIGURES

LIST OF TABLES

1.0 INTRODUCTION

The work described in this report was performed for Sandia National Laboratories (SNL) as a part of the Yucca Mountain Project (YMP). SNL is one of the principal organizations participating in the project, which is managed by the U. S. Department of Energy's (DOE) Nevada Operations Office (NVO). The project is a part of the DOE's program to safely dispose of the radioactive waste from nuclear power plants.

The DOE has determined that the safest and most feasible method currently known for the disposal of such wastes is to emplace them in mined geologic repositories. The YMP is conducting detailed studies of the Yucca Mountain area on and near the Nevada Test Site (NTS) in southern Nevada to determine the feasibility of developing a repository.

Numerical models that simulate the geologic disposal of nuclear waste have been traditionally divided into three scales. This division is based on the geometric detail of the physical phenomenon being studied. A *very-near-field* model focuses only on the phenomenon in the rock within a few meters of the waste container. A *near-field* model provides a prediction of a phenomenon in the rock around the disposal drift; the rock mass considered includes the pillar between disposal drifts and the rock extending several drift diameters above and below the waste disposal drift. A *far-field* model predicts a phenomenon within a geometric boundary extending vertically from the ground surface down several thousand meters below the repository horizon and laterally several thousand meters beyond the edges of the repository. Although each type of model is equally important in the study of geologic nuclear waste disposal, this report focuses on the construction of thermal and mechanical far-field models.

Far-field models provide information about thermomechanical effects in the rock induced by the presence of a repository. The thermomechanical effects are investigated in the far-field domain. The phenomena are investigated on a time scale that starts at the time of waste emplacement and lasts through 50,000 yr of waste isolation. The construction of finite element far-field models in tuff started in 1979 as part of the YMP. The YMP is investigating a potential repository site at Yucca Mountain, located on and adjacent to the NTS. The early far-field models were generic and did not include many of the site-specific features of Yucca Mountain. The continuous effort to characterize this potential repository site has resulted in far-field models that incorporate greater detail about the geometry, stratigraphy, and material properties of Yucca Mountain.

As part of the YMP unit evaluation study [Johnstone et al., 1984], thermomechanical far-field models aided in the selection of the Topopah Spring lithologic unit as the horizon to host the repository at Yucca Mountain. The models described in this report are based on site-specific information about this potential repository site at Yucca Mountain and include data obtained after the unit evaluation study.

2.0 OBJECTIVE

The objective of this effort is to construct thermal and mechanical numerical far-field models of Yucca Mountain. These models use information regarding mechanical properties, thermal properties, initial temperatures, thermal/mechanical stratigraphy, and in situ stress that has been updated since the unit evaluation study [Johnstone et al., 1984]. The models will serve as a basis for planning future studies of rock response to the presence of the repository.

3.0 SCOPE

The construction of the enhanced far-field models is based on information regarding the topography and thermal/mechanical stratigraphy at Yucca Mountain [SNL, 1987] and on a previous far-field model of Yucca Mountain [Johnstone et al., 1984]. The creation of the finite element mesh closely adheres to the topography and thermal/mechanical stratigraphy supplied. Provisions for specifying boundary conditions (thermal and mechanical) are built into the mesh. A check regarding adequate mesh refinement and appropriate boundary conditions was performed and is reported in Appendix A.

The thermal model constructed uses the finite element computer program SPECTROM-41 [D. K. Svalstad, *Documentation of SPECTROM-41: A Finite Element Heat Transfer Analysis Program*, draft]. The data used in SPECTROM-41 represent a conceptual model of the heat transfer problem to be analyzed. The data include the far-field mesh with defined boundary conditions, the material behavior defined in terms of thermophysical properties, the characteristics of the nuclear waste type and thermal decay, and the initial temperature conditions of the model.

The mechanical model uses the finite element computer program SPECTROM-31 [S. W. Key and D. A. Labreche, *SPECTROM-31: A Finite Element Computer Program for the Large Deformation, Static, and Quasi-Static Response of Planar and Axisymmetric Solids*, draft]. The data for SPECTROM-31 represent a conceptual model of the mechanical problem to be analyzed. The data include the far-field mesh with appropriate boundary conditions defined, the material behavior defined in terms of mechanical properties and rock strength parameters, the definition of the initial (in situ) stress field, and the temperature history of the far-field domain supplied by the output from SPECTROM-41.

No specific analyses using these models were conducted as part of this study. However, with the far field models described here, studies of the effects of waste emplacement on the thermal and mechanical response of the repository site can now be conducted.

4.0 MODEL CONSTRUCTION

4.1 MATERIAL CHARACTERIZATION

The far-field model of Yucca Mountain is based on the cross section CC' shown in Figure 4-1. This figure shows the topography and the thermal/mechanical stratigraphy of the mountain, as well as the approximate location of the water table. In addition, Figure 4-1 also shows the location of several faults, labeled C2 through C7. Each stratum in Figure 4-1 is differentiated based on thermomechanical behavior rather than lithology [SNL, 1987]. The approximate location of the repository horizon within the cross section CC' is also shown in Figure 4-1. The repository is situated in the Topopah Spring member, which has a low percentage of lithophysae. A map of Yucca Mountain (Figure 4-2), shows the location of the CC' cross section and the location of various drillholes.

Material properties and model input parameters are given in Table 4-1 [SNL, 1987] for each of the stratigraphic units of Figure 4-1. The thermal conductivity, volumetric heat capacity, and coefficient of thermal expansion vary with temperature. This variation is provided to account for the possible boiling of the pore water in the rock. This phenomenon will be explained further in Section 4.3, which discusses the thermal model.

Although there is no site-specific information regarding the material behavior of the faults identified in Figure 4-1, the presence of the faults is acknowledged in the model by virtue of their location. If data on the material behavior of the faults become available at a later date, these data may be incorporated to model fault behavior.

The type of nuclear waste considered in this far-field model is a combination of 10-year-old spent nuclear fuel from pressurized water reactors (PWR) and boiling water reactors (BWR). It is assumed that 60 percent of the initial areal power density (APD) of the repository is attributable to PWR spent fuel and 40 percent to BWR spent fuel. The thermal decay characteristics used for the 10-year-old PWR and BWR spent fuel are those given by SNL [1987]. The thermal decay characteristics of the combined PWR and BWR spent fuel used in the model is shown in Figure 4-3, and decay and time constants are given in Table 4-2.

4.2 FINITE ELEMENT MESH

The finite element mesh shown in Figure 4-4 defines the geometric boundaries of the far-field domain. Eight-noded quadrilateral elements are used. The mesh was constructed on the basis of the cross section CC' in Figure 4-1; however, the boundaries have been extended horizontally and vertically down beyond the region

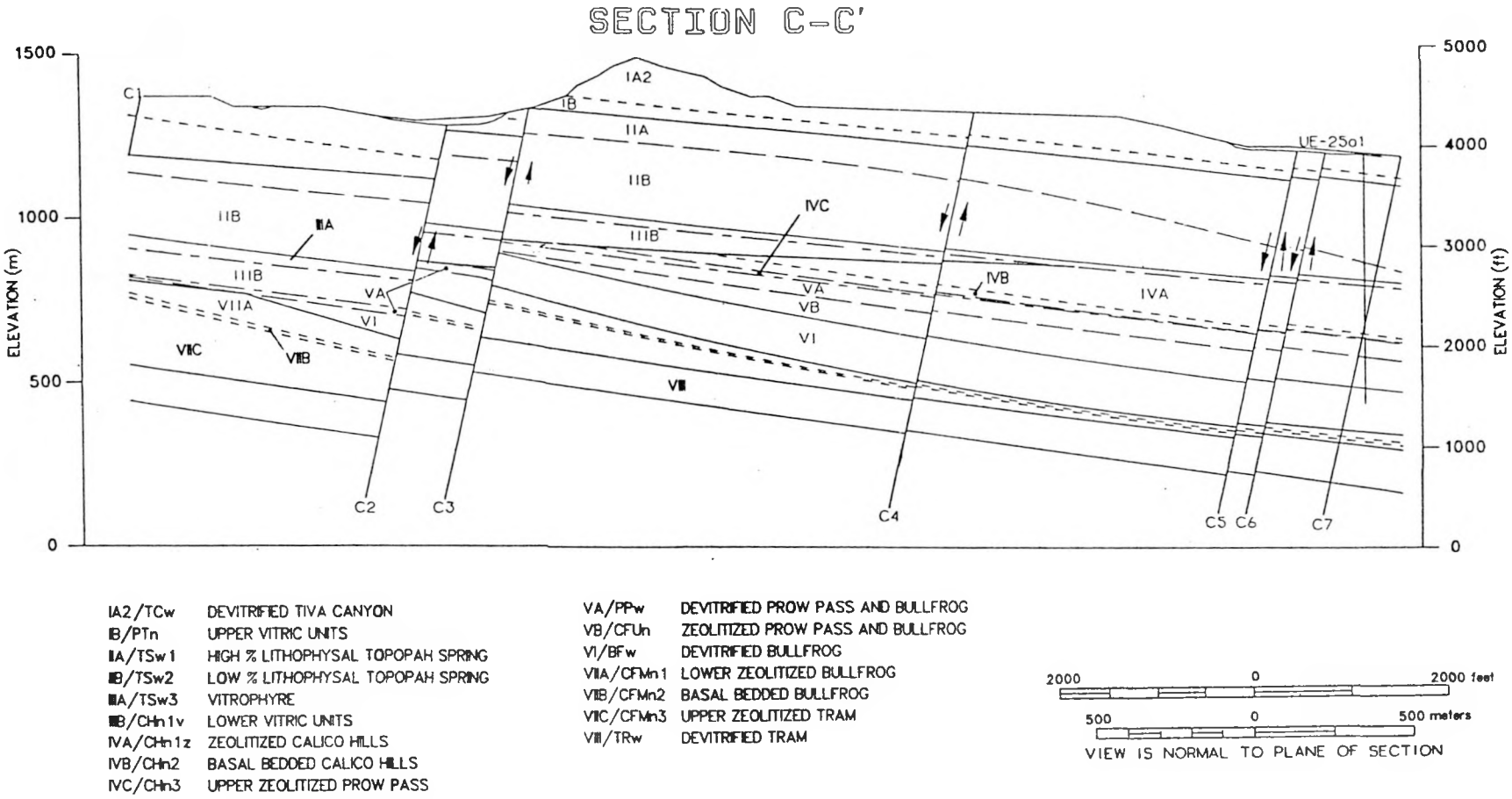

Figure 4-1. Thermomechanical Stratigraphy in Cross Section CC' at Yucca Mountain [SNL, 1987].

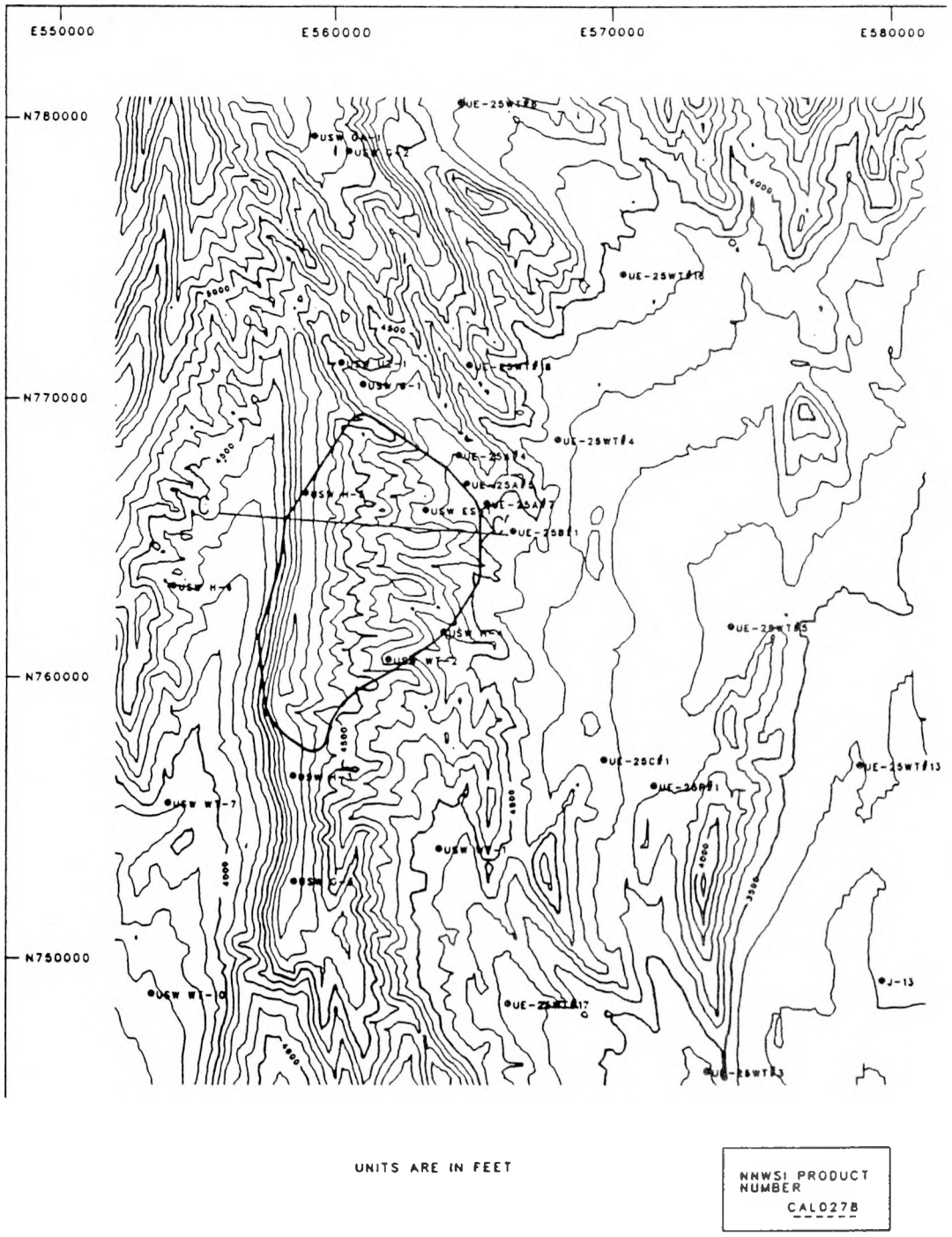

Figure 4-2. Map of Yucca Mountain Showing the Location of Cross Section CC' and the Location of Various Drillholes.

Table 4-1. Material Properties and Model Input Parameters of Yucca Mountain
[SNL, 1987]

Property	Unit[a]										
	IA2 TCw	IB PTn	IIA TSw1	IIB,IIIA TSw2,3	IIIB CHn1v	IVA,B,C CHn1z,2,3	VA PPw	VB CFUn	VI BFw	VIIA,B,C CFMn1,2,3	VIII TRw
Young's modulus, E (GPa)	15.4	2.3[b]	7.3[b]	15.1	2.4	3.5	6.05	3.8	5.4	5.4	8.8
Poisson's ratio, ν	0.10	0.18	0.18[b]	0.20	0.15	0.17	0.20	0.16	0.13	0.15	0.18
Specific weight, $\rho_{bs}g$ (MPa/m^3)[c]	.022555	.018632	.022163	.022849	.017456	.018534	.021084	.019025	.021868	.020496	.022751
Uniaxial compressive strength, σ_0 (MPa)	77.3	11.1	33.4	75.4	8.4	13.5	25.3	15.5	20.8	22.3	35.9
Tensile strength, σ_T (MPa)	9.3	1.0	4.0	6.5	1.0	1.6	3.0	1.9	2.5	2.7	4.3
Coeff. of thermal exp., $\alpha_1 \times 10^{-6}$ (°C^{-1})	8.7	−70.0	10.7	10.7	−70.0	6.7	8.3	6.7	8.3	6.7	8.3
Temp. range (°C)	<100.	<100.	<200.	<200.	<100.	<100.	<100.	<100.	<100.	<100.	<100.
$\alpha_2 \times 10^{-6}$ (°C^{-1})	8.7	−11.5	31.8	31.8	−11.5	−52.0	−12.0	−29.4	−12.0	−16.2	−12.0
Temp. range (°C)	100–125	100–125	200–350	200–350	100–125	100–150	100–125	100–150	100–125	100–150	100–125
$\alpha_3 \times 10^{-6}$ (°C^{-1})	8.7	−8.0	15.5	15.5	−8.0	−2.4	10.9	4.4	10.9	1.5	10.9
Temp. range (°C)	>125.	>125.	350–400	350–400	>125.	>150.	>125.	>150.	>125.	>150.	>125.
Matrix cohesion,[b] S_m (MPa)	22.4	4.6	11.5	22.1	3.3	5.1	8.7	5.7	7.2	7.8	11.5
Matrix angle of int. friction, Φ_m (deg)	29.7	11.2	20.9	29.2	13.4	15.8	21.1	17.8	21.6	20.5	24.8
Joint cohesion, S_j (MPa)	1.0	1.0	1.0	1.0	1.0	0.4	1.0	0.4	1.0	0.4	1.0
Joint angle of int. friction, Φ_j (deg)	38.7	38.7	38.7	38.7	38.7	28.8	38.7	28.8	38.7	28.8	38.7
Joint tensile strength (MPa)	0.1	0.1	0.1	0.1	0.1	0.0	0.1	0.0	0.1	0.0	0.1

(Table is continued on following page)

Table 4-1 (continued)

Property	Unit[a] IA2 TCw	IB PTn	IIA TSw1	IIB,IIIA TSw2,3	IIIB CHn1v	IVA,B,C CHn1z,2,3	VA PPw	VB CFUn	VI BFw	VIIA,B,C CFMn1,2,3	VIII TRw
Brittle/ductile trans. pressure,[d] σ_n (MPa)	−92.7	−6.0	−25.0	−87.1	−4.1	−17.6	−18.5	−23.2	−15.3	−42.1	−31.0
Thermal conductivity,[b]											
k_1 (T< 100°C)	2.00	1.49	1.19	1.85	1.21	1.35	1.86	1.31	2.00	1.48	2.09
k_2 (100 ≤T≤ 125°C)	1.95	1.43	1.10	1.73	1.12	1.20	1.61	1.18	1.68	1.31	1.94
k_3 (T> 125°C)	1.90	1.37	1.00	1.61	1.02	1.03	1.35	1.04	1.35	1.13	1.79
(W/mK)											
Volum. heat capacity,[b]											
ρC_{p_1} (T< 100°C)	0.070	0.078	0.061	0.069	0.078	0.077	0.077	0.077	0.085	0.082	0.082
ρC_{p_2} (100 ≤T≤ 125°C)	0.838	0.321	0.386	0.308	0.880	0.520	0.605	0.478	0.737	0.425	0.599
ρC_{p_3} (T> 125°C)	0.042	0.058	0.045	0.057	0.040	0.042	0.052	0.045	0.053	0.049	0.057
(W·yr/m^{3}K)											
Boiling Low	100.	100.	100.	100.	100.	100.	100.	100.	100.	100.	100.
range (°C) High	125.	125.	125.	125.	125.	150.	125.	150.	125.	150.	125.
Wet bulk density,[b] ρ_{bs} (kg/m^3)	2300.	1900.	2260.	2330.	1780.	1890.	2150.	1940.	2230.	2090.	2320.

[a]The first set of unit designators was in use at the time of this study; the second set was established later.

[b]Value differs from SNL [1987] because it was obtained from preliminary data in a draft version of the document.

[c]$g = 9.8065$ m/s^2.

[d]Brittle/ductile transition pressure (where negative values indicate compression)

$$
\begin{aligned}
I: \quad \tau &= S_m + \tan(\Phi_m) \times \sigma_n \text{ (Mohr-Coulomb criterion for matrix)} \\
II: \quad \tau &= S_j + \tan(\Phi_j) \times \sigma_n \text{ (Mohr-Coulomb criterion for failed matrix)} \\
I &= II, \text{ and solve for } \sigma_n : \\
\sigma_n &= \frac{(S_j - S_m)}{[\tan(\phi_m) - \tan(\phi_j)]}.
\end{aligned}
$$

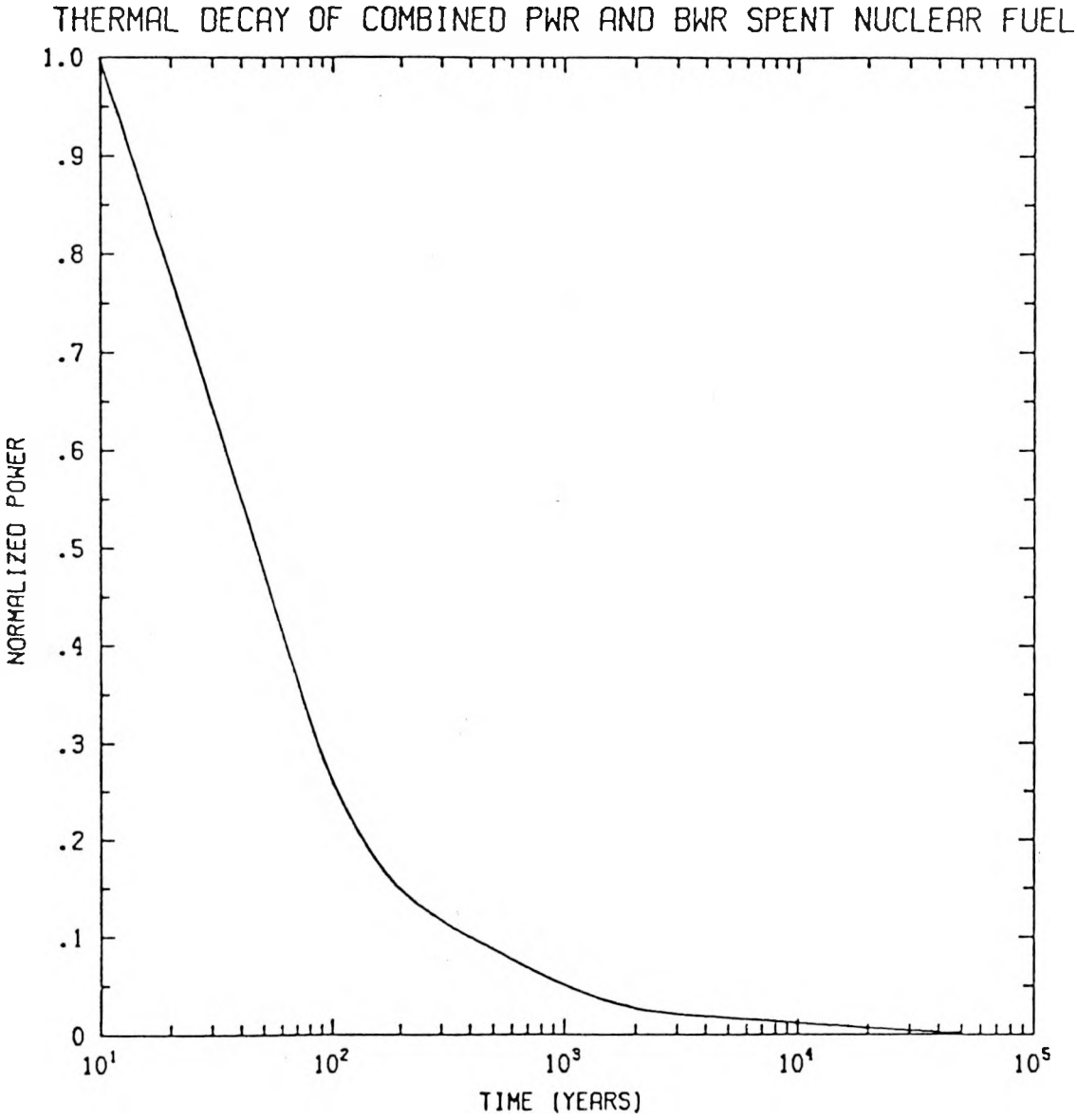

Figure 4-3. Thermal Decay Characteristics of Combined 60 Percent PWR and 40 Percent BWR Spent Fuel.

Table 4-2. Thermal Power Decay of Combined 60 Percent PWR and 40 Percent BWR Spent Fuel

Time (Years)[a]	NP[b]
10	1.0000
20	0.7786
50	0.4763
100	0.2618
200	0.1488
500	0.0880
1,000	0.0515
2,000	0.0276
5,000	0.0178
10,000	0.0128
20,000	0.0075
50,000	0.0027

[a]Years after discharge from the reactor.

[b]NP denotes normalized thermal power.

of Yucca Mountain shown in Figure 4-1. This extension is necessary to avoid violation of the boundary conditions used in the thermal and mechanical models, which are discussed in Sections 4.3.2 and 4.4.2, respectively. The region of the far-field model provided by Figure 4-1 is within the dashed rectangle in Figure 4-4.

The mesh closely matches the topography, thermal/mechanical stratigraphy, location of the repository, and the location of the faults as laid out in Figure 4-1. Figure 4-5 shows the thermal/mechanical stratigraphy as it is defined by the finite element mesh.

Mesh refinement has been provided in regions of the far field most likely to be affected by the repository and in regions where the rates of change of temperature and displacement are expected to be high. The far-field mesh shown in Figure 4-4 contains 3,281 nodal points in 1,050 elements and has a nodal bandwidth of 96. The issues of sufficient mesh refinement and appropriate boundary conditions for this far-field model are discussed in Appendix A.

4.3 THERMAL MODEL

4.3.1 Finite Element Code SPECTROM–41

The finite element heat transfer computer program SPECTROM–41 is an integral part of the SPECTROM (Special Purpose Engineering Codes for Thermal/-ROck Mechanics) series of computer programs. The program is capable of solving

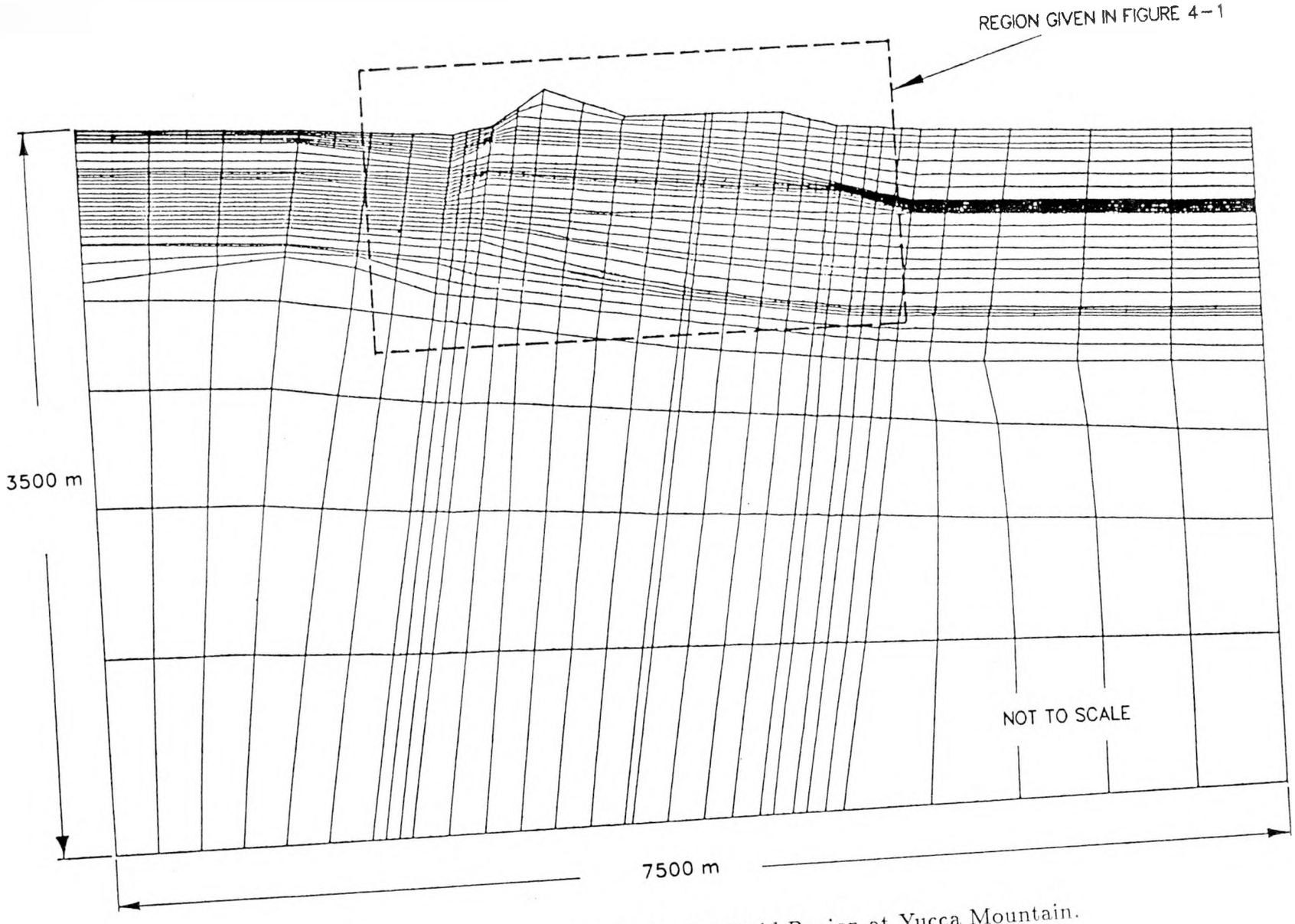

Figure 4-4. Finite Element Mesh of the Far-Field Region at Yucca Mountain.

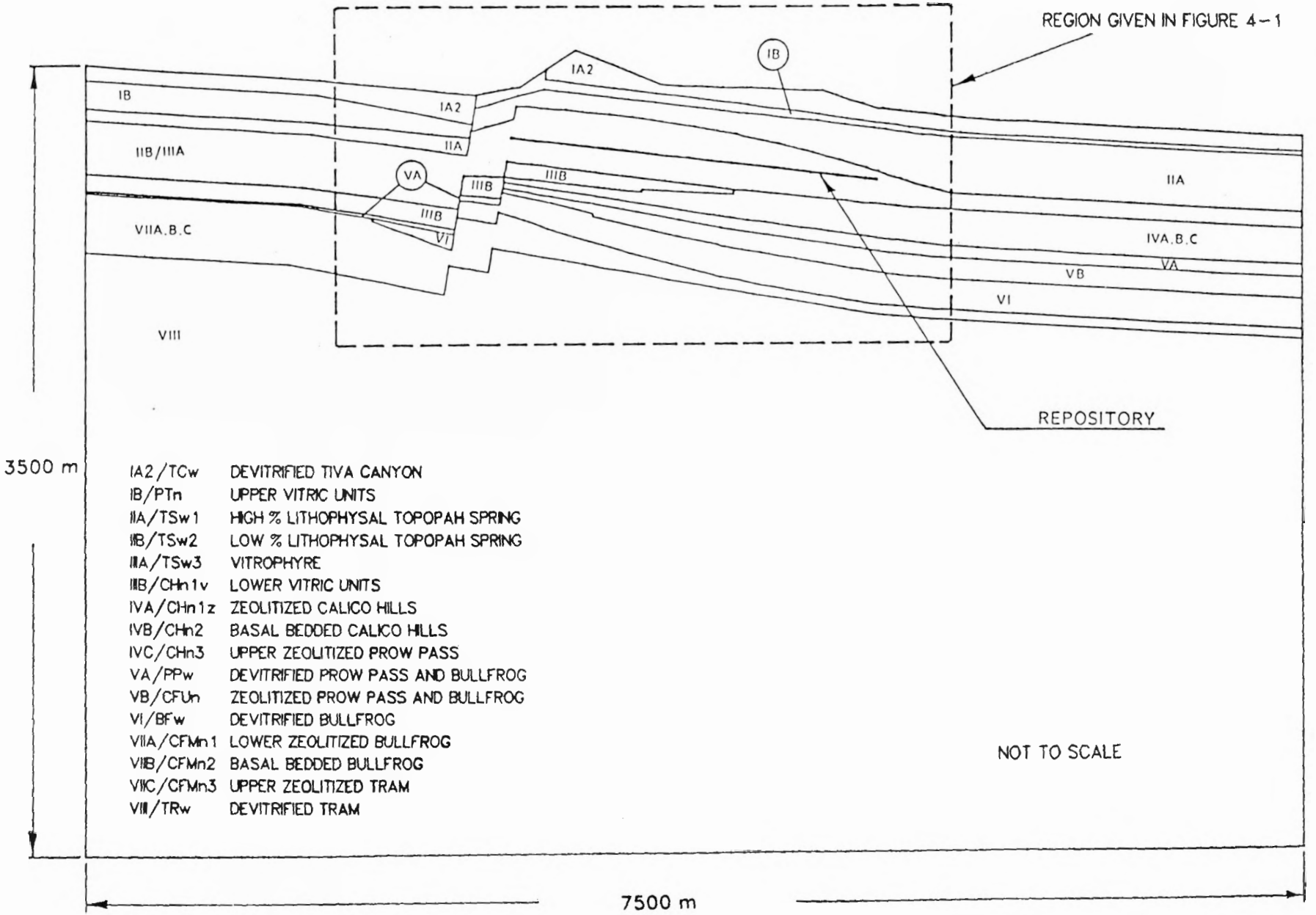

Figure 4-5. Thermal/Mechanical Stratigraphy Defined by the Finite Element Mesh.

two-dimensional (x-y) and axisymmetric (r-z) steady-state or transient-conductive heat transfer problems with a variety of boundary conditions. The program uses isoparametric elements, and the finite element equations involving the spatial temperature distribution are obtained from a variational formulation [Wilson and Nickell, 1966]. The program is also capable of solving heat transfer problems involving phase change, which is a phenomenon that may take place in the far field in the form of pore water boiling.

4.3.2 Conceptualized Thermal Model

The conceptual thermal model illustrated in Figure 4-6 is a two-dimensional (x-y) model with boundary conditions as follows.

- The two vertical boundaries are sufficiently far removed from the repository that they are assumed to be perfectly insulated or adiabatic.
- The modeled ground surface is a convective boundary chosen so that any temperature rise at the surface can be detected.
- The lower horizontal boundary is a constant flux boundary.

The convective heat transfer coefficient used is 1 $W/m^2°C$ and the air temperature used is 16.5°C. This is an estimate of the annual average air temperature approximately 12 mi southeast of the potential repository site at Yucca Mountain. The initial temperatures in the thermal far-field model are based on temperature measurements from drillholes USW H–4, USW H–5, and USW G–4 at Yucca Mountain [Sass et al., 1988]. Figure 4-7 shows the location of these drillholes projected onto the cross section CC'. Using the material characterization, stratigraphy, and geometry presented in Sections 4.1 and 4.2, along with the boundary conditions presented above, a constant upward flux of 0.040 W/m^2 along the lower horizontal boundary was selected to give the most reasonable match between the predicted steady-state temperatures in the far field and those measured in the drillholes. Some variation outside the immediate vicinity of the repository was accepted in order to optimize the comparison in the repository region. The comparison between measured and predicted temperatures for the three drillholes is given in Figures 4-8, 4-9, and 4-10. In Figure 4-11, temperature contours illustrate the initial thermal conditions in the far field.

The repository is modeled as a 4-m-thick heat generating plate. The plate thickness is approximately equal to the length of a waste container. The repository is modeled as infinitely long in the out-of-plane direction (normal to the paper), a consequence inherent in the two-dimensional model. In this model, it is assumed that all the waste is emplaced instantaneously. This assumption is conservative and will result in predicted rock temperatures slightly higher than those of actual conditions where waste is emplaced sequentially.

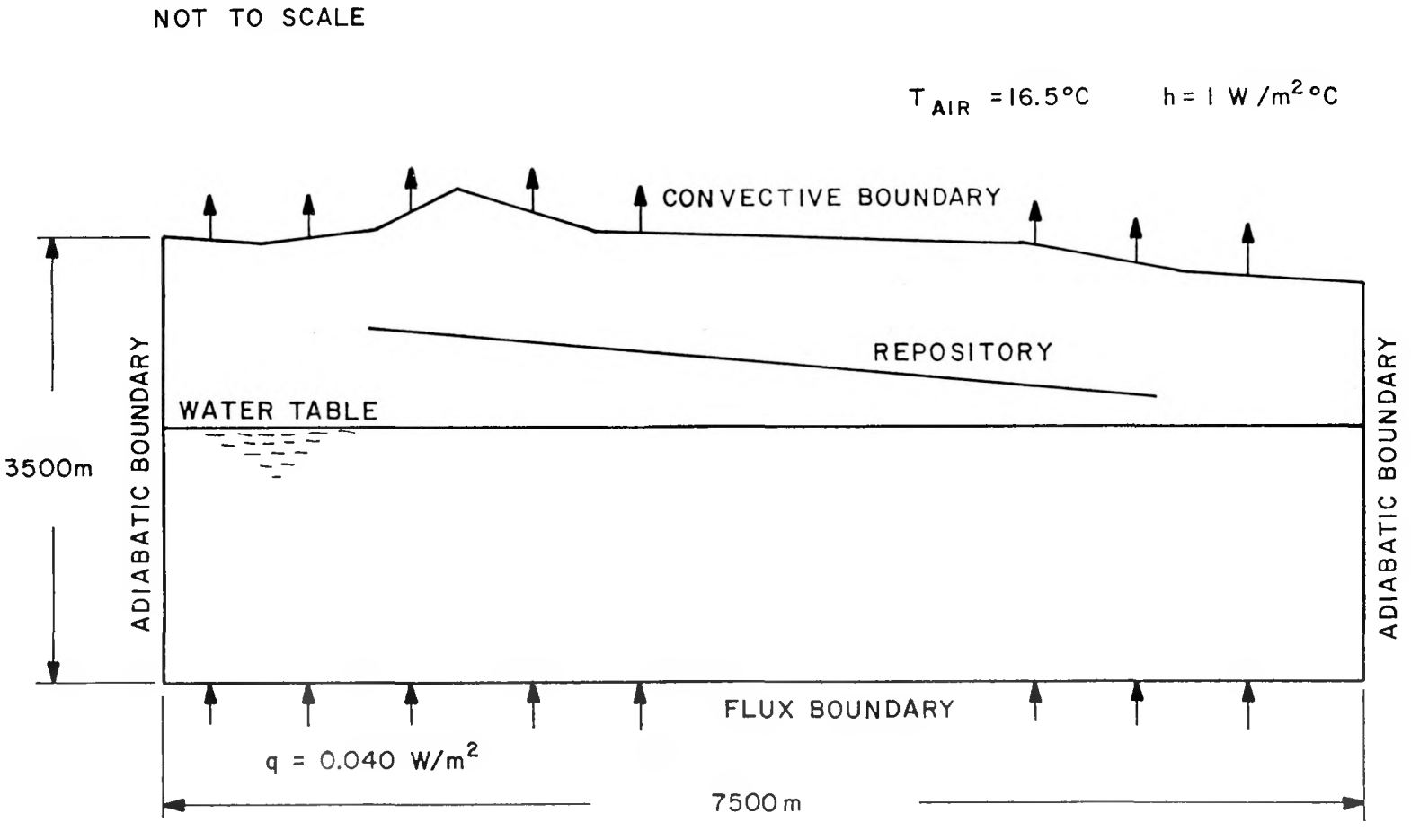

Figure 4-6. Conceptualized Thermal Far-Field Model of Yucca Mountain

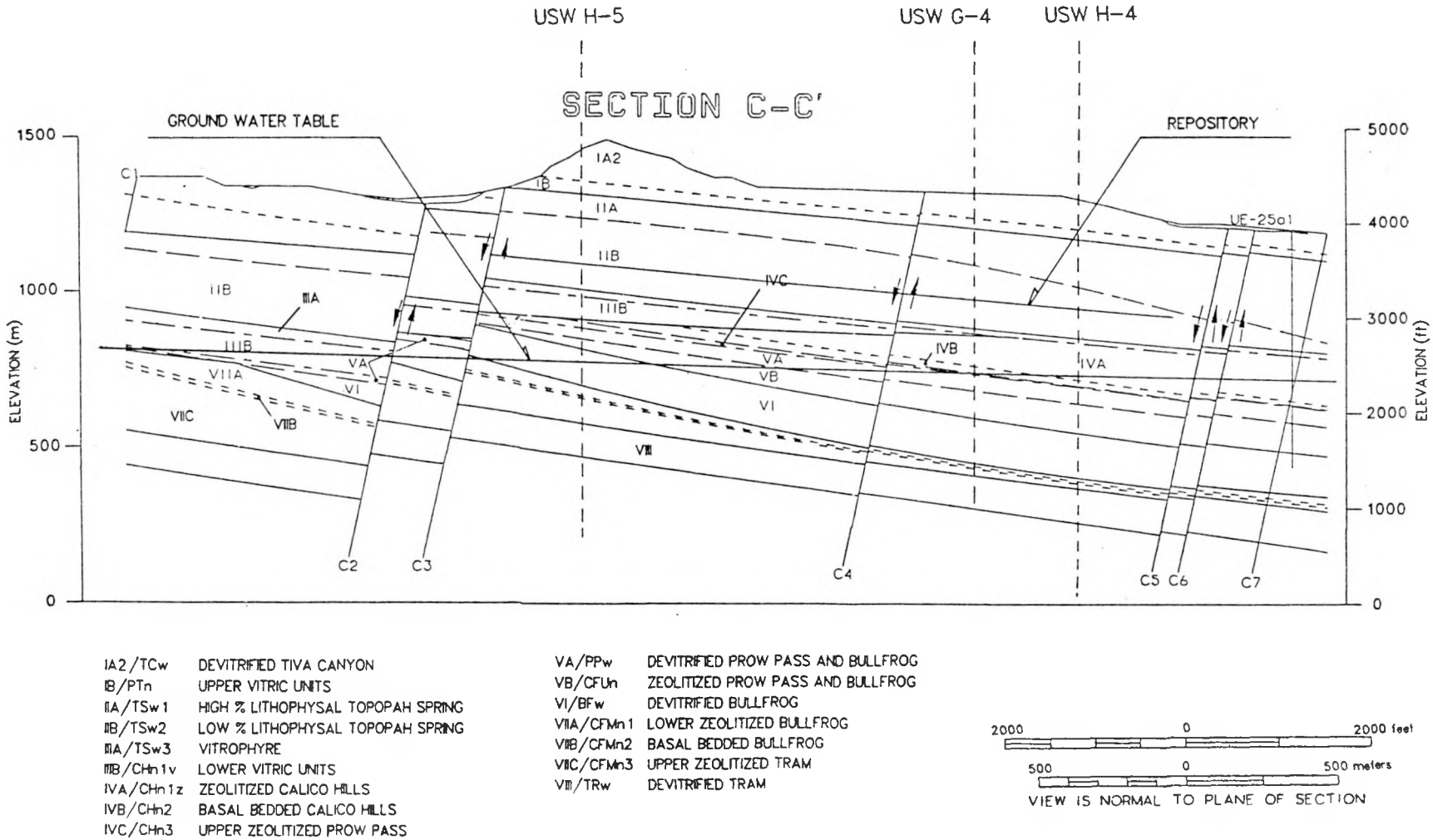

Figure 4-7. Projection of Drillholes USW H–4, USW H–5, and USW G–4 onto Cross Section *CC'*

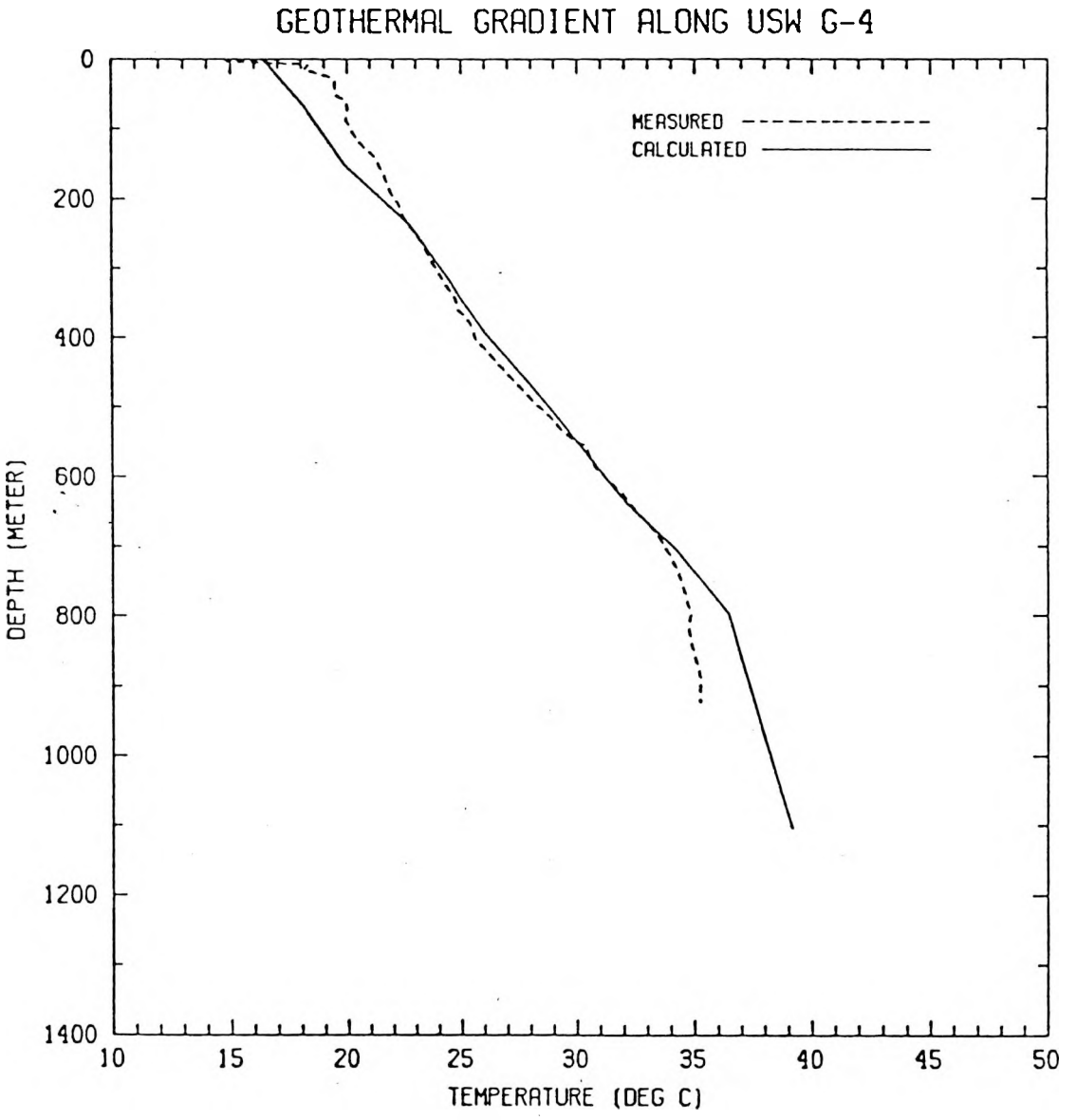

Figure 4-8. Measured and Predicted Temperatures along Drillhole USW G–4 at Yucca Mountain.

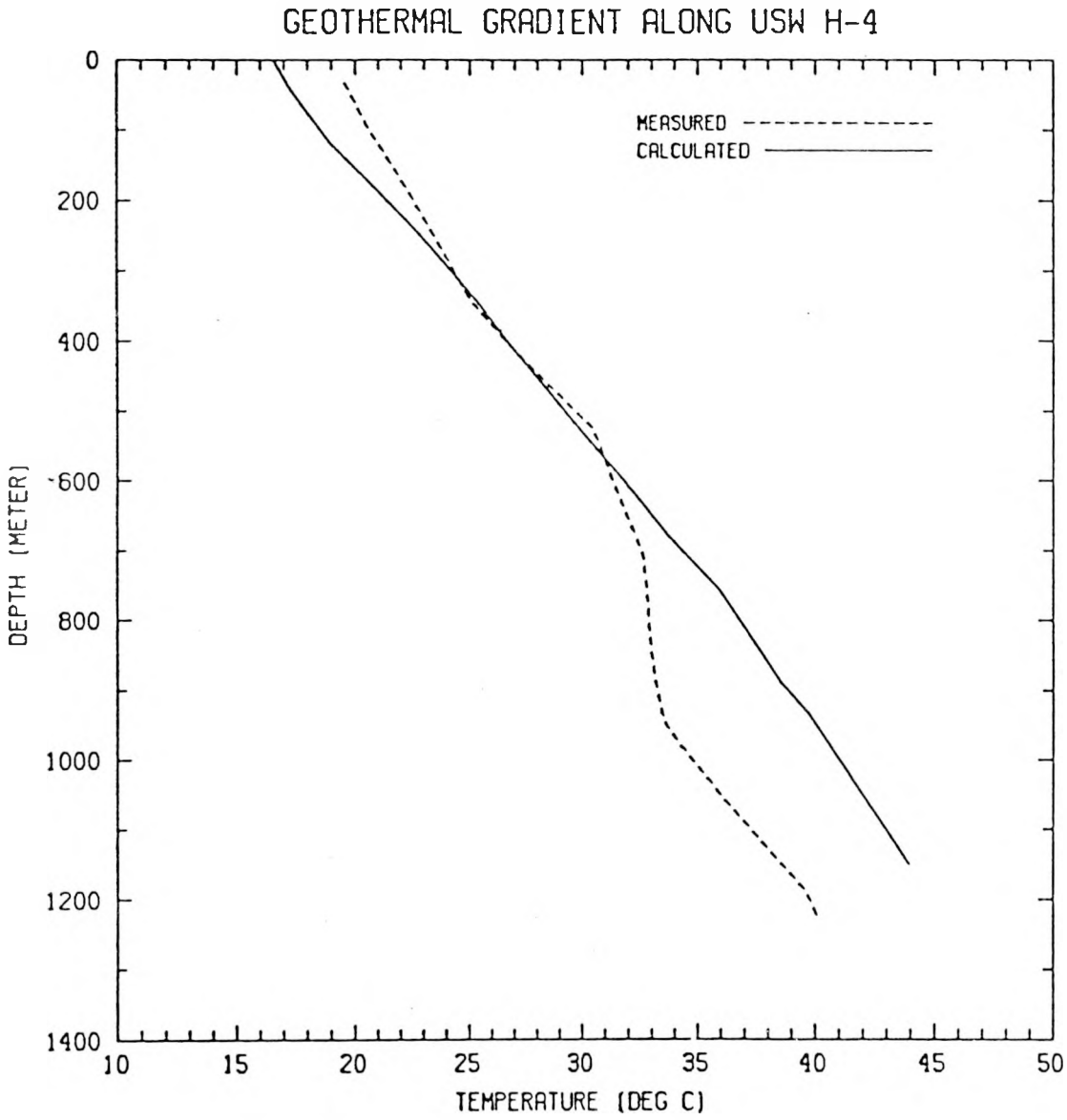

Figure 4-9. Measured and Predicted Temperatures along Drillhole USW H–4 at Yucca Mountain.

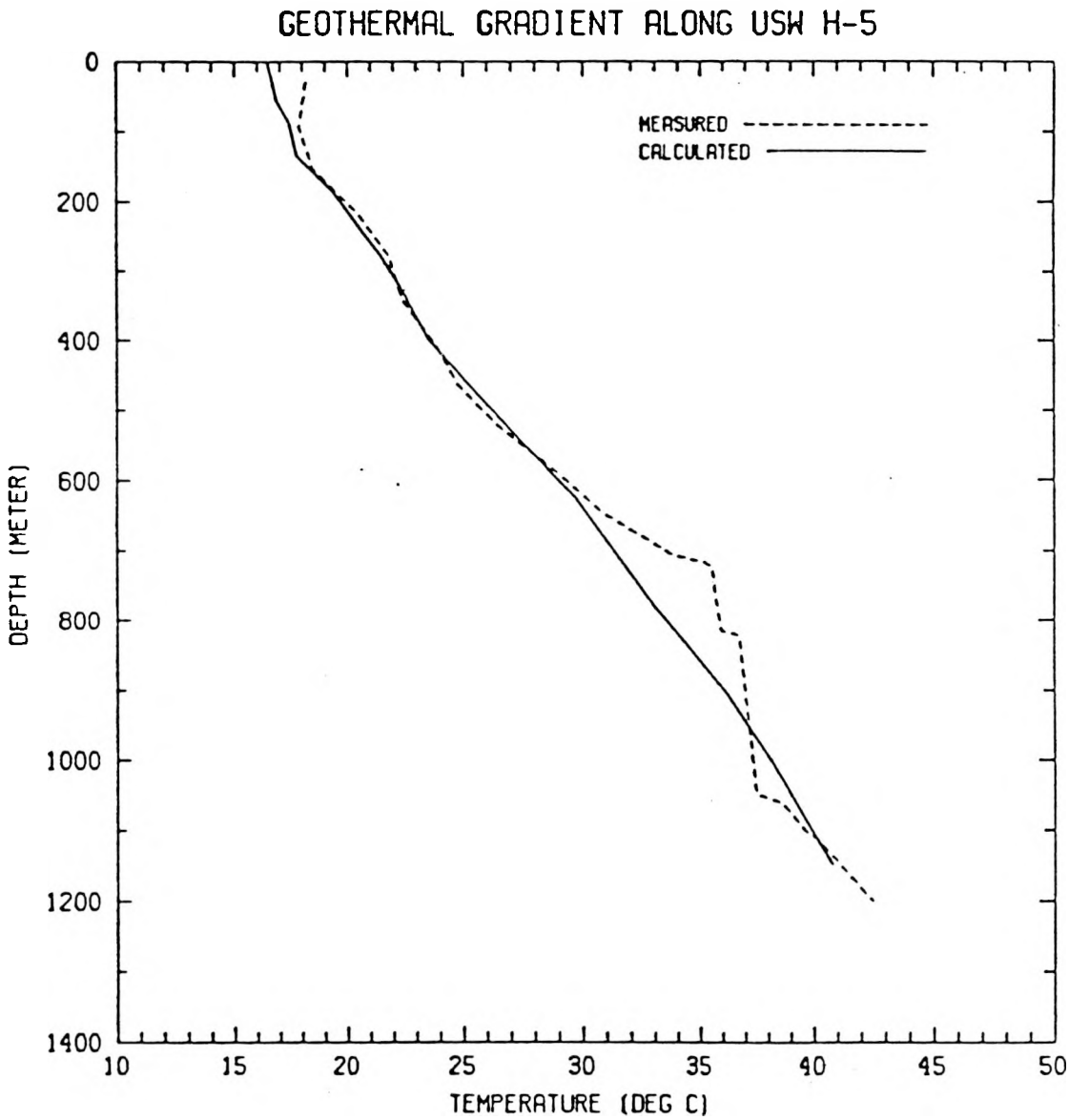

Figure 4-10. Measured and Predicted Temperatures along Drillhole USW H-5 at Yucca Mountain.

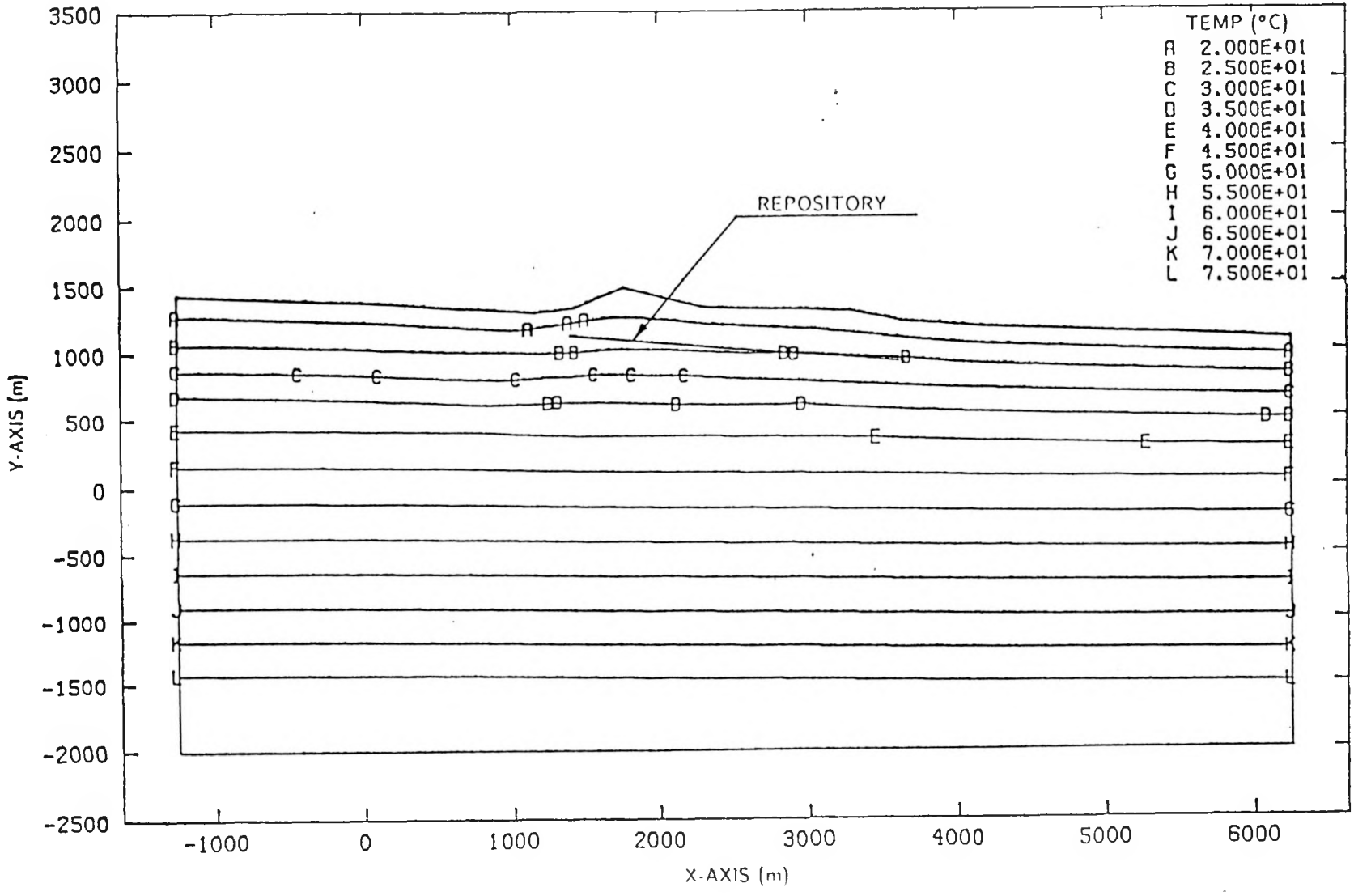

Figure 4-11. Temperature Contours (°C) Showing Initial Conditions of the Far-Field Region at Yucca Mountain.

Although the repository in its entirety is located above the static water table, the rock in this region remains about 80 percent saturated. If the rock is heated to temperatures beyond 100°C (assuming atmospheric conditions), the pore water in the rock may boil. The simulation of boiling has been included in the model and is shown qualitatively in Figure 4-12. To avoid ill conditioning of the heat transfer problem, the boiling phenomenon is simulated over a temperature range (T_1, T_2). The boiling model illustrated in Figure 4-12 responds differently when temperatures increase and decrease. The thermal conductivity and volumetric heat capacity are changed twice as temperatures increase; i.e., first, when the temperature reaches the onset of boiling (T_1) and, second, when the temperature increases beyond the range of boiling (T_2). When the temperature exceeds T_2, the rock is essentially dry. As temperatures decrease, the thermal conductivity and volumetric heat capacity change at temperature T_1, which now becomes the onset of resaturation. The model implies that the energy consumed during the process of boiling (i.e., the heat of vaporization in dehydrating the rock) does not return upon resaturation of the rock. This energy is assumed to be lost from the system. In reality, the heat of vaporization would be recovered if the vapor cooled within the modeled region.

The boiling range for each of the stratigraphic units of Figure 4-1 is given in Table 4-1, along with the respective values of the thermal conductivity (k_1, k_2, k_3) and volumetric heat capacity (ρC_{p_1}, ρC_{p_2}, ρC_{p_3}).

4.4 MECHANICAL MODEL

4.4.1 Finite Element Code SPECTROM–31

SPECTROM–31 is a finite element computer program for the large-deformation elastic and inelastic, static and quasi-static response of axisymmetric (r-z) solids and two-dimensional (x-y) solids in plane strain or plane stress. The program allows for pressure and displacement boundary conditions. The initial stress field can be caused by body forces, or the initial stress field can be prescribed. The program uses isoparametric elements and is based on an eight-noded biquadratic displacement assumption. Thermal stresses in SPECTROM–31 are computed on the basis of a precalculated thermal history, such as that calculated using SPECTROM–41. The program allows the user to choose from several material models.

4.4.2 Conceptualized Model

The conceptual mechanical finite element far-field model of Yucca Mountain is shown in Figure 4-13. It is a two-dimensional plane strain model that maintains the complex stratigraphic definition of Figure 4-1 in terms of element geometry, as well as the definition of the material properties of each stratigraphic unit. The rock is characterized as an elastic/plastic, isotropic, heterogeneous continuum with one ubiquitous vertical joint set. The constitutive model uses an approach similar

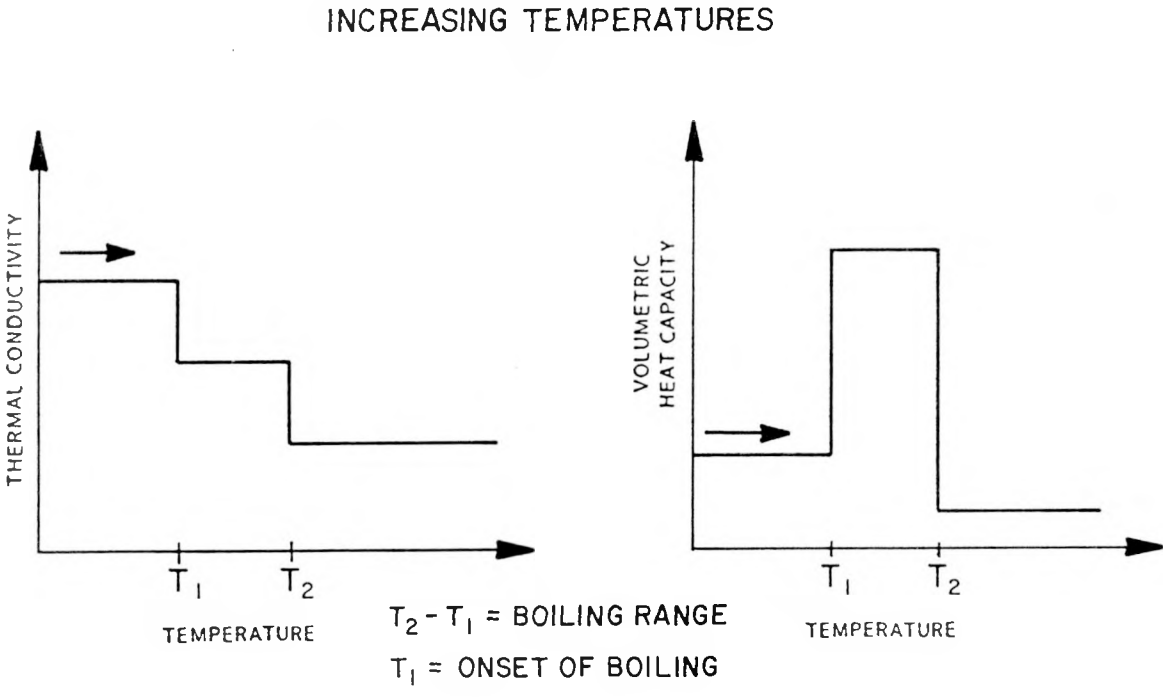

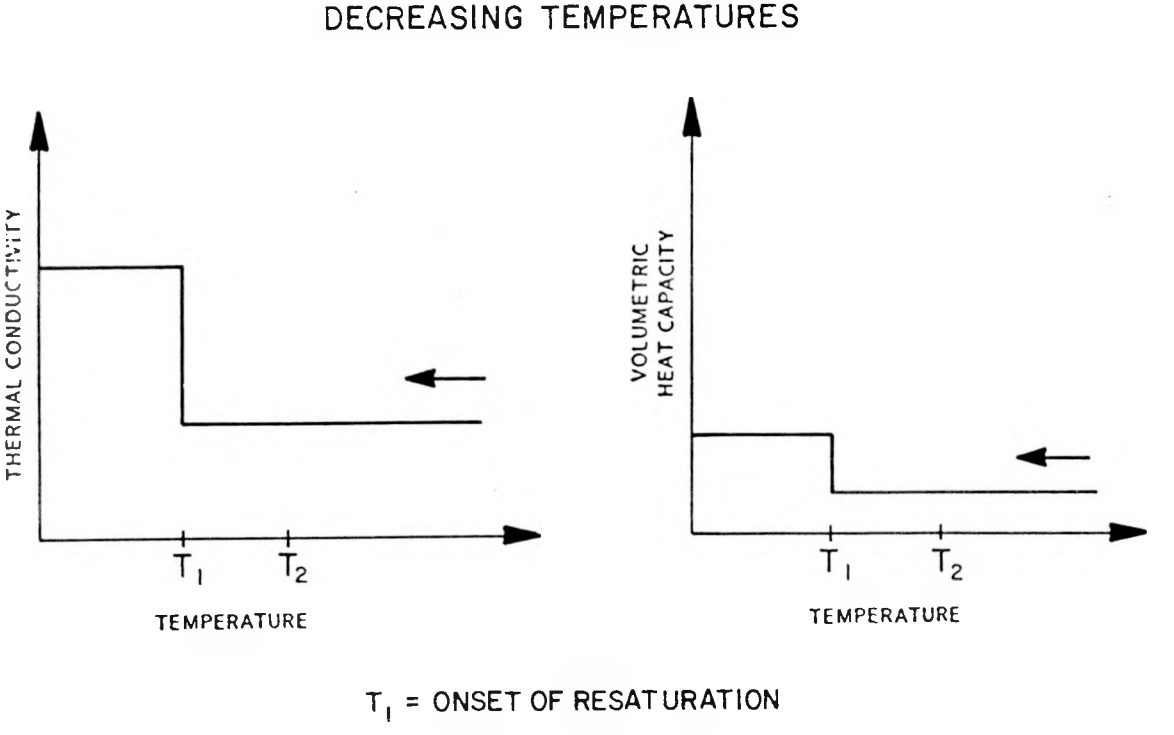

Figure 4-12. Qualitative Illustration of the Model that Simulates Boiling.

to the one used by Thomas [1980]. The onset of plastic response in the matrix material and of the joints is governed by a Mohr-Coulomb criterion. Plasticity of the joints is evaluated both in shear (fracture slip) and in tension (fracture opening). The graphical output from SPECTROM–31 to illustrate plasticity is "X" and "O," where "X" symbolizes fracture slip and "O" symbolizes fracture opening.

The displacement boundary conditions used are illustrated in Figure 4-13, and are as follows

- The two vertical boundaries are placed at a sufficient distance from the repository to assure that perturbations on the boundary are negligible; the boundaries are therefore restrained from horizontal movement.
- The lower horizontal boundary is also placed at sufficient distance from the repository to specify that it be restrained from vertical movement.
- The lower left and right corner nodes are restrained from vertical and horizontal movement, a combination of the above two boundary conditions.
- The ground surface is unrestrained (traction free).

Initial conditions are based on a gravitational stress field [Bauer et al., 1985]; i.e., the vertical stress is equal to the weight of the overburden, and the horizontal stresses are caused by the Poisson's effect. Figures 4-14 and 4-15 illustrate the in situ stress field at Yucca Mountain as it is predicted by the mechanical model for the particular conditions given.

The coefficient of thermal expansion, which was found to be a function of temperature [SNL, 1987], will, in some instances, induce positive strain (contraction) with increasing temperatures. The thermal expansion coefficients of each stratigraphic unit are given in Table 4-1, along with the respective dehydration ranges.

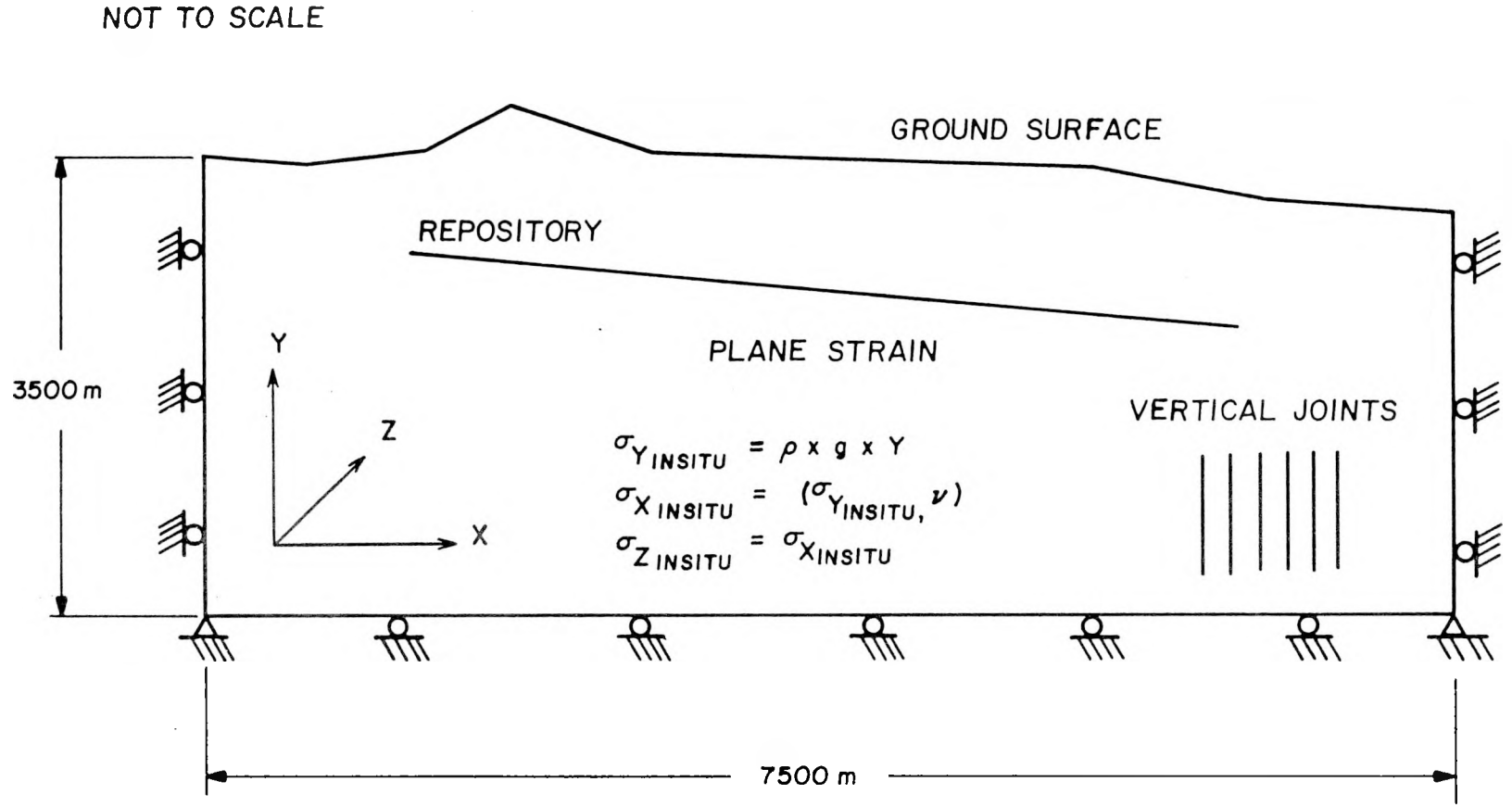

Figure 4-13. Conceptualized Mechanical Far-Field Model of Yucca Mountain

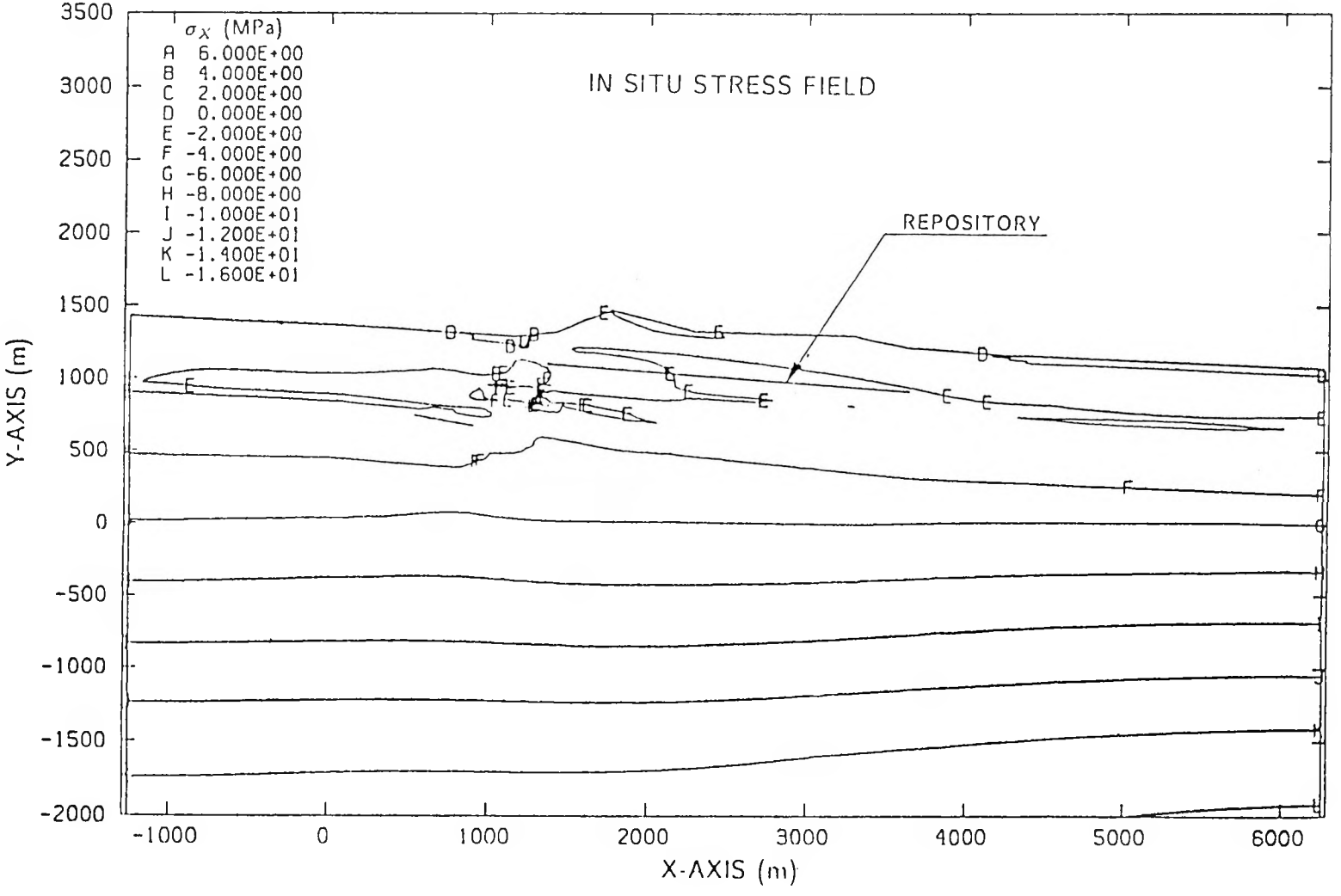

Figure 4-14. Contours of Predicted Initial Horizontal Stress (MPa) in the Far Field at Yucca Mountain.

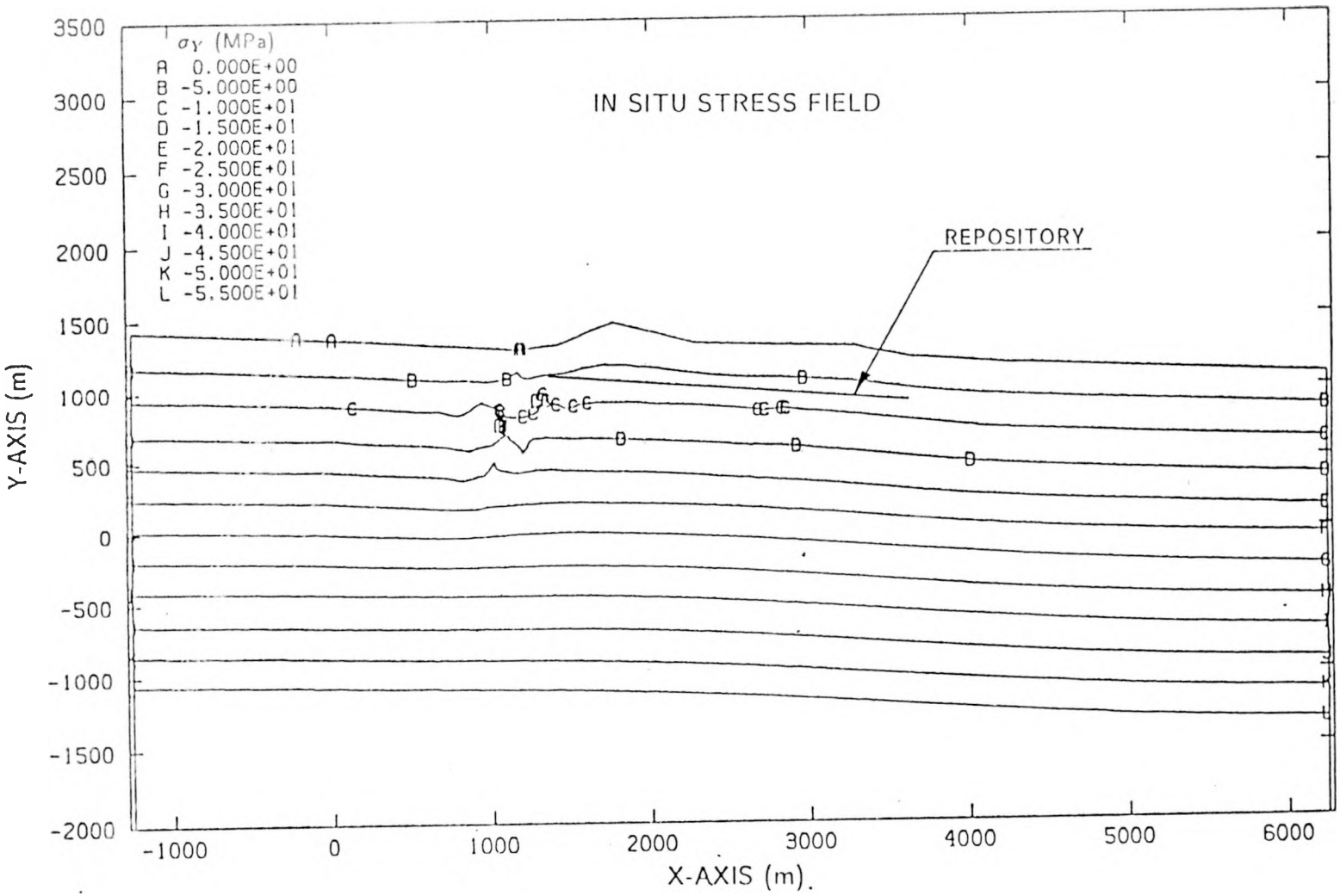

Figure 4-15. Contours of Predicted Initial Vertical Stress (MPa) in the Far Field at Yucca Mountain.

5.0 ARCHIVED DATA

The specific thermal and mechanical far-field models described in the previous sections are preserved in terms of computer programs, update files, and program input files. These files are archived at RE/SPEC Inc. and were also submitted to SNL on magnetic tape upon completion of the analysis. The two finite element computer programs, SPECTROM–41 and SPECTROM–31, represent the basic tools used to obtain solutions to the thermal and mechanical far-field problems, respectively.

Update files, which add additional capability but do not otherwise alter the computer programs, are sometimes necessary in order to account for special features of a problem not generally covered by the "basic version" of the computer program. For SPECTROM–41, the process of pore water boiling is an example of a special feature.

It is the input files that define the environment within which the phenomena of heat transfer and material behavior are studied. The input files tailor specific model characteristics by defining the materials that are modeled, as well as by defining their constitutive, structural, and geometric details.

The following paragraph identifies the files constructed specifically to create the Yucca Mountain thermal and mechanical far-field models described in this report.

The files related to the thermal far-field model are as follows.

[RSI058.017.TB.RUN41.UPD41]BOIL.UPD;26

> This is an update file containing programming that enables the computer program SPECTROM–41 to simulate the process of pore water boiling. The updates are specific to the thermal far-field model of Yucca Mountain described in this report.

[RSI058.017.TB.FFMESH]MESH41.DAT;3

> This is an input file to the program SPECTROM–41. The file defines the far-field domain of Yucca Mountain in terms of nodal point coordinates, boundary conditions, and element material type according to the format required by SPECTROM–41.

[RSI058.017.TB.RUN41.41FFRUN]READ41.DAT;13

This is an input file to SPECTROM–41 that contains the necessary information to simulate the thermal response of the far field to a spent fuel repository at Yucca Mountain, for a time period of 50,000 yr. The initial APD is 57 kW/acre.

The files related to the mechanical far-field model are as follows:

[RSI058.017.TB.FFMESH]MESH.DAT;1

This is an input file to the program SPECTROM–31. This file defines the far-field domain in terms of nodal point coordinates, boundary conditions, and element material type according to the SPECTROM–31 format.

[RSI058.017.TB.RUN31]31INPUT.DAT;12

This is an input file to SPECTROM–31 that contains the necessary information to simulate the in situ stress field at Yucca Mountain by gravitational loading. The file also contains information necessary to complete a thermomechanical simulation of Yucca Mountain for a time period of 50,000 yr.

[RSI058.017.TB.RUN41.41FFRUN]TEMP31.BIN;3

This is an input file to SPECTROM–31 used only if a thermomechanical simulation of Yucca Mountain is performed. The file contains temperatures of the far field at discrete times from initial waste disposal to 50,000 yr of waste isolation. The file was created from a thermal simulation using the program SPECTROM–41 for the condition of spent fuel disposal with an initial APD of 57 kW/acre.

These files have been stored permanently on a magnetic tape by using the BACKUP utility program provided for the Digital Equipment Corporation VAX 11/750 computer. The files are stored on the magnetic tape as a SAVE SET in the RE/SPEC Analysis Archive uniquely identified by the number 0588444. The files can be retrieved from the magnetic tape using the same BACKUP utility program by anyone familiar with the Digital Equipment Corporation VAX/VMS operating system.

6.0 CONCLUSION

A thermomechanical finite element far-field model has been constructed that reflects the material properties and structural character of Yucca Mountain that have been updated since the unit evaluation study [Johnstone et al., 1984]. The model is a result of a continuous effort to characterize a potential repository site at Yucca Mountain. The primary purpose of the thermomechanical far-field model is to aid in the understanding of the effects and consequences related to the permanent isolation of nuclear waste in a repository at Yucca Mountain by providing information about changes in temperatures, displacements, and stresses in the rock resulting from the presence of the repository.

Although the model is perceived to be an accurate and realistic representation of the potential repository site at Yucca Mountain, it remains an idealized description of the mountain. It is important to keep this fact in mind when interpreting the results provided by the model.

The work to characterize the repository site at Yucca Mountain will culminate with the excavation of the Exploratory Shaft Facility (ESF). As data are gathered from the ESF and perhaps from additional boreholes, these far-field models may be revised. The revisions may include updated material properties and stratigraphy and appropriate constitutive models to provide current results upon which decisions regarding design and construction of the repository may be based.

REFERENCES

Bauer, S., J. Holland, and D. K. Parrish, 1985. *Implications About In Situ Stress at Yucca Mountain*, Proceedings 26th U.S. Symposium on Rock Mechanics, Rapid City, South Dakota, pp. 1113-1120. (HQS.880517.1611)

Johnstone, J. K., R. R. Peters, and P. F. Gnirk, 1984. *Unit Evaluation at Yucca Mountain, Nevada Test Site: Summary Report and Recommendation*, SAND83–0372, Sandia National Laboratories, Albuquerque, New Mexico. (NNA.870519.0052)

Sandia National Laboratories, 1987. SAND84–2641, *Site Characterization Plan Conceptual Design Report*, Volume 4, H. R. MacDougall, L. W. Scully, and J. R. Tillerson, compilers, Albuquerque, New Mexico. (NNI.880902.0014-.0019)

Sass, J., A. Lachenbruch, W. W. Dudley, Jr., S. S. Priest, and R. J. Munroe, 1988. *Temperature, Thermal Conductivity and Heat Flow Near Yucca Mountain, Nevada: Some Tectonic and Hydologic Implications,* OFR87–649, U.S. Geological Survey Letter Report. (NNA.890123.0010)

Thomas, R. K., 1980. *A Material Constitutive Model for Jointed Rock Mass Behavior*, SAND80–1418, Sandia National Laboratories, Albuquerque, New Mexico. (HQS.880517.3249)

Wilson, E. L. and R. E. Nickell, 1966. *Application of the Finite Element Method to Heat Conduction Analysis*, Nuclear Engineering and Design, Vol. 4, pp. 276–286. (NNA.891109.0119)

APPENDIX A

A CHECK OF THE FAR-FIELD MESH REFINEMENT AND BOUNDARY CONDITIONS

APPENDIX A
LIST OF FIGURES

APPENDIX A
A CHECK OF THE FAR-FIELD MESH REFINEMENT AND BOUNDARY CONDITIONS

The following study has been performed to investigate the influence the current mesh refinement and adopted boundary conditions may have on the results predicted by the thermomechanical far-field models.

To investigate the influence of mesh refinement, two finite element meshes were applied to the same two-dimensional far-field problem. The refinement of each mesh required that (1) the repository and each layer of stratigraphy be modeled, and (2) the refinement be greatest near the repository in the location of the highest temperature and stress gradients. Figure A-1 shows Mesh I, which has close to the same refinement as the mesh for Yucca Mountain defined in Section 4.2. Figure A-2 shows Mesh II, which has the same vertical refinement but twice the horizontal refinement of Mesh I. In essence, the second mesh has element aspect ratios that are closer to one. Comparing results from both meshes reveals whether the aspect ratios caused by the coarseness of the first mesh significantly affected the performance of the element in this problem and hence significantly affected the results. For convenience, both meshes were generated in rectangular form, thus allowing for a vertical plane of symmetry to be used along the center of the model.

SPECTROM–41 described in Section 4.3.1, was the finite element heat transfer computer program used. The conceptual thermal model shown in Figure A-3 defines a thermal/mechanical stratigraphy similar to that of Yucca Mountain. Boundary and initial conditions are the same as those described in Section 4.3.2. The model does not, however, take into account boiling of the pore water that exists in the rock. This feature was omitted to minimize computer time and cost and does not affect the outcome of this study. Therefore, for each stratigraphic unit in this model, the constant thermal conductivity (k_1) and volumetric heat capacity (ρC_{p_1}) listed in Table 4-1 were used.

The thermal model was used to investigate a waste isolation period of 50,000 yr using both Mesh I and Mesh II. The waste was spent nuclear fuel as defined in Section 4.1, and the initial APD was 57 kW/acre (14.1 W/m^2). Results can best be illustrated as contours in the far-field domain of the difference in the temperature predicted with the two meshes. Figures A-4 through A-10 show this difference from the time 10 yr after waste emplacement to 150 yr of waste isolation. There is a difference of about -3°C at 10 yr after the initial waste emplacement. The negative sign means Mesh I "underpredicts" relative to Mesh II. A positive sign means Mesh I "overpredicts" relative to Mesh II. The difference at 10 yr appears in the vicinity of the edges of the repository and represents approximately 6 percent difference in the temperature predicted using the two different meshes. During the period from 10 to 150 yr, the difference decreases to about 1°C (less than 1 percent difference) and appears in the immediate vicinity of the repository. Beyond 150 yr,

the difference in temperature predicted using the two different meshes becomes much less than 1°C. The difference in temperatures predicted beyond the vicinity of the repository is always shown to be less than 1°C.

The mechanical finite element code SPECTROM–31 discussed in Section 4.4.1 was used to investigate the effect of mesh refinement on the mechanical results. The conceptual mechanical model is shown in Figure A-11. The boundary and initial conditions are the same as those described in Section 4.4.2. The temperatures predicted by the thermal model at 10, 50, 100, and 2,000 yr were used in the mechanical model to predict thermomechanical effects. Contours of the predicted horizontal and vertical stress using both Mesh I and Mesh II are given in Figures A-12 to A-27. These figures show that there is virtually no difference in the predicted stress contours using the two different meshes. Figures A-28 to A-35 show the predicted joint activity using Mesh I and Mesh II. At 10 yr, the lateral extent of the joint activity predicted using Mesh II is slightly greater than the lateral extent predicted using Mesh I; however, the vertical extent is the same. For subsequent times, the amount of joint activity predicted is virtually the same for Mesh I and Mesh II.

Comparison of predicted horizontal and vertical displacements between Mesh I and Mesh II are given in Figures A-36 to A-45 for nodal locations along the ground surface of the model. These displacements include those that result simulating gravity stresses in the model at the zero solution time. The displacements predicted are virtually the same using both Mesh I and Mesh II.

It appears from these results that the additional refinement provided in Mesh II has very little effect on the predicted outcome of the thermal and mechanical models. Thus, for the far-field models described in the main body of this report, the thermal and mechanical effects induced in the rock by the radioactive waste repository are predicted with sufficient accuracy using the refinement of the far-field domain provided by Mesh I.

For a boundary value problem, the boundary conditions should be chosen so that no adverse effects are imposed on the events investigated. For the present thermal and mechanical far-field models, the boundary conditions must attempt to provide for models of infinite extent. Therefore, the vertical and lower horizontal boundaries have been located at great distance from the region of interest around the repository so that their presence will have minimal or no adverse effect on the prediction of temperatures, displacements, and stresses. For both the thermal and mechanical far-field models, temperatures, displacements, and stresses were investigated along the lower horizontal boundary and along the right vertical boundary of models represented by Mesh I. For the thermal model, the predicted temperatures should remain constant along the lower horizontal and the right vertical boundaries for the period of time investigated, because these boundaries are expected to represent an infinite extent. In Figures A-46 to A-48, temperature histories are shown for nodal points that are on the boundaries investigated. Along the right vertical boundary (nodal points 46 and 1,127 in Figures A-46

and A-47) temperatures remain constant for the time period investigated. Along the lower horizontal boundary immediately below the repository (nodal point 1 in Figure A-48), there is a temperature rise of about 1.5°C at 50,000 yr. This temperature rise, however, occurs thousands of years after the maximum temperatures are reached in the vicinity of the repository and is of no consequence to the events investigated because these boundaries are expected to represent an infinite extent.

In Figures A-49 to A-58, stresses and displacements are shown along the lower horizontal and right vertical boundaries of the far-field model. Because stresses are determined at integration points only (four integration points per element located inside the element), they do not necessarily represent boundary values. The displacements are evaluated at nodal points; thus, they do represent boundary values. It is assumed in the present mechanical far-field model that stresses and displacements along the lower horizontal and the right vertical boundaries will remain at their initial values throughout the time period analyzed. For the thermal model, the time period analyzed was 50,000 yr. However, the time period analyzed for the mechanical model was 2,000 yr. With the material model (elastic/plastic with ubiquitous joints) used, the mechanical events investigated have been shown to reach a maximum within 2,000 yr [Brandshaug and Svalstad, 1984]. Figures A-49 to A-58 show that stresses and displacements along the boundaries remain fairly constant for the 2,000 yr investigated. The small variations that occur are not believed to have any effect on the mechanical events taking place in the vicinity of the repository.

The investigation of the thermal and mechanical events along the lower horizontal and right vertical boundaries of the thermal and mechanical far-field models indicates that these boundaries are not affected by the events in the vicinity of the repository.

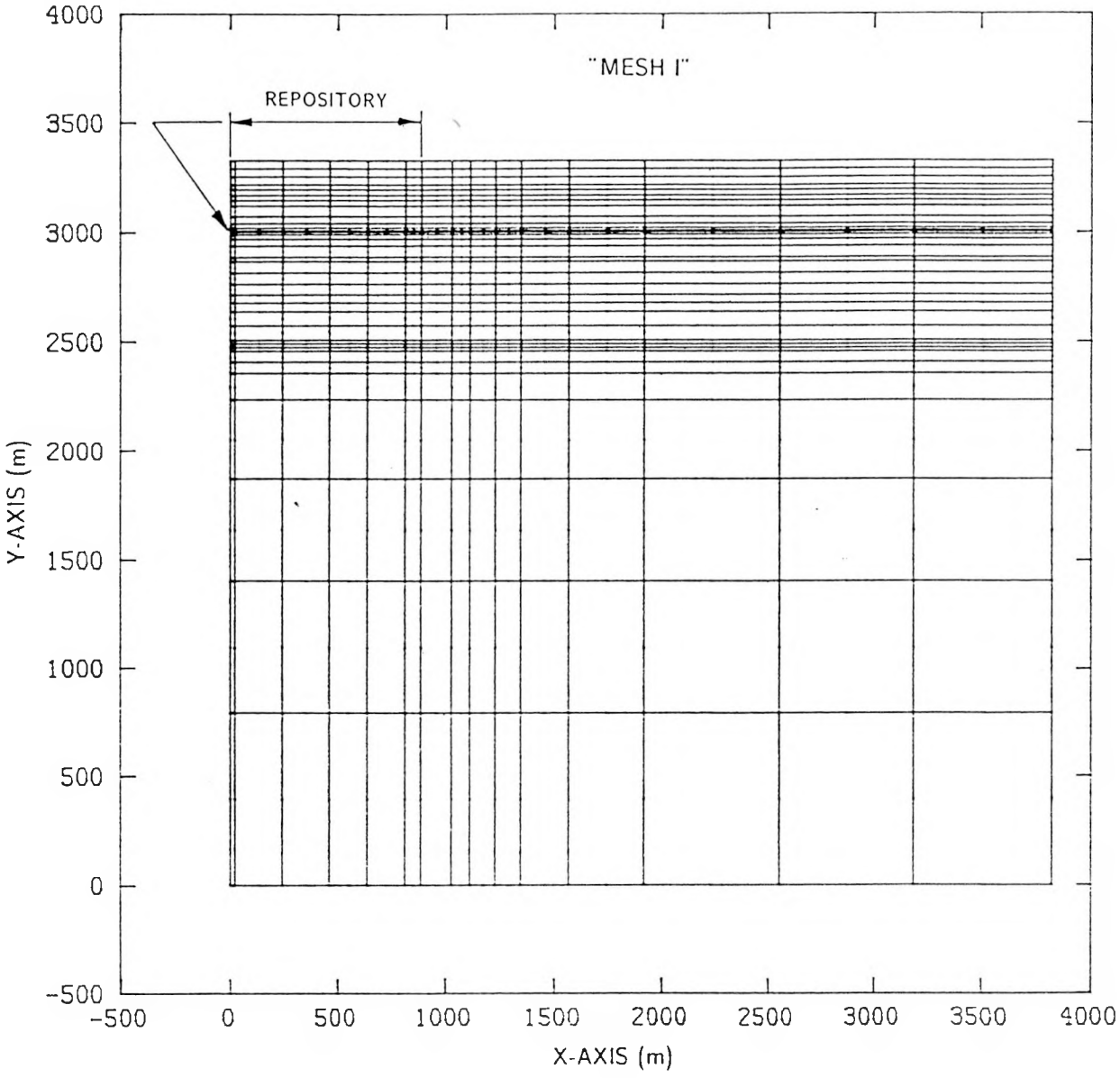

Figure A-1. Finite Element Mesh (Mesh I) of a Rectangular Far-Field Region.

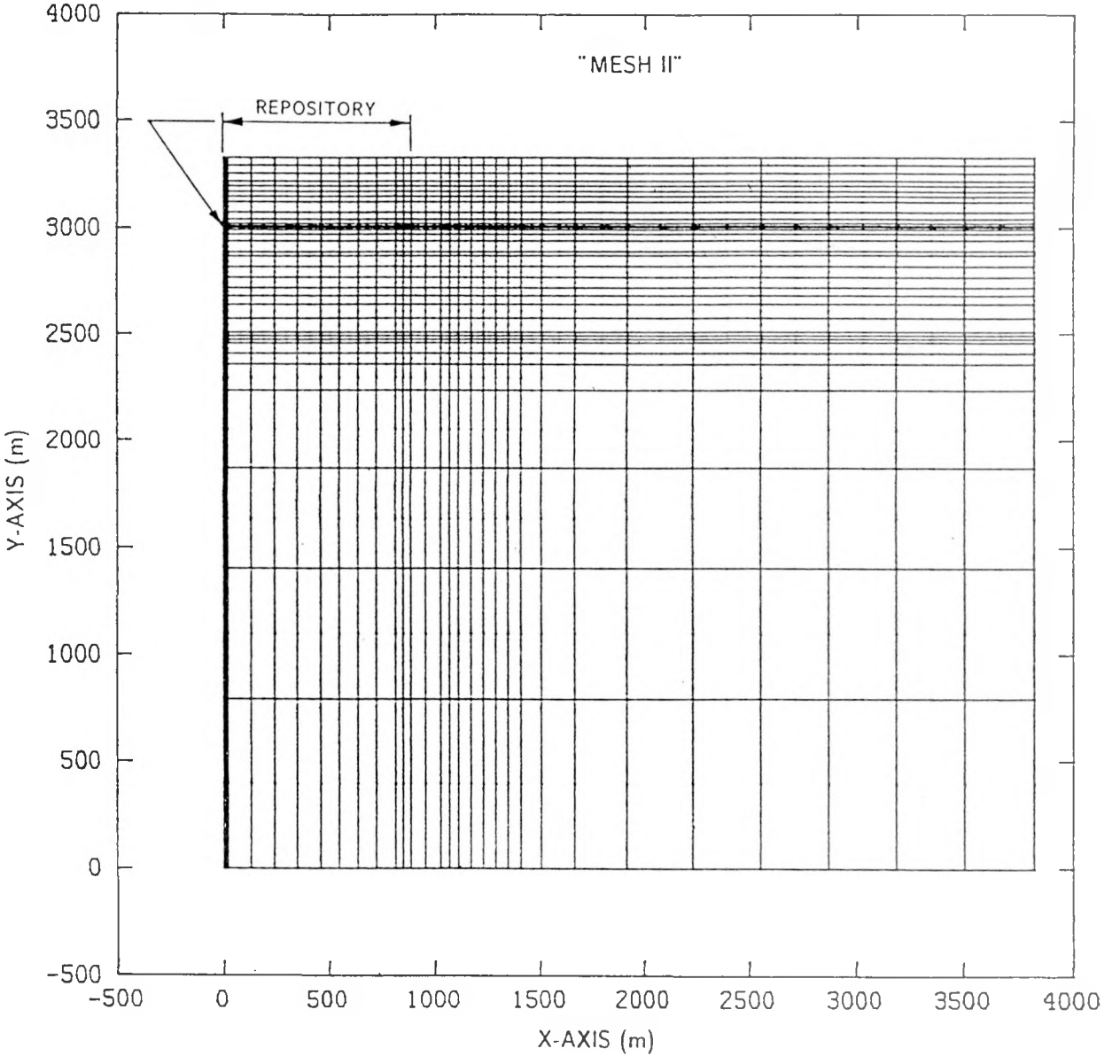

Figure A-2. Finite Element Mesh (Mesh II) of a Rectangular Far-Field Region.

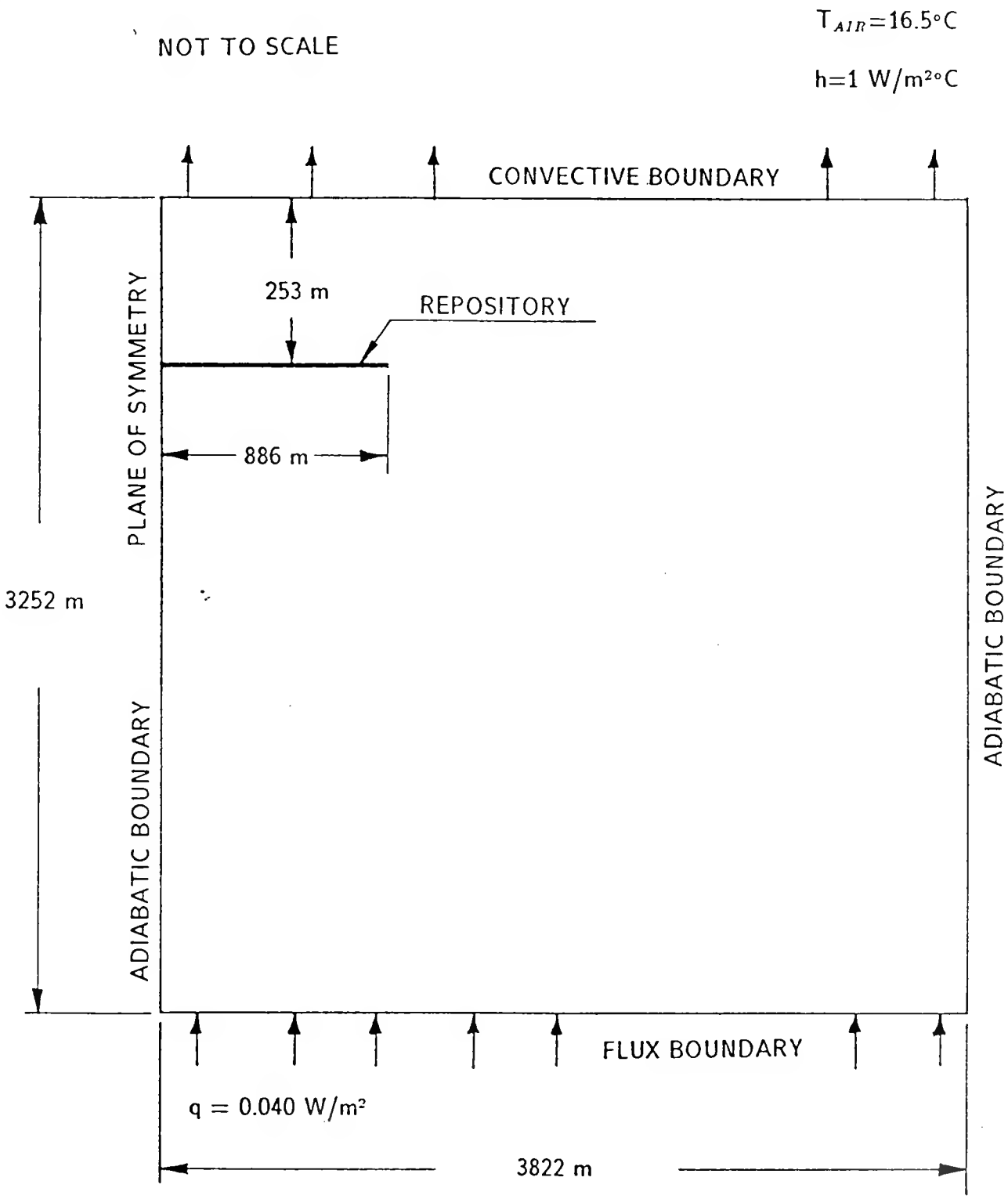

Figure A-3. Conceptualized Thermal Far-Field Model.

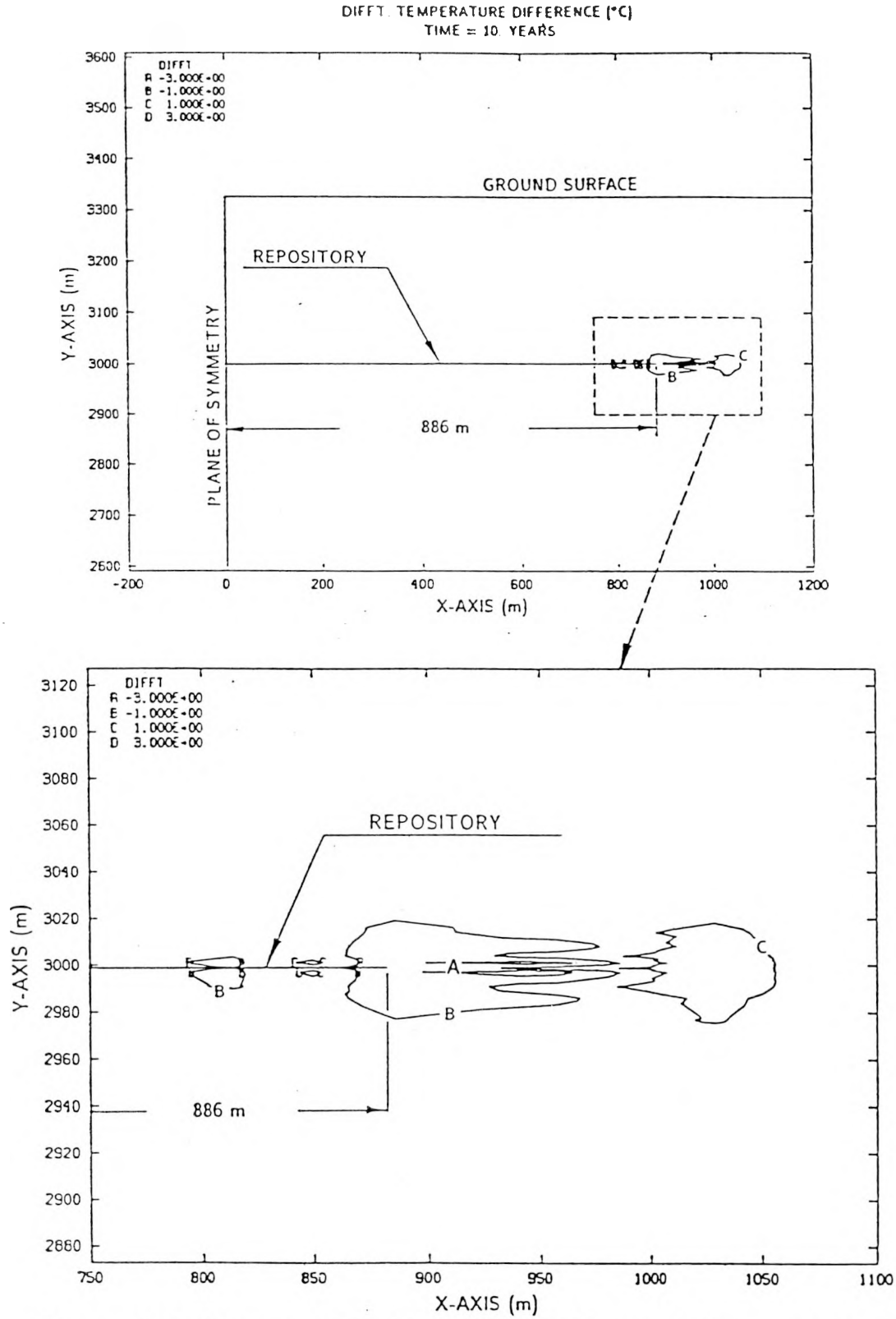

Figure A-4. Contours of the Temperature Difference (°C) Between Mesh I and Mesh II at 10 Yr. Negative Contours Indicate Mesh I "Underpredicts" Relative to Mesh II. Positive Contours Indicate the Opposite.

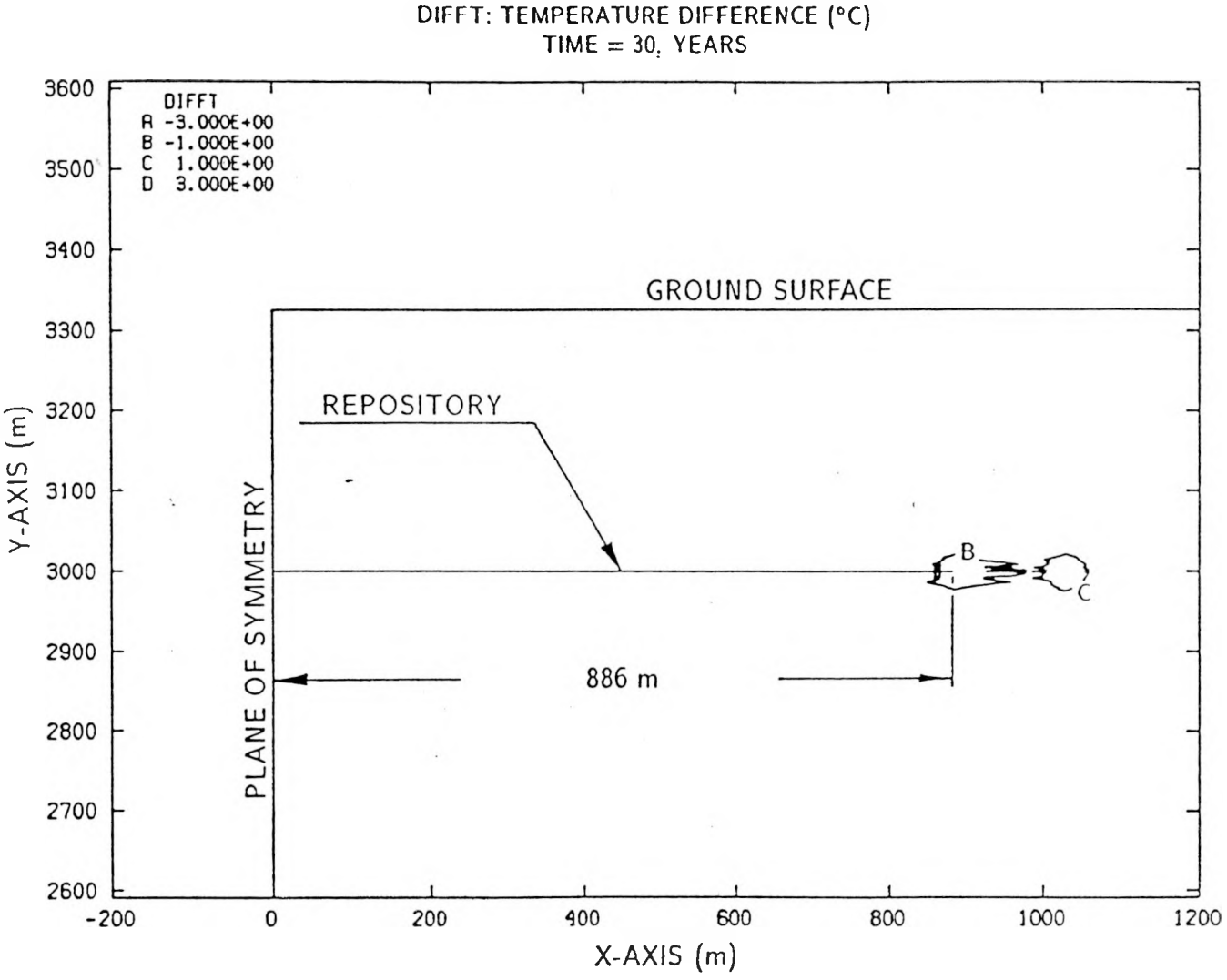

Figure A-5. Contours of the Temperature Difference (°C) Between Mesh I and Mesh II at 30 Yr. Negative Contours Indicate Mesh I "Underpredicts" Relative to Mesh II. Positive Contours Indicate the Opposite.

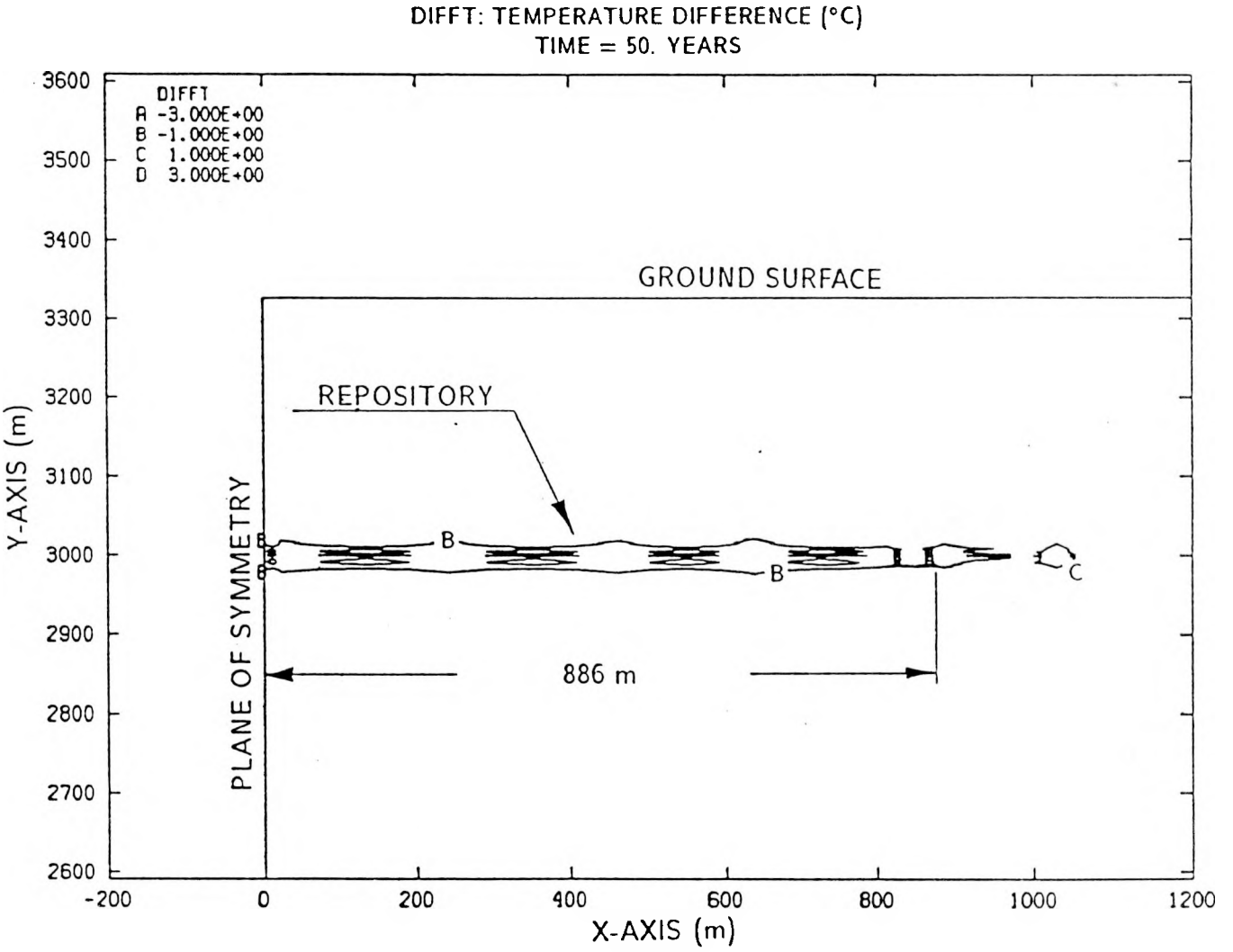

Figure A-6. Contours of the Temperature Difference (°C) Between Mesh I and Mesh II at 50 Yr. Negative Contours Indicate Mesh I "Underpredicts" Relative to Mesh II. Positive Contours Indicate the Opposite.

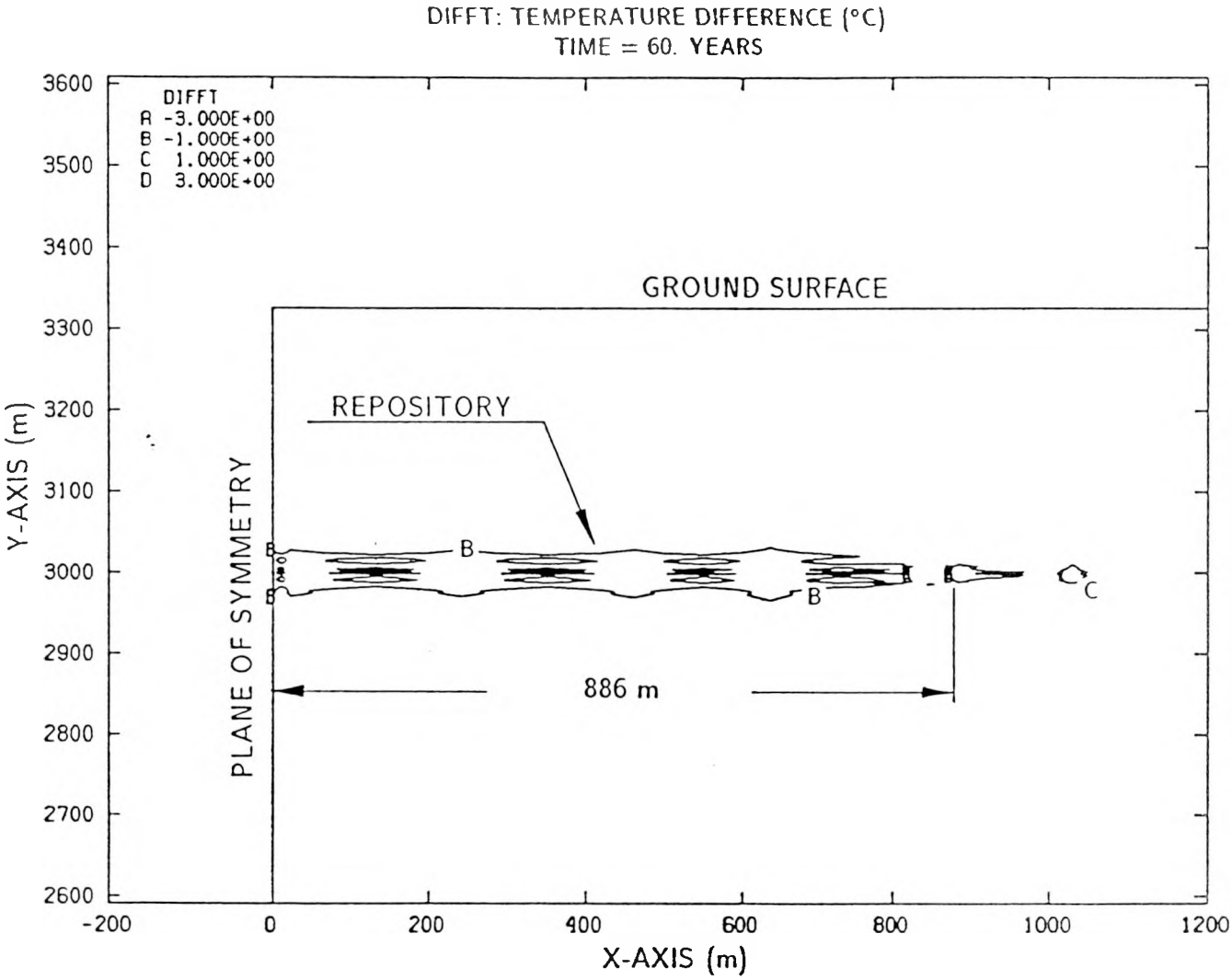

Figure A-7. Contours of the Temperature Difference (°C) Between Mesh I and Mesh II at 60 Yr. Negative Contours Indicate Mesh I "Underpredicts" Relative to Mesh II. Positive Contours Indicate the Opposite.

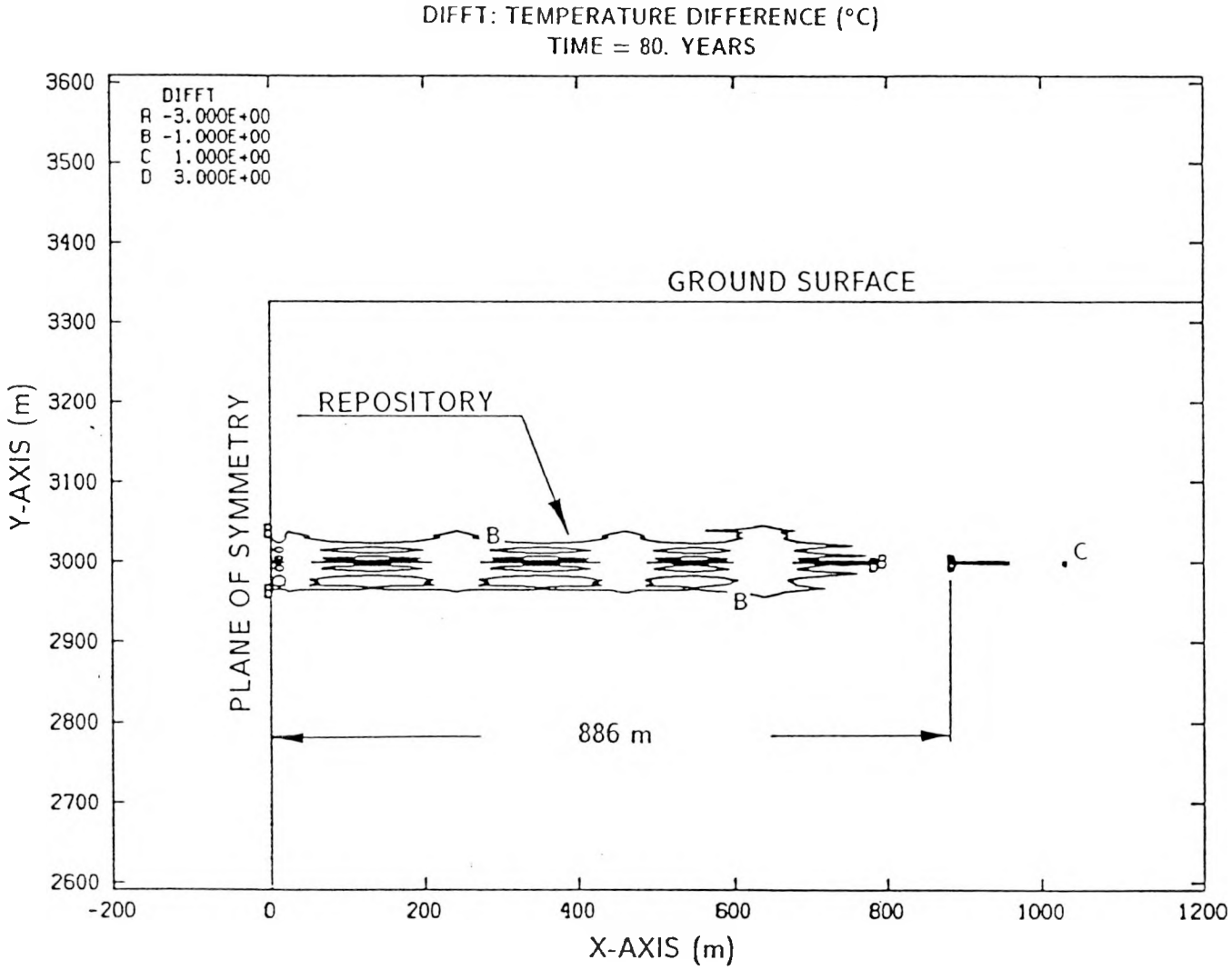

Figure A-8. Contours of the Temperature Difference (°C) Between Mesh I and Mesh II at 80 Yr. Negative Contours Indicate Mesh I "Underpredicts" Relative to Mesh II. Positive Contours Indicate the Opposite.

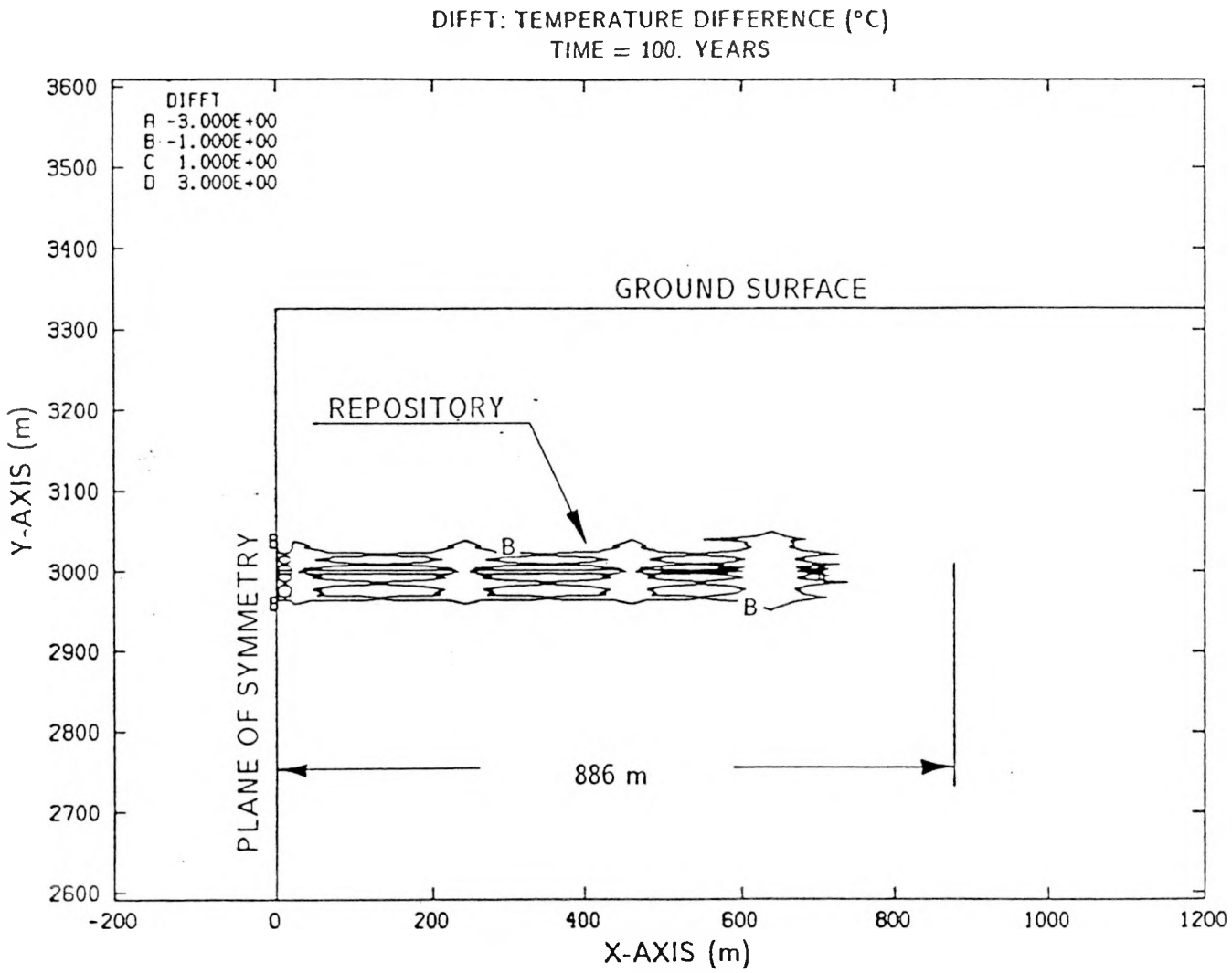

Figure A-9. Contours of the Temperature Difference (°C) Between Mesh I and Mesh II at 100 Yr. Negative Contours Indicate Mesh I "Underpredicts" Relative to Mesh II. Positive Contours Indicate the Opposite.

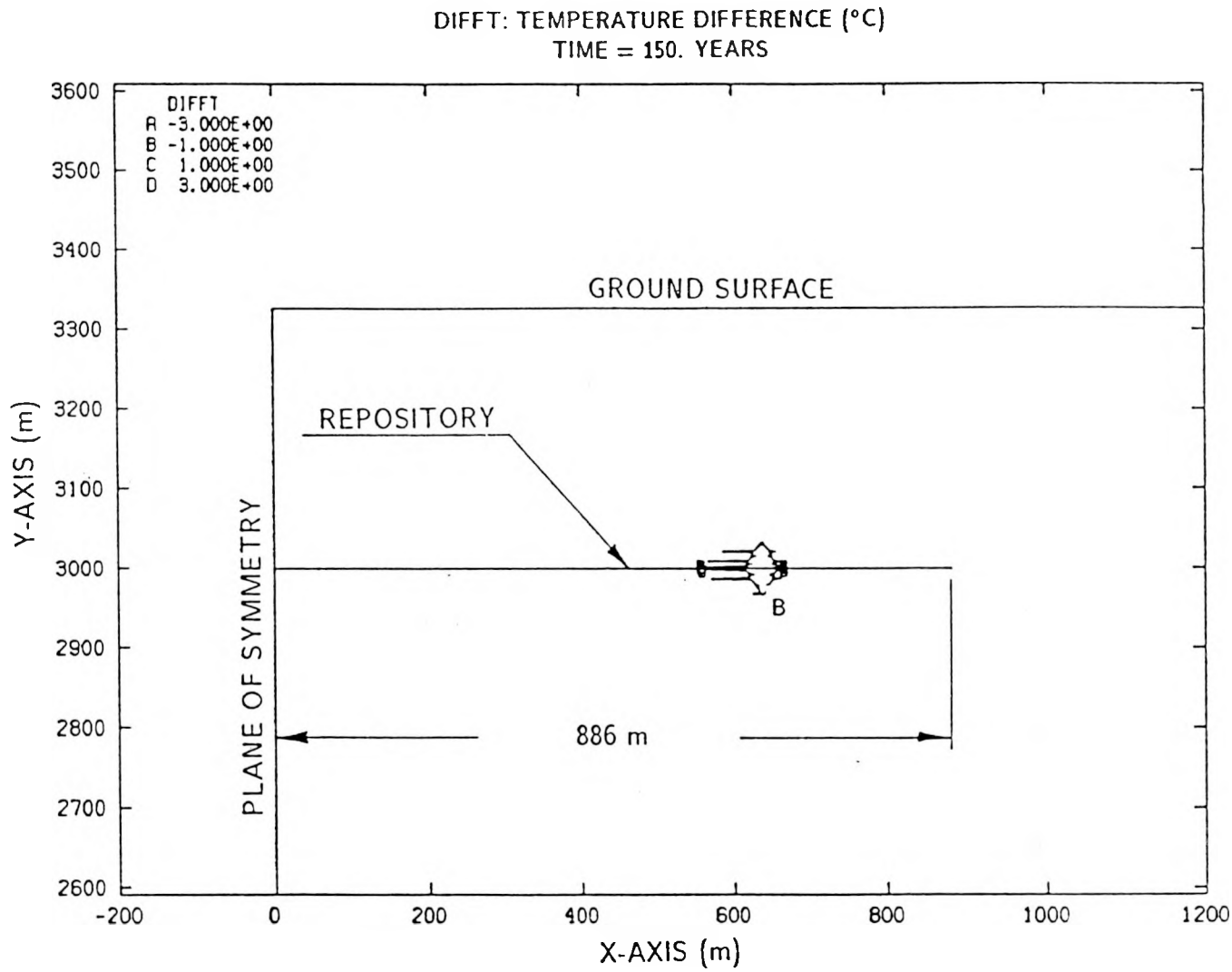

Figure A-10. Contours of the Temperature Difference (°C) Between Mesh I and Mesh II at 150 Yr. Negative Contours Indicate Mesh I "Underpredicts" Relative to Mesh II. Positive Contours Indicate the Opposite.

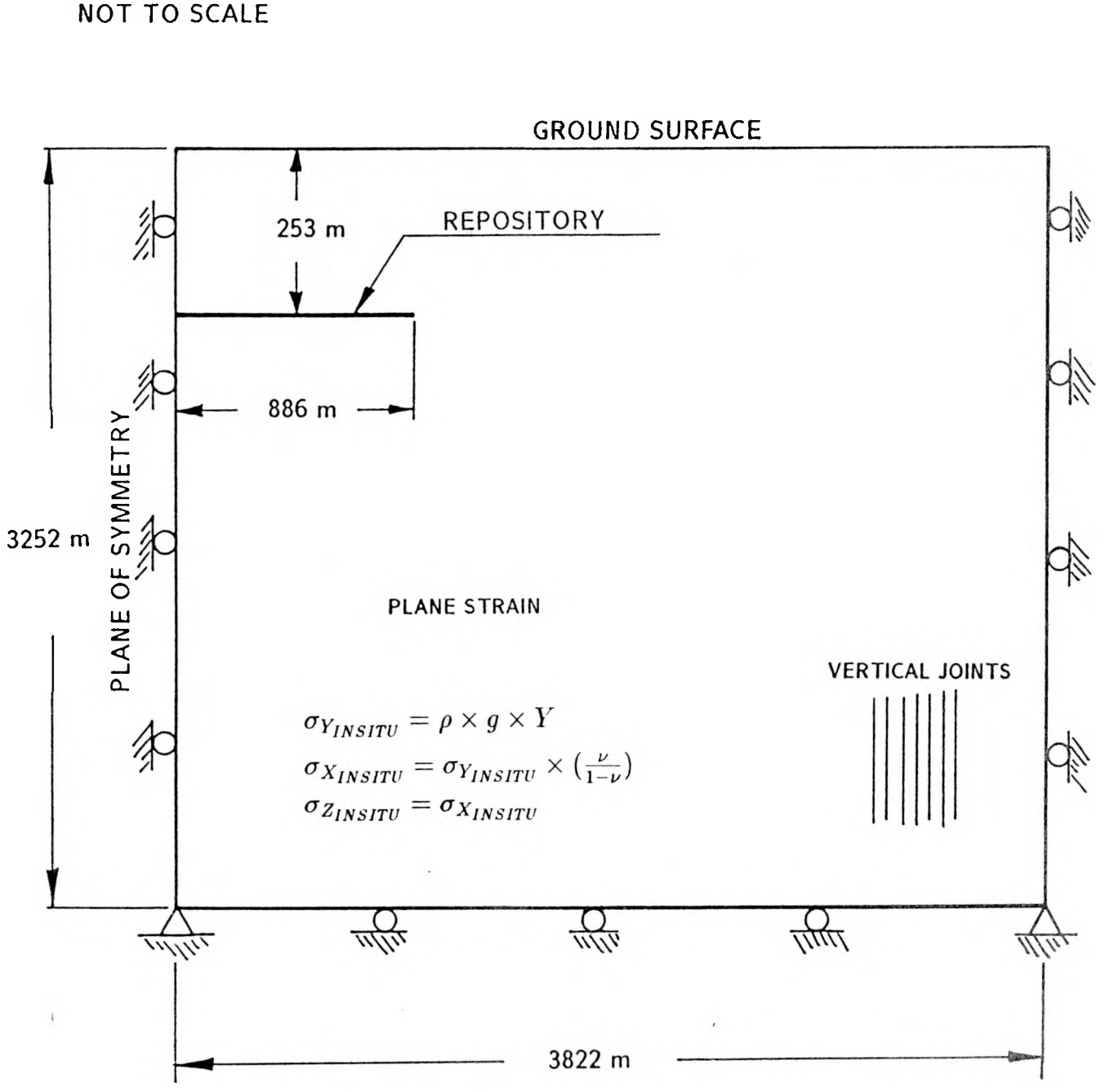

Figure A-11. Conceptualized Mechanical Far-Field Model.

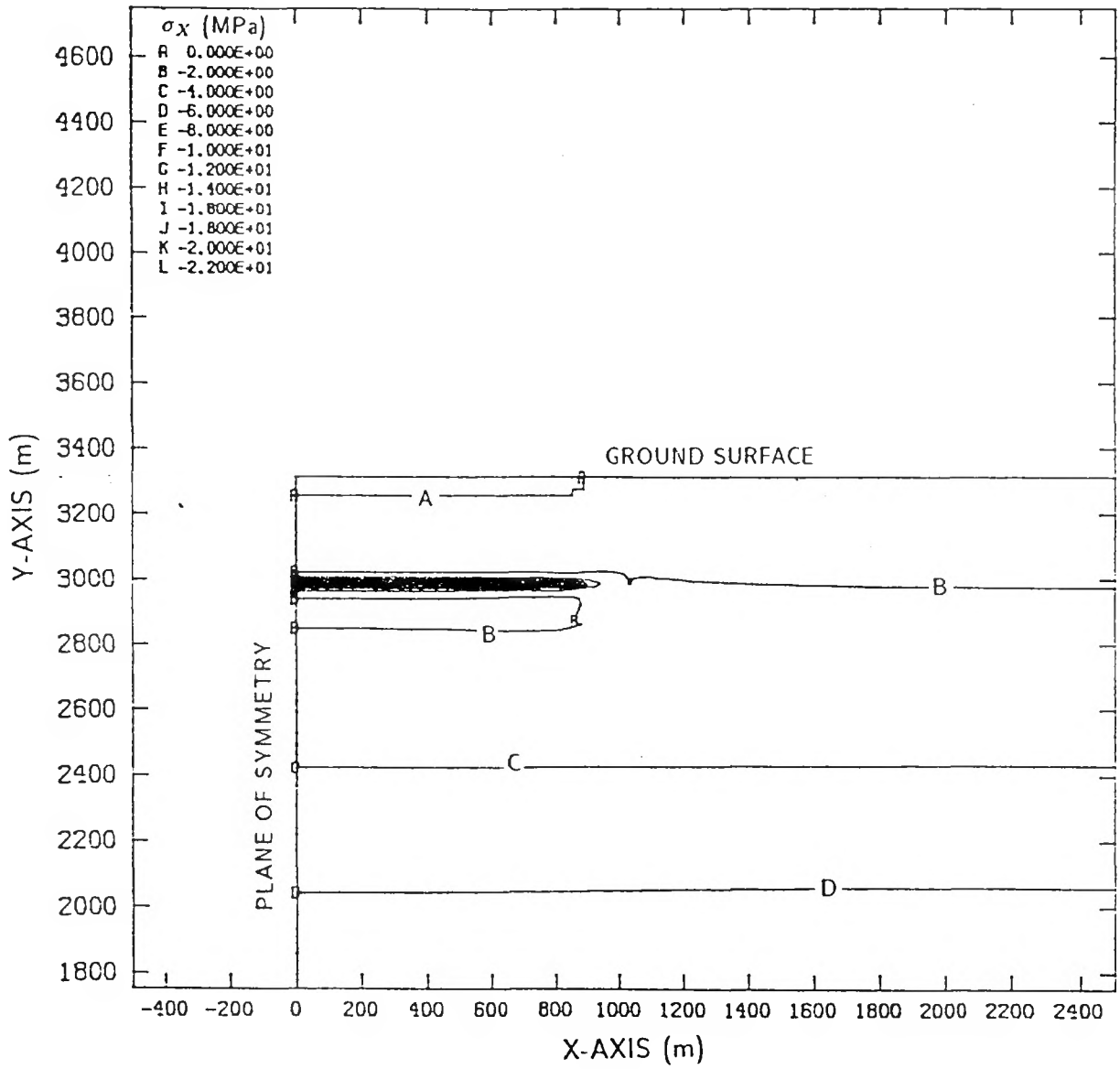

Figure A-12. Contours of Predicted Horizontal Stress (MPa) at 10 Yr Using Mesh I.

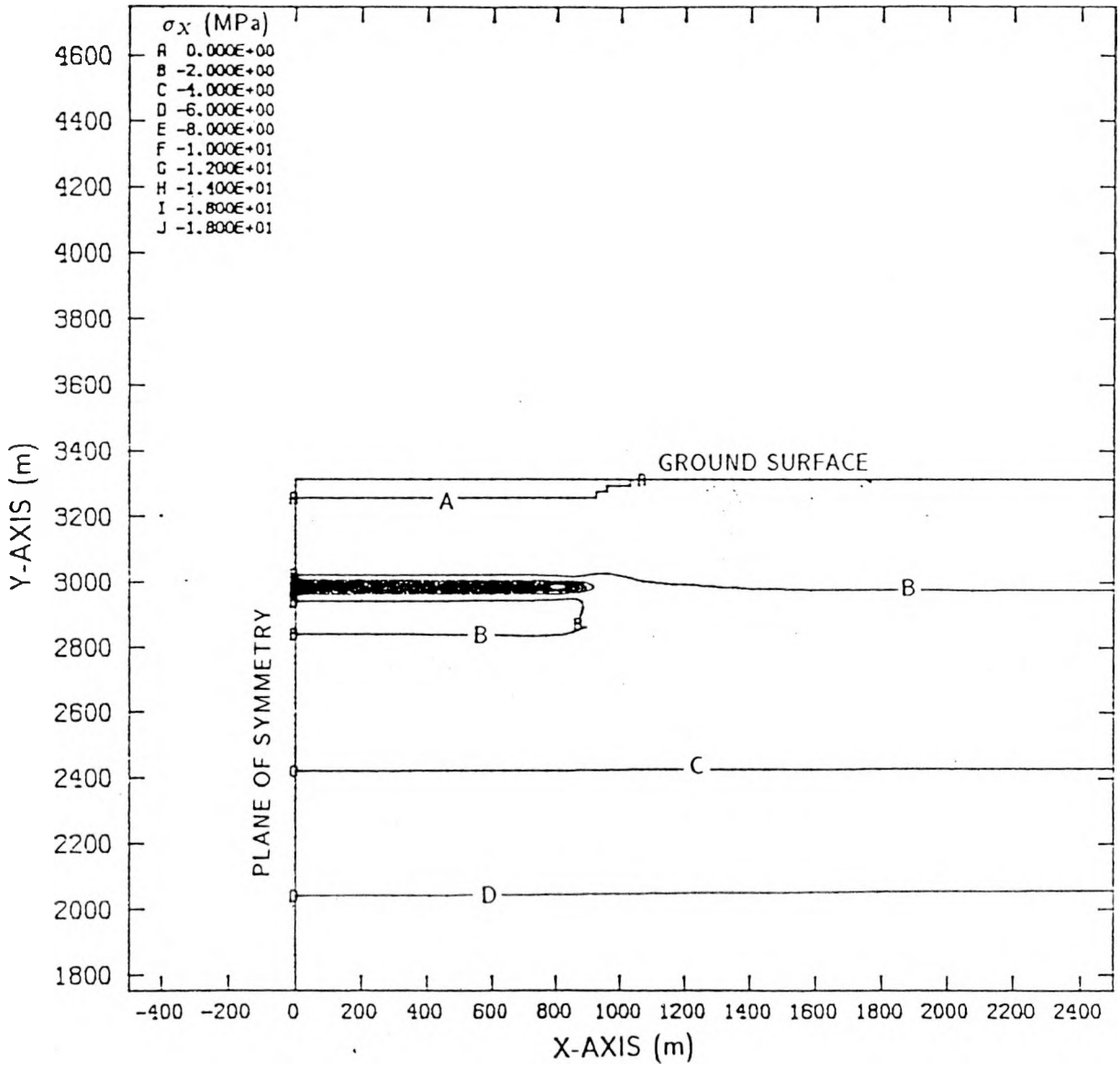

Figure A-13. Contours of Predicted Horizontal Stress (MPa) at 10 Yr Using Mesh II.

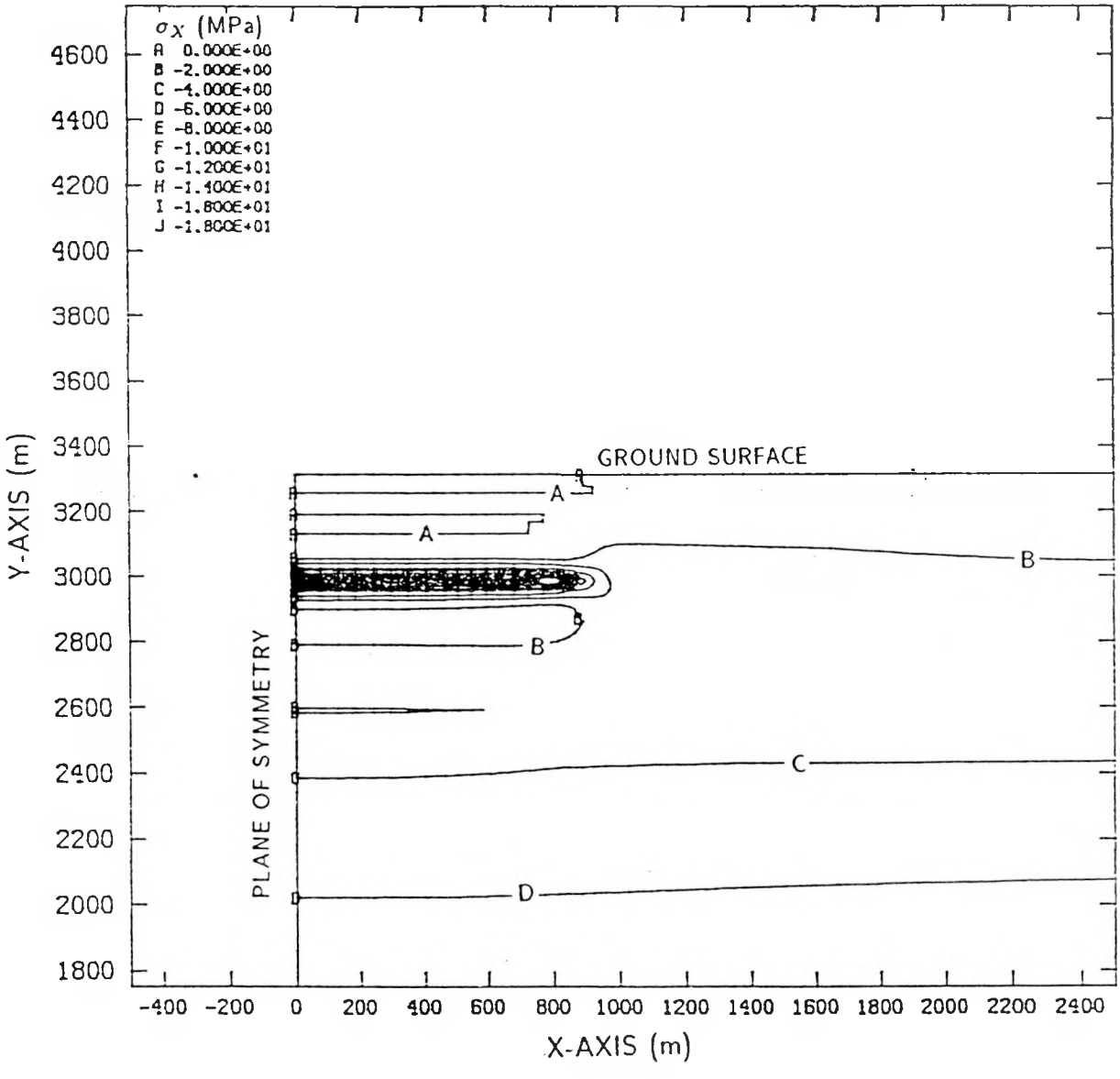

Figure A-14. Contours of Predicted Horizontal Stress (MPa) at 50 Yr Using Mesh I.

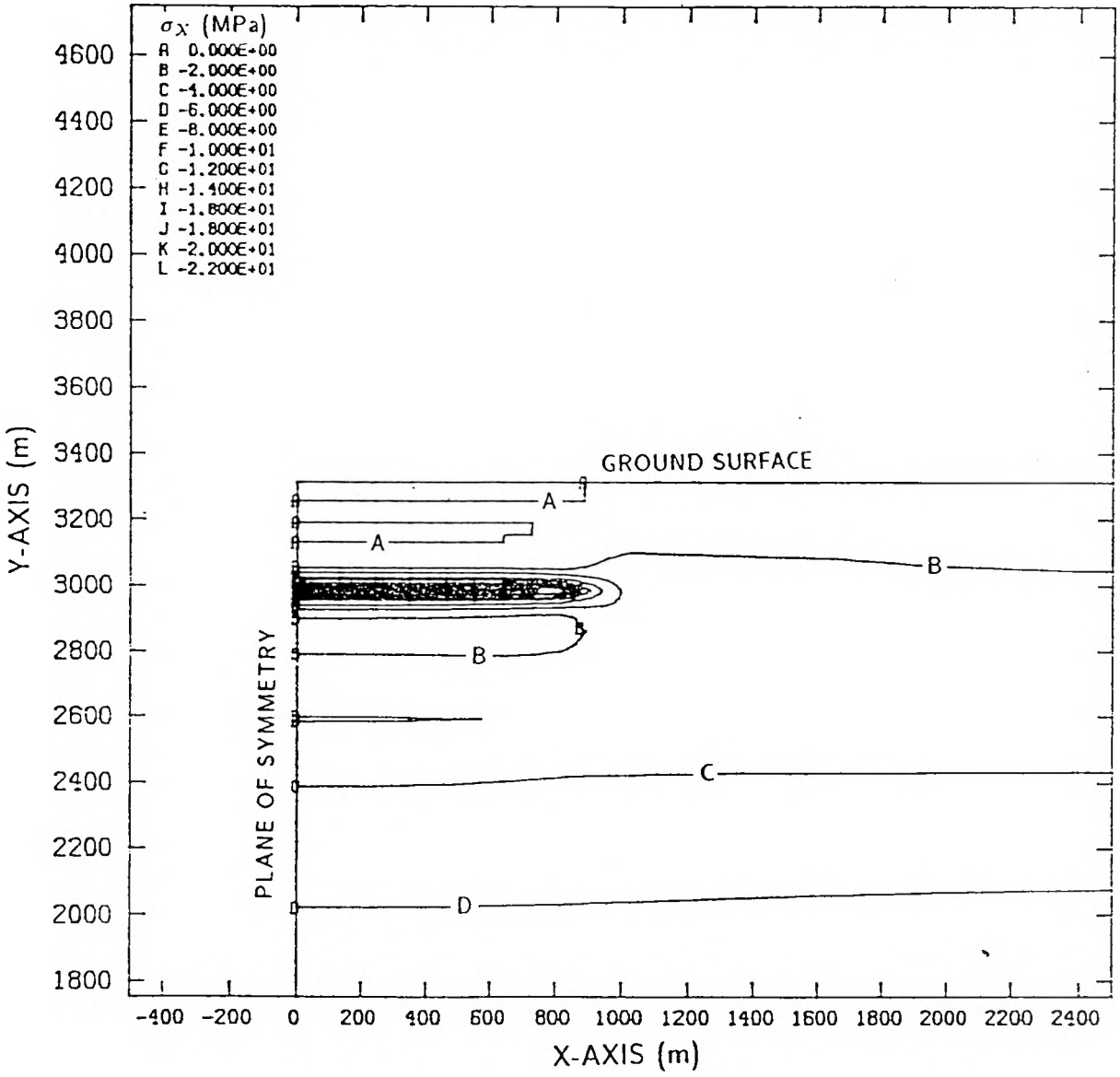

Figure A-15. Contours of Predicted Horizontal Stress (MPa) at 50 Yr Using Mesh II.

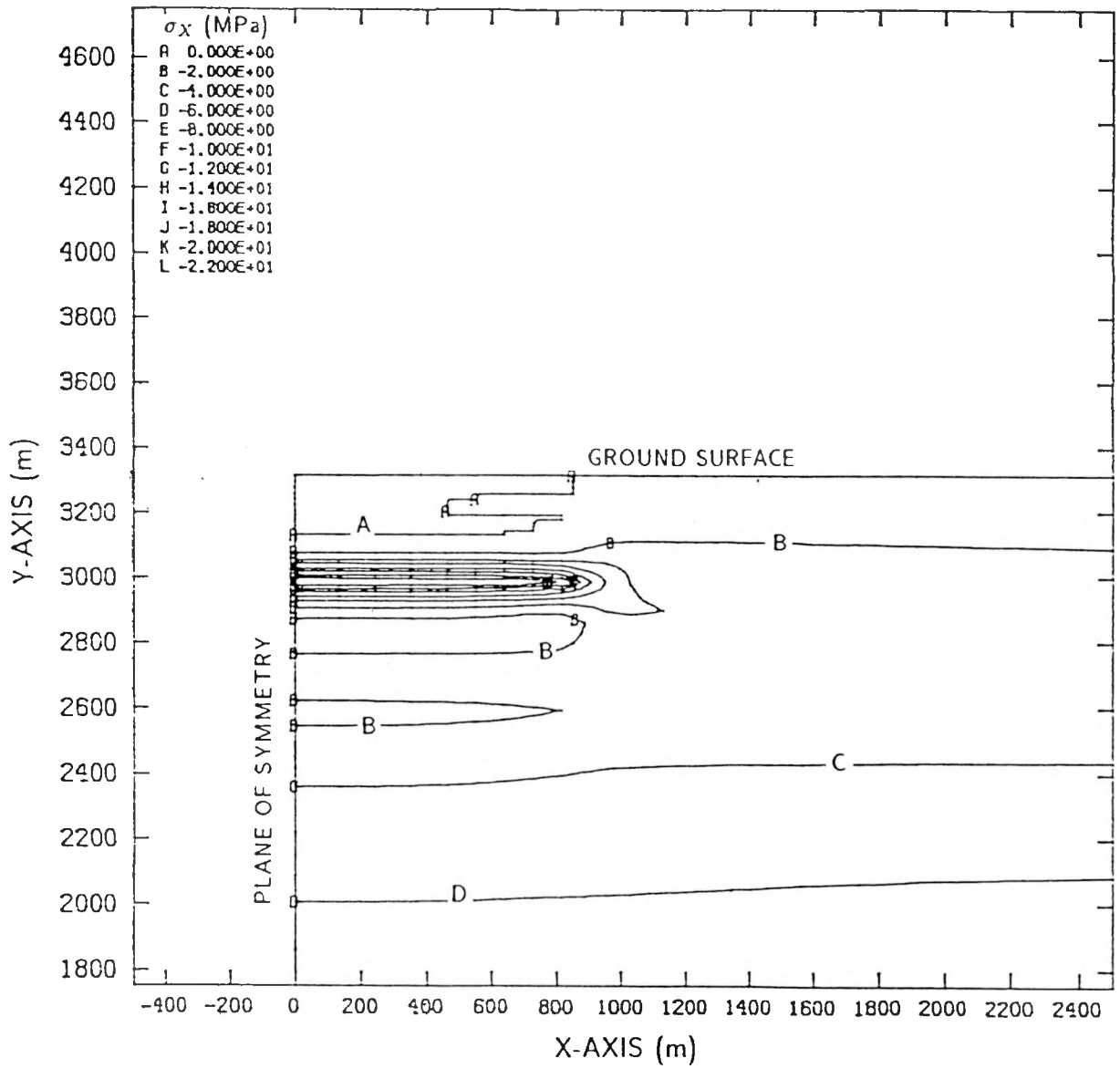

Figure A-16. Contours of Predicted Horizontal Stress (MPa) at 100 Yr Using Mesh I.

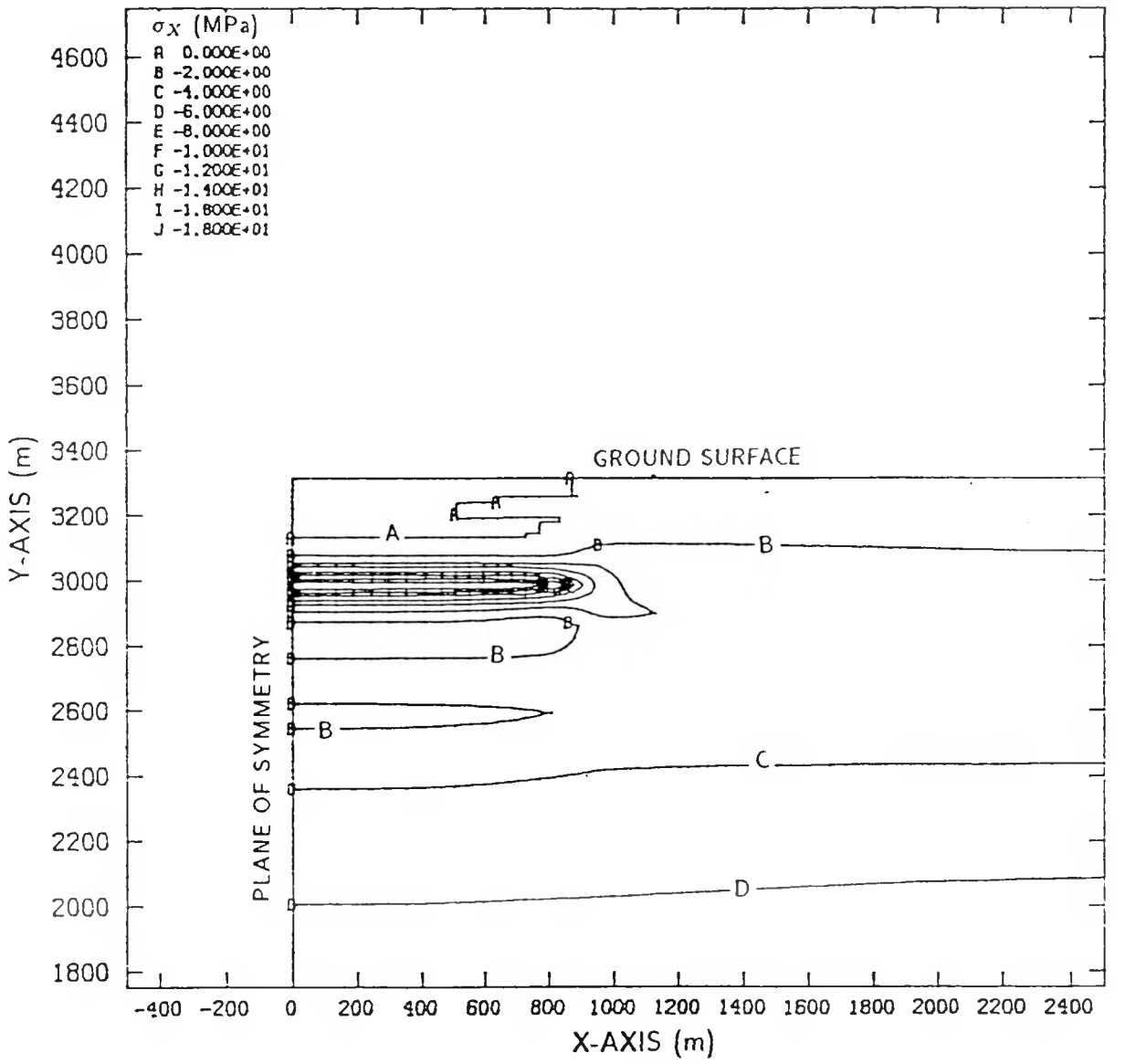

Figure A-17. Contours of Predicted Horizontal Stress (MPa) at 100 Yr Using Mesh II.

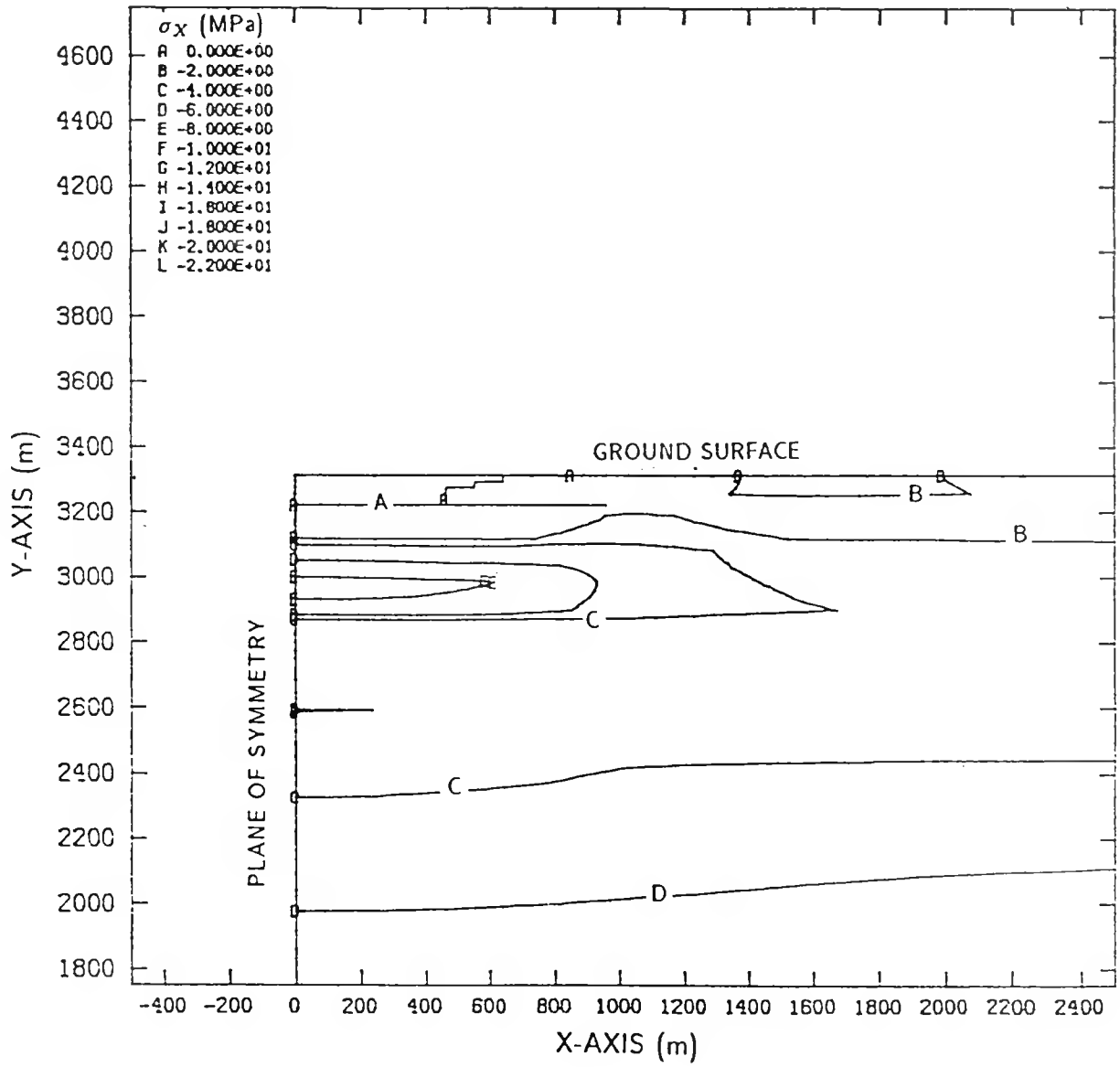

Figure A-18. Contours of Predicted Horizontal Stress (MPa) at 2,000 Yr Using Mesh I.

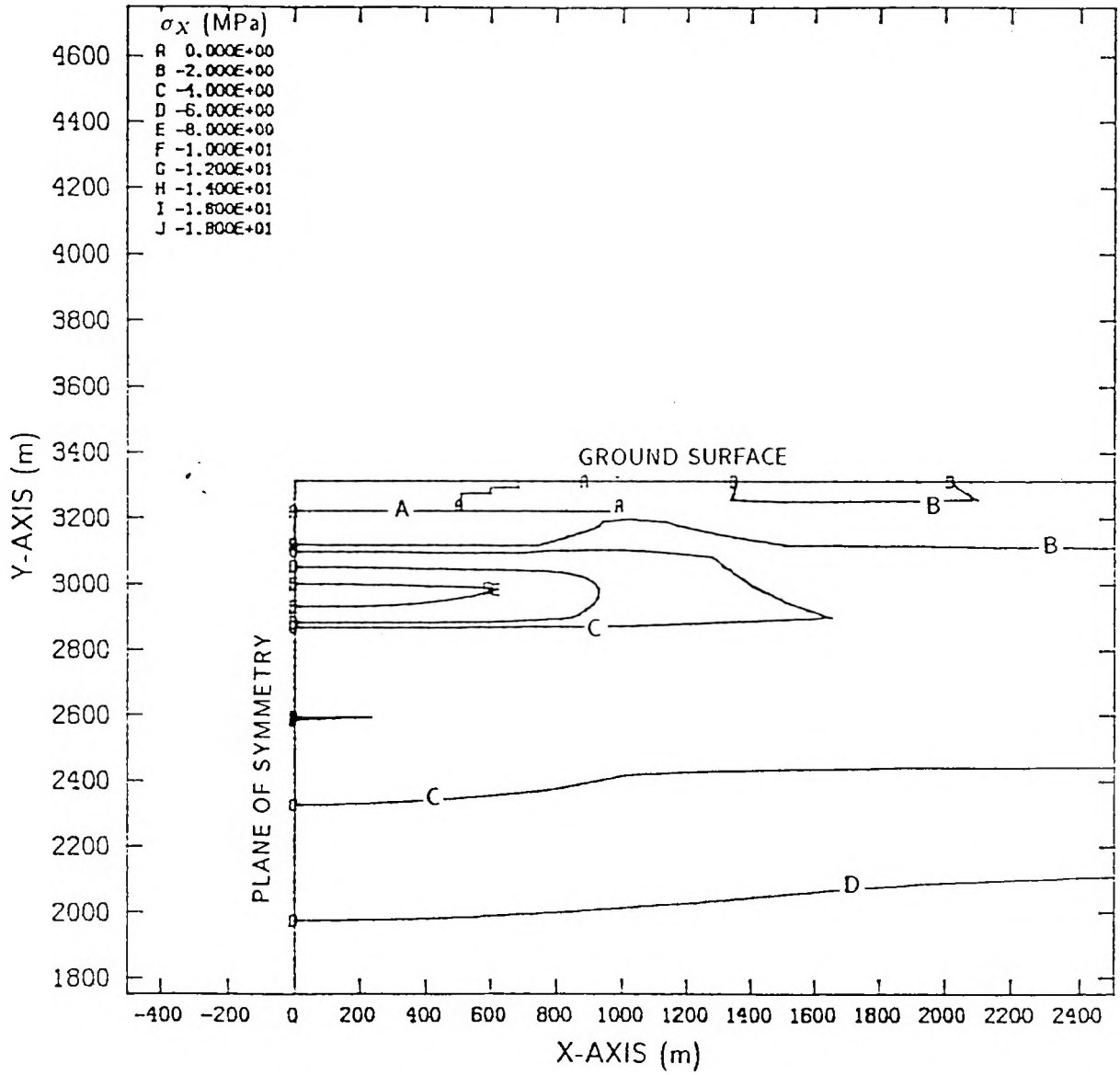

Figure A-19. Contours of Predicted Horizontal Stress (MPa) at 2,000 Yr Using Mesh II.

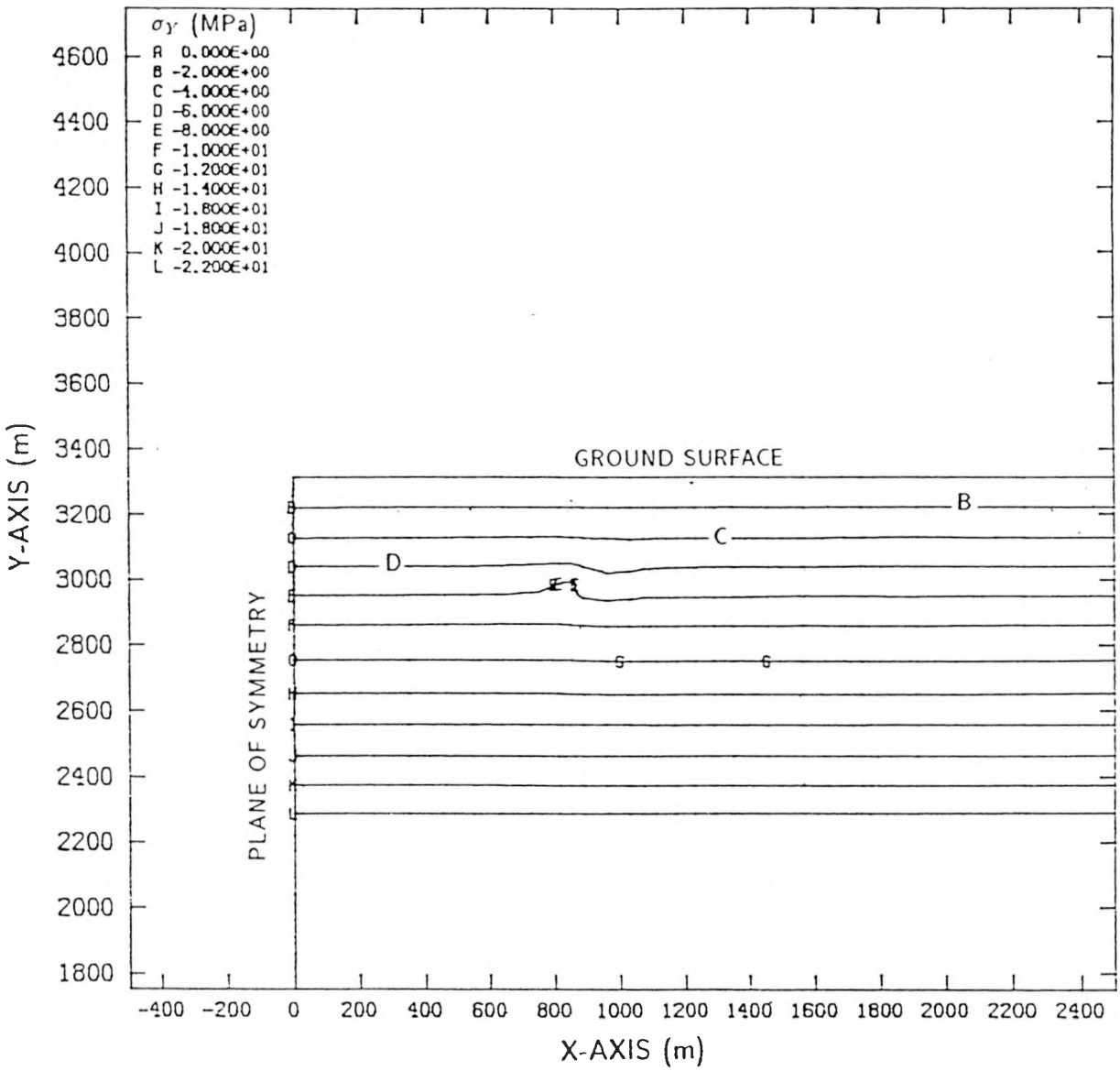

Figure A-20. Contours of Predicted Vertical Stress (MPa) at 10 Yr Using Mesh I.

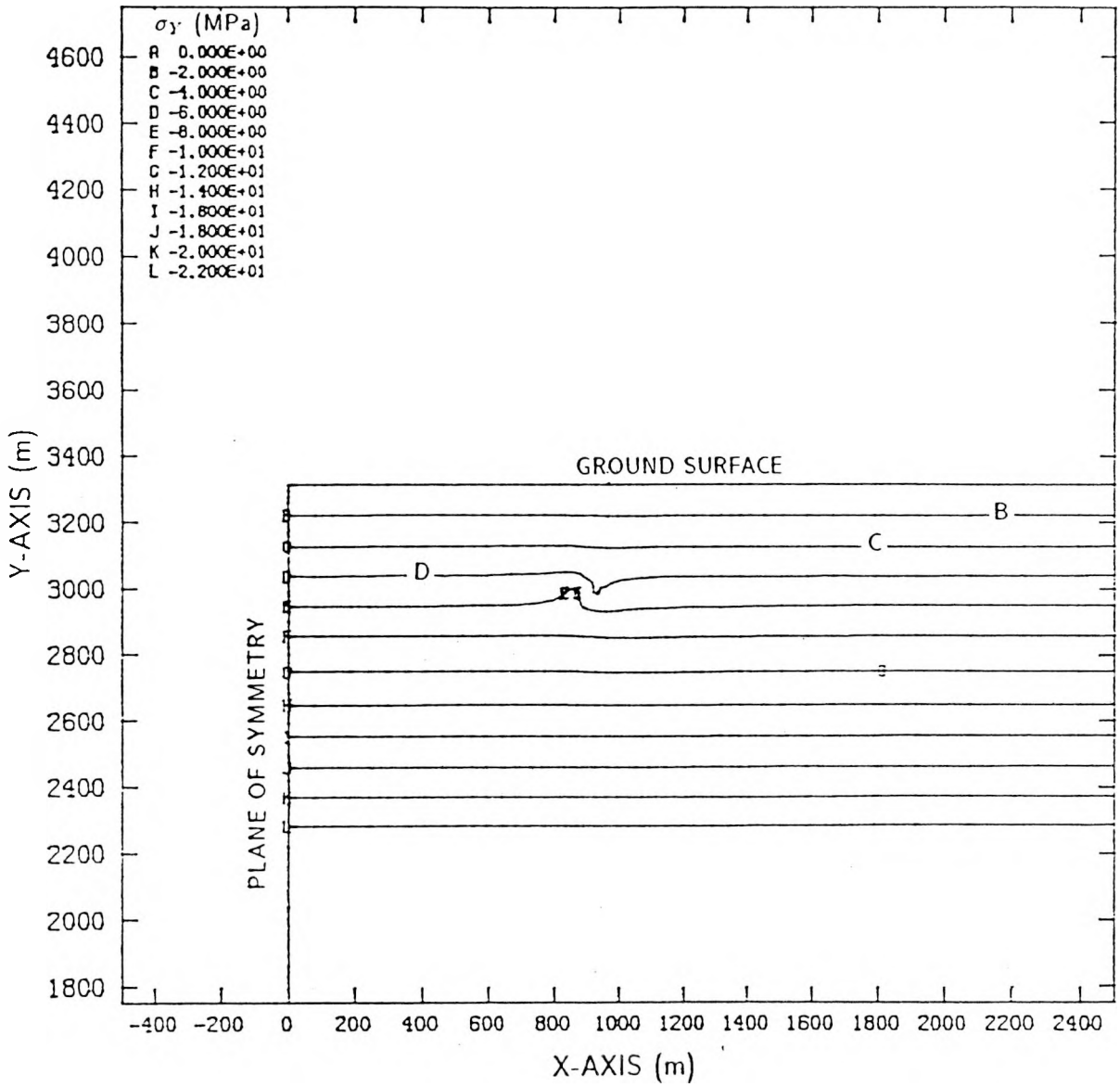

Figure A-21. Contours of Predicted Vertical Stress (MPa) at 10 Yr Using Mesh II.

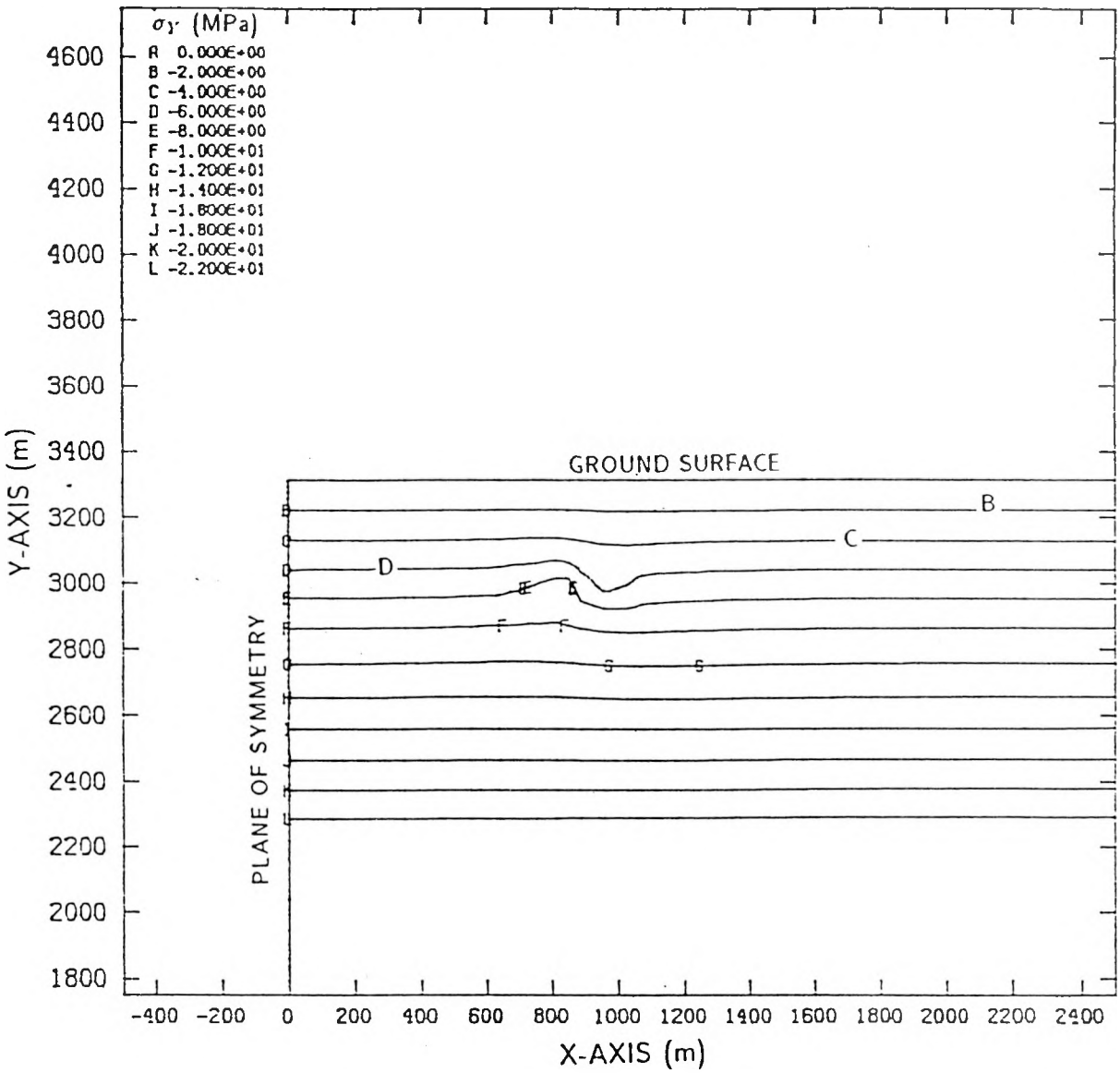

Figure A-22. Contours of Predicted Vertical Stress (MPa) at 50 Yr Using Mesh I.

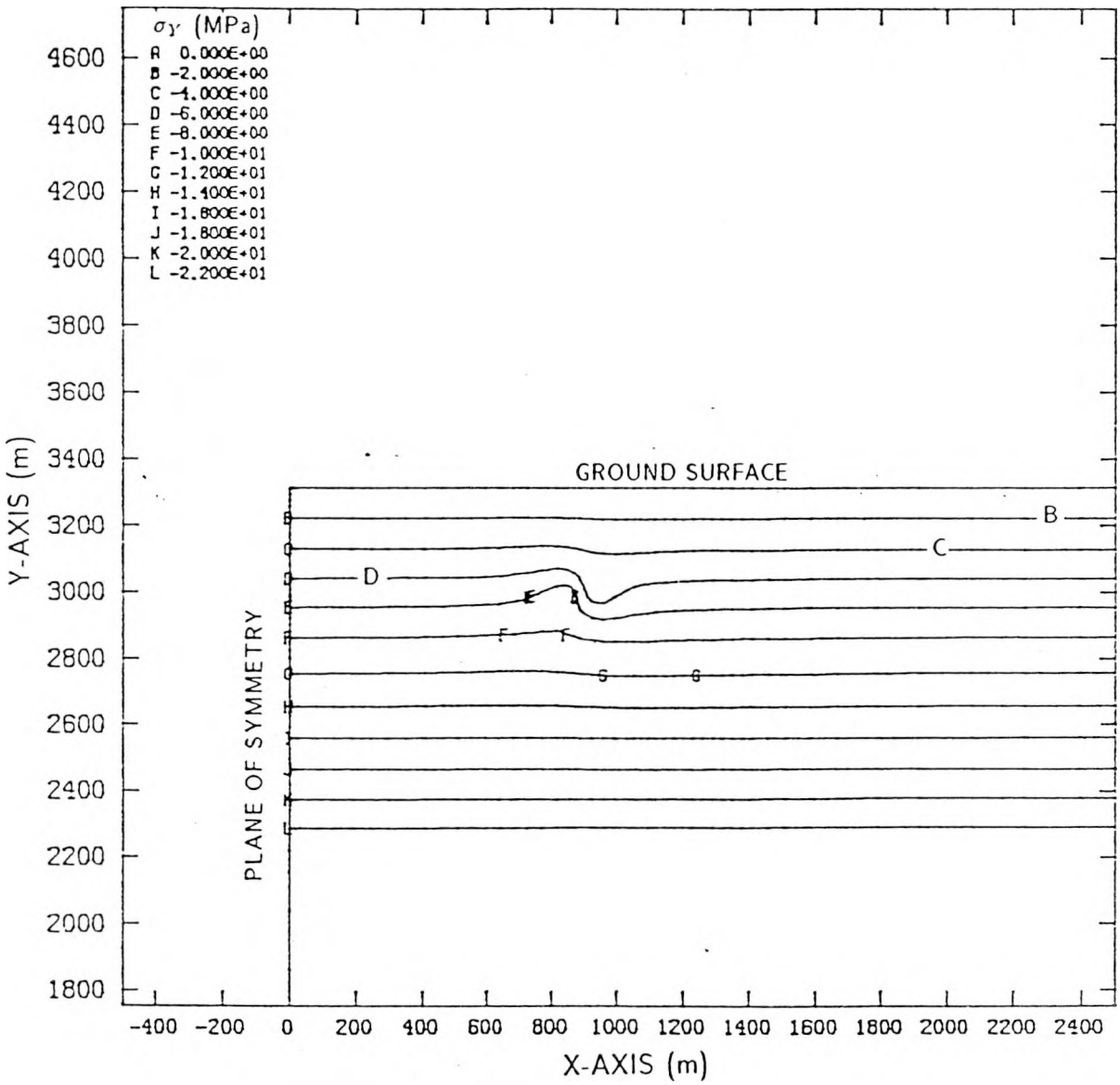

Figure A-23. Contours of Predicted Vertical Stress (MPa) at 50 Yr Using Mesh II.

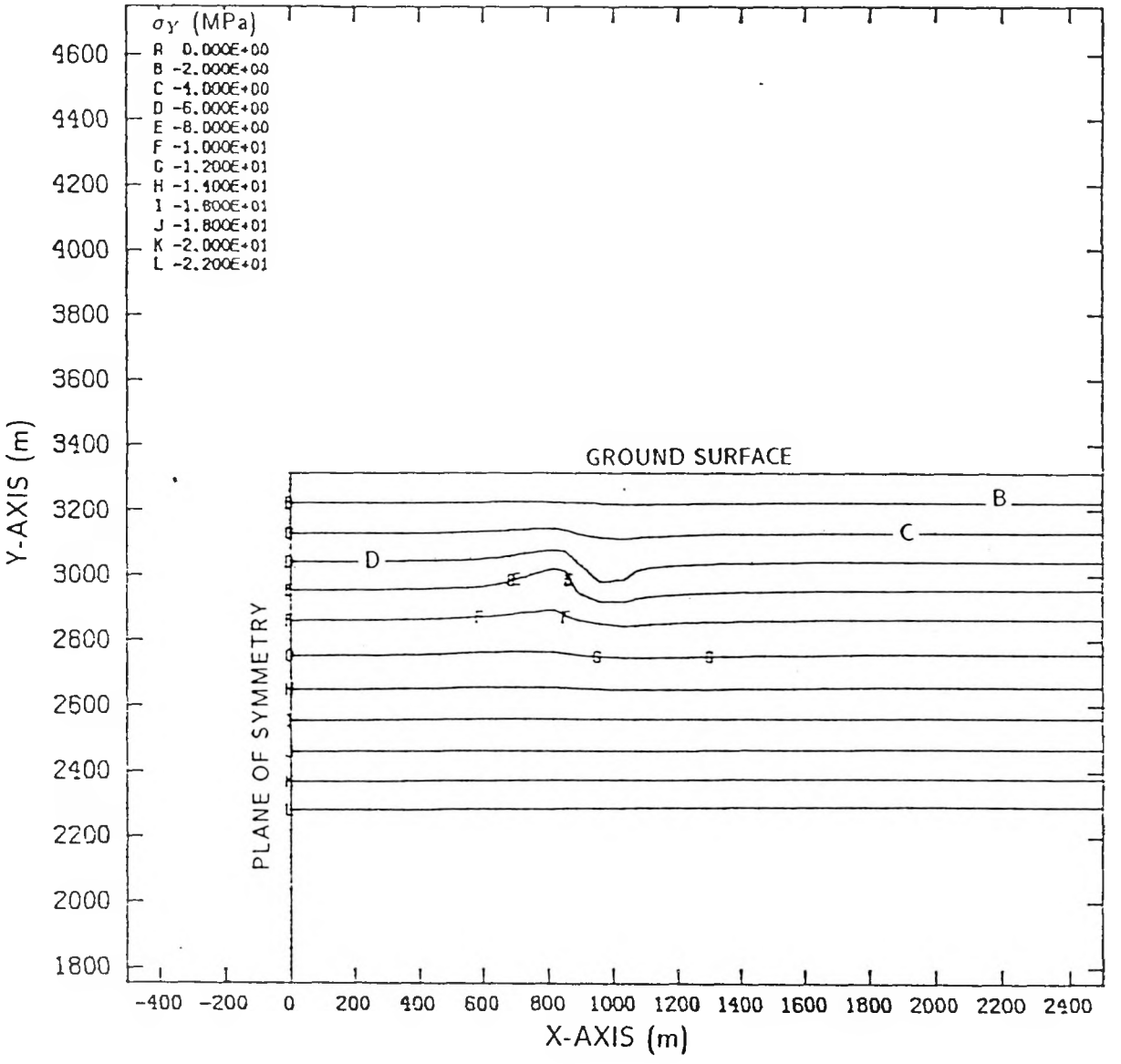

Figure A-24. Contours of Predicted Vertical Stress (MPa) at 100 Yr Using Mesh I.

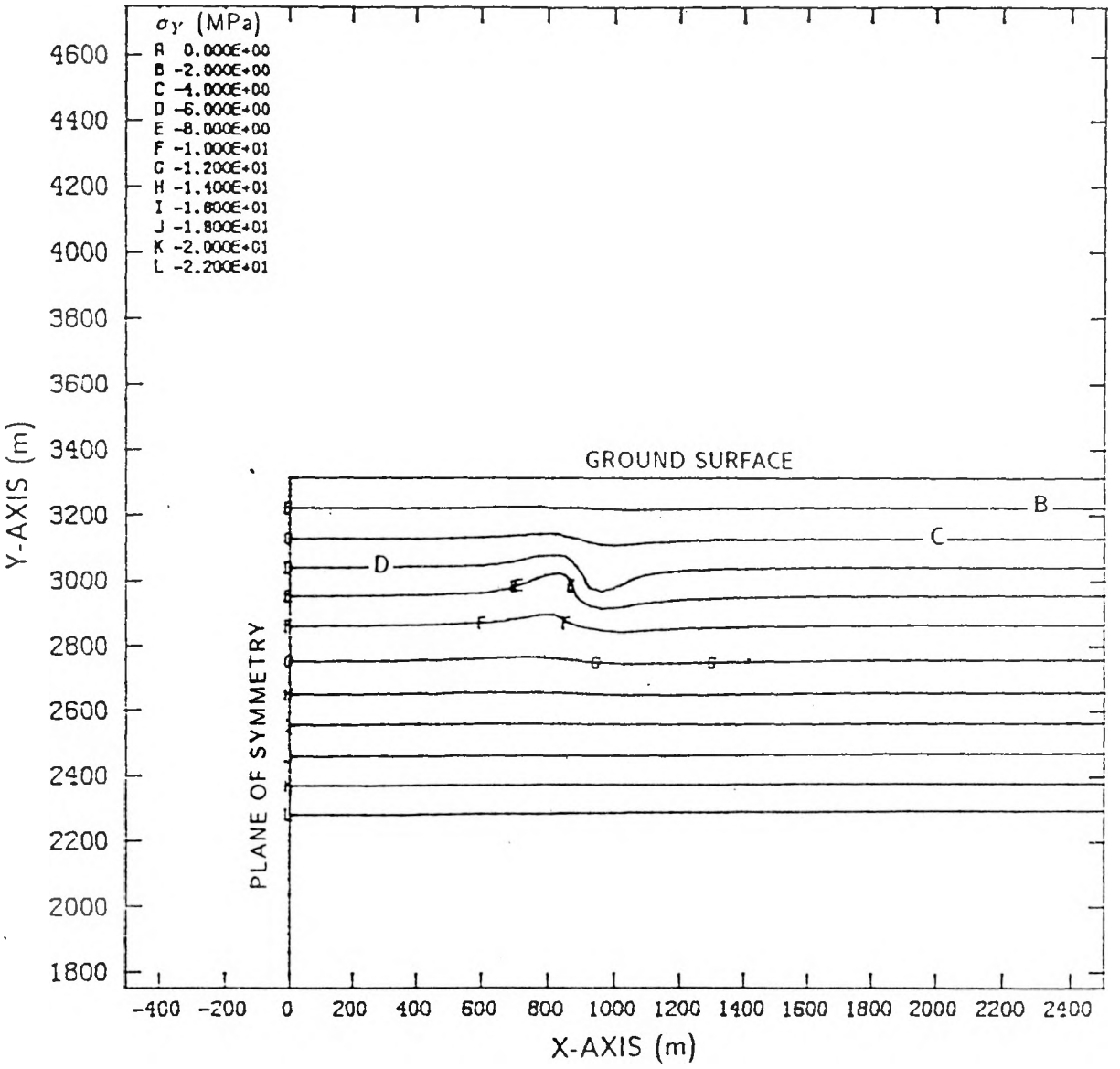

Figure A-25. Contours of Predicted Vertical Stress (MPa) at 100 Yr Using Mesh II.

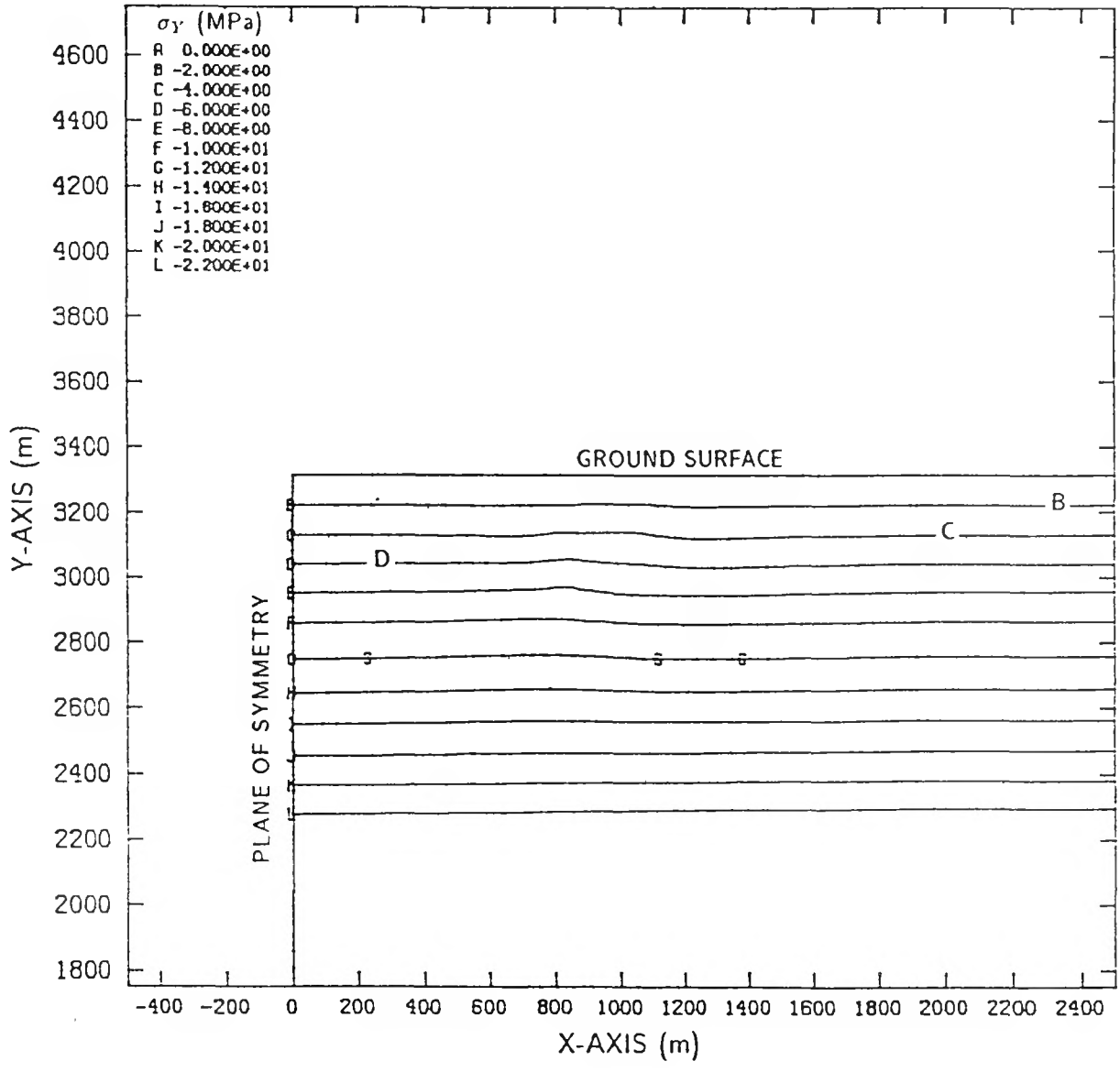

Figure A-26. Contours of Predicted Vertical Stress (MPa) at 2,000 Yr Using Mesh I.

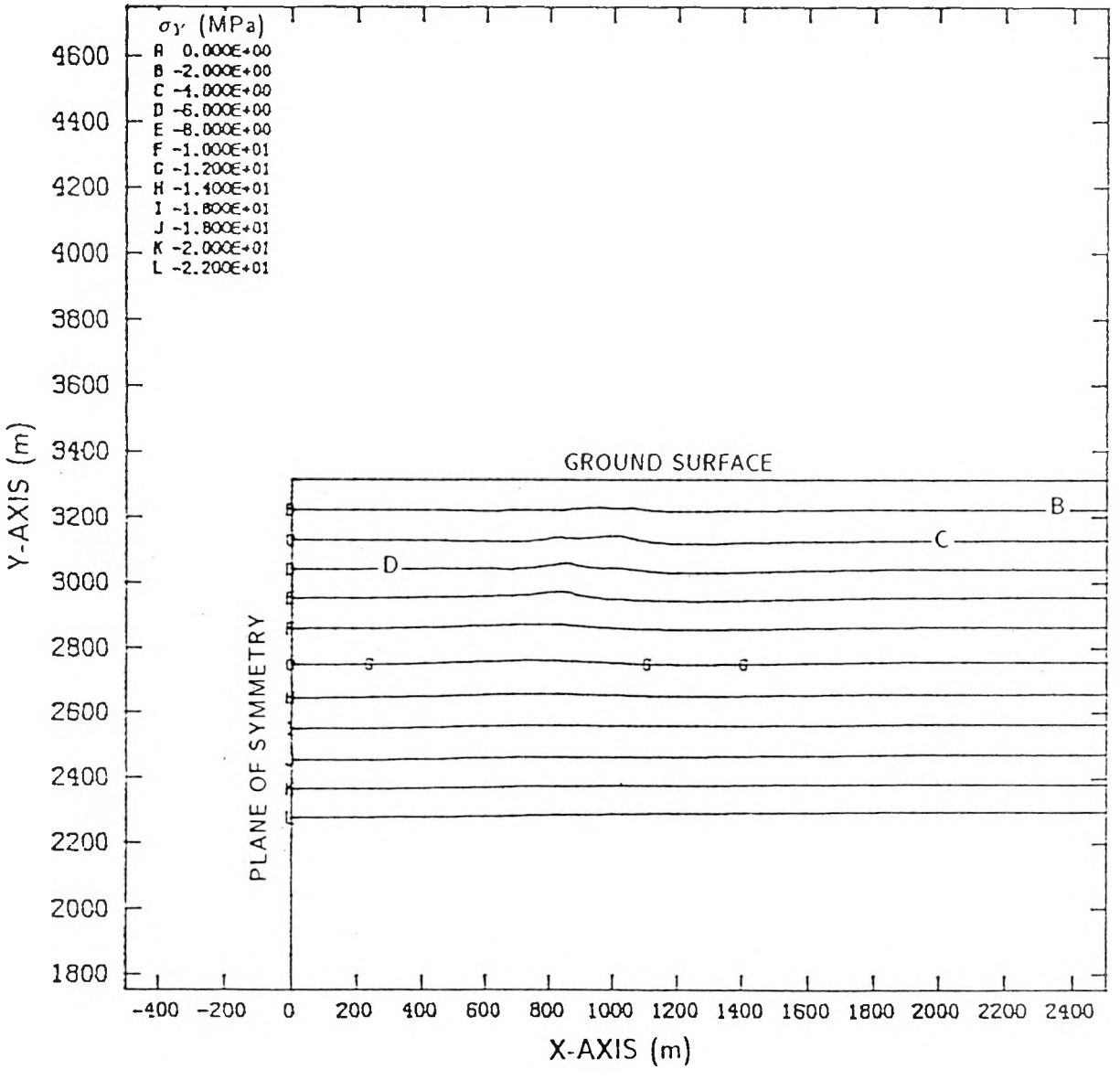

Figure A-27. Contours of Predicted Vertical Stress (MPa) at 2,000 Yr Using Mesh II.

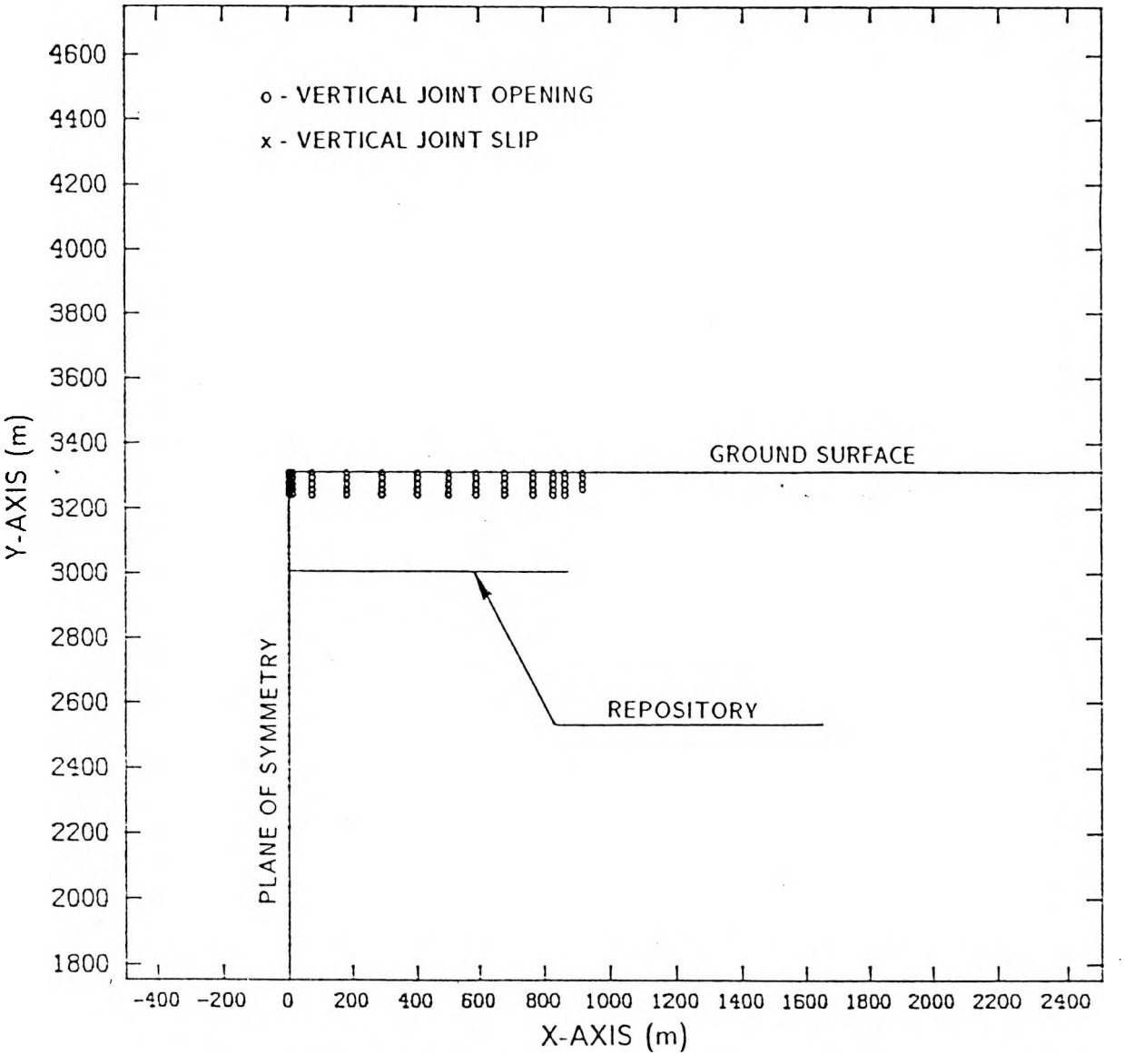

Figure A-28. Predicted Joint Activity at 10 Yr Using Mesh I.

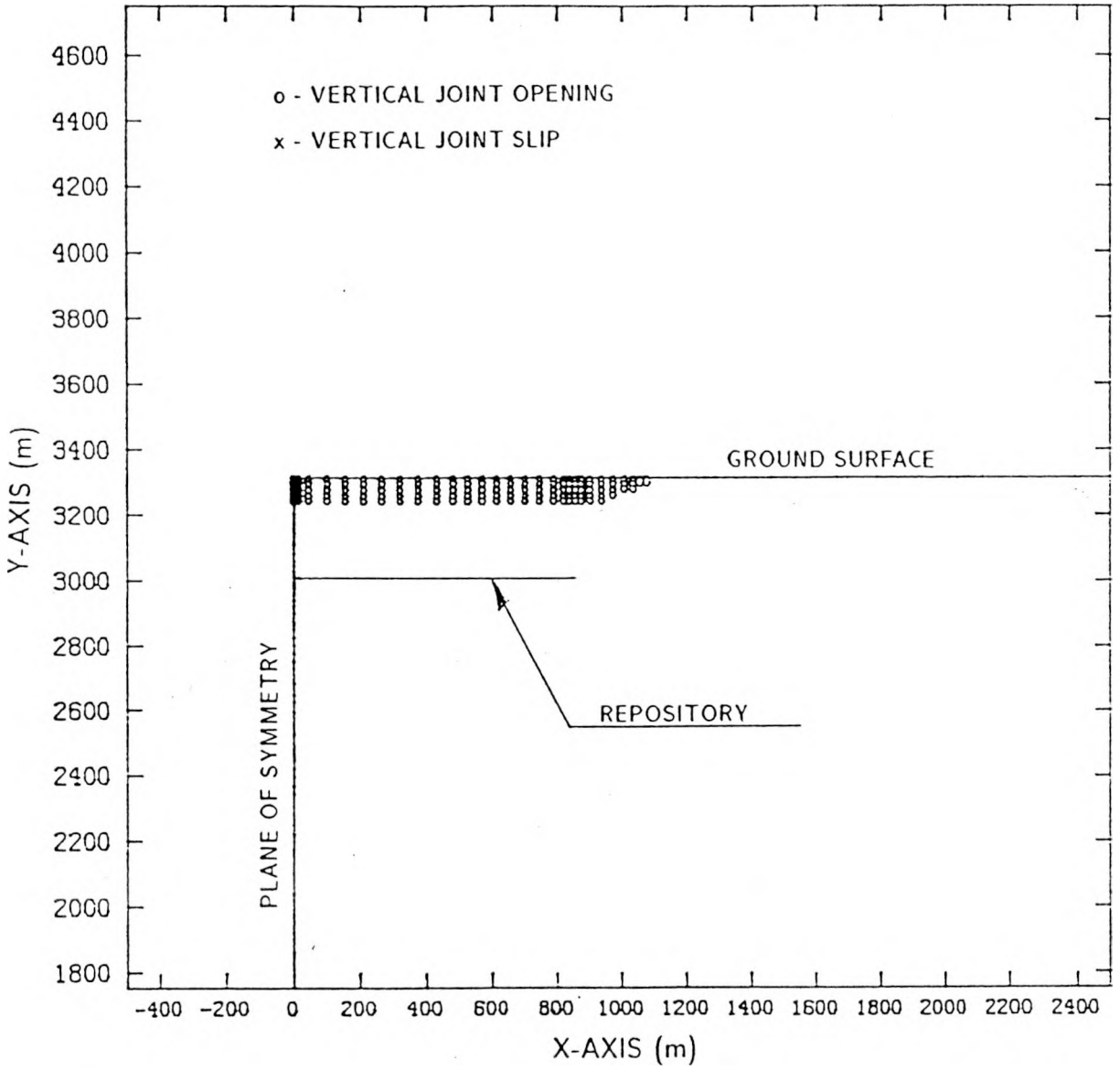

Figure A-29. Predicted Joint Activity at 10 Yr Using Mesh II.

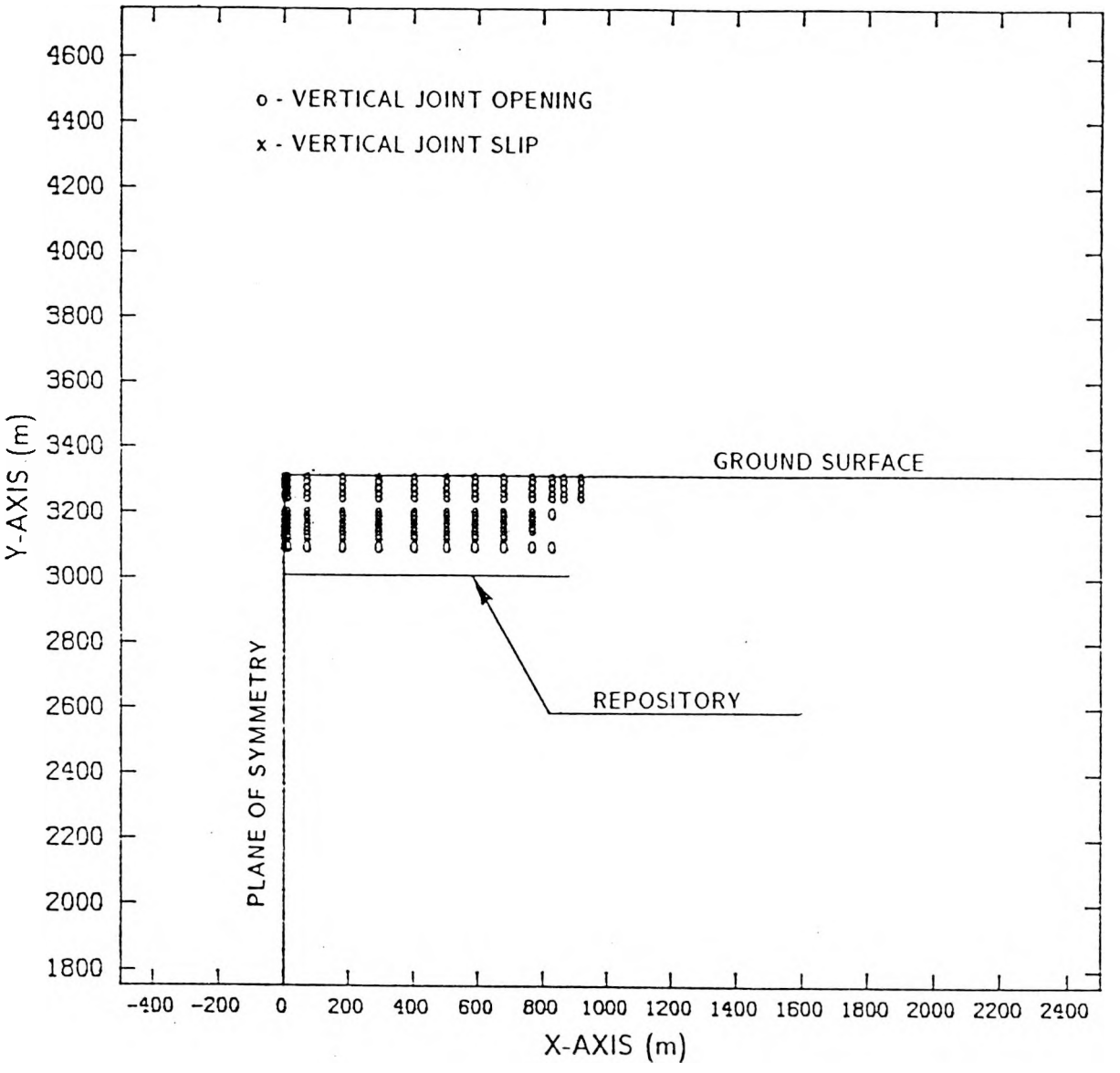

Figure A-30. Predicted Joint Activity at 50 Yr Using Mesh I.

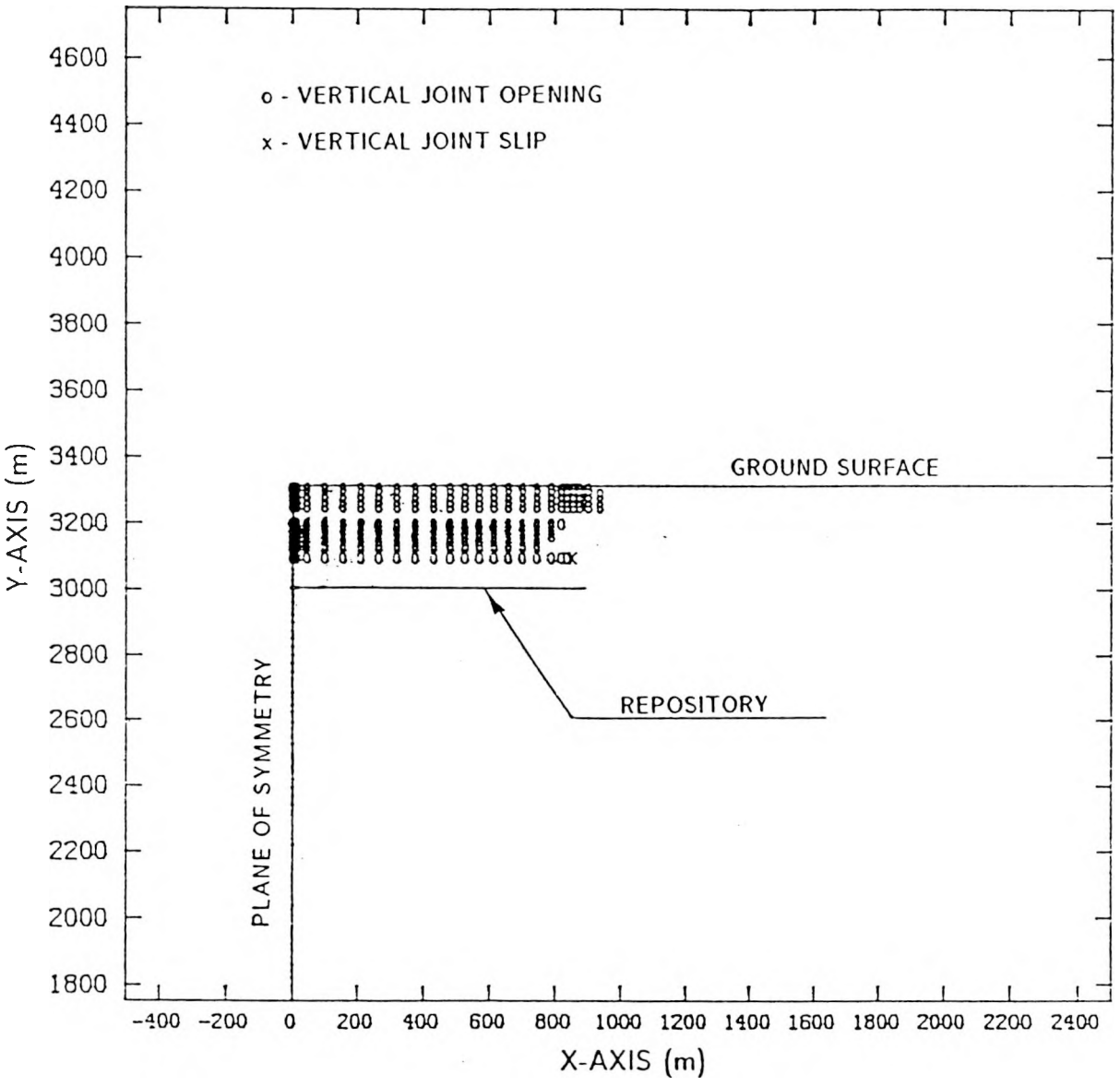

Figure A-31. Predicted Joint Activity at 50 Yr Using Mesh II.

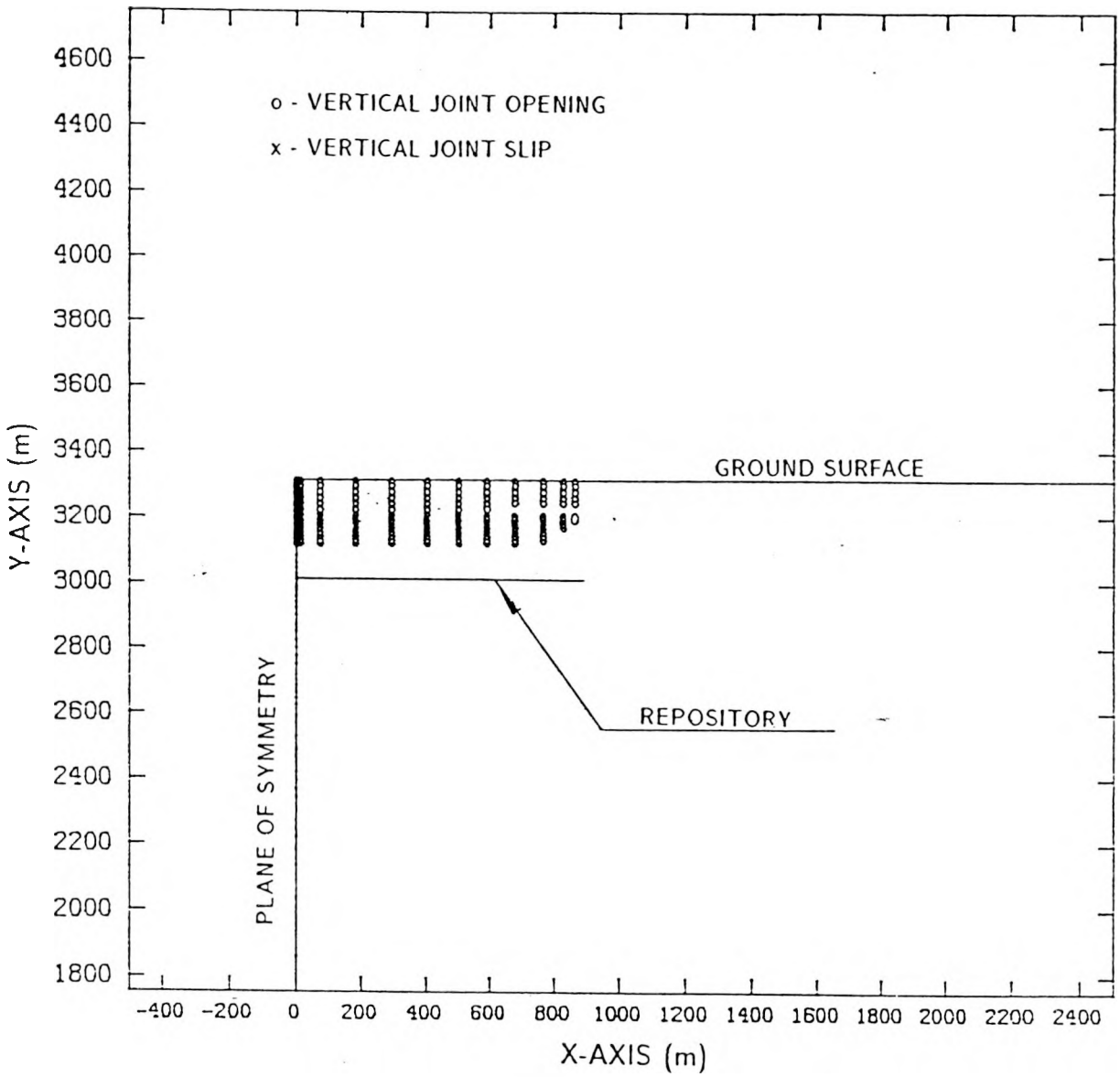

Figure A-32. Predicted Joint Activity at 100 Yr Using Mesh I.

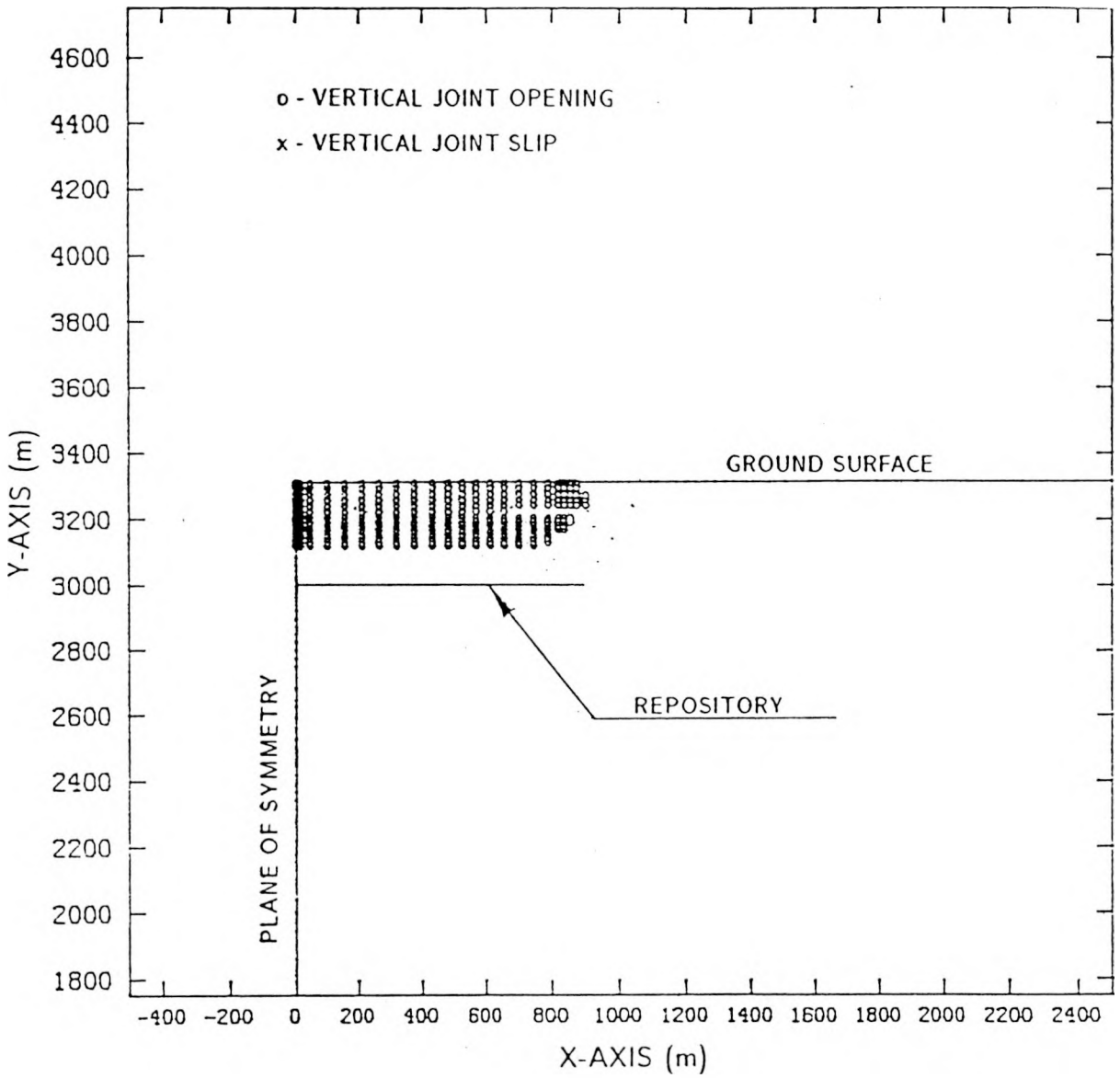

Figure A-33. Predicted Joint Activity at 100 Yr Using Mesh II.

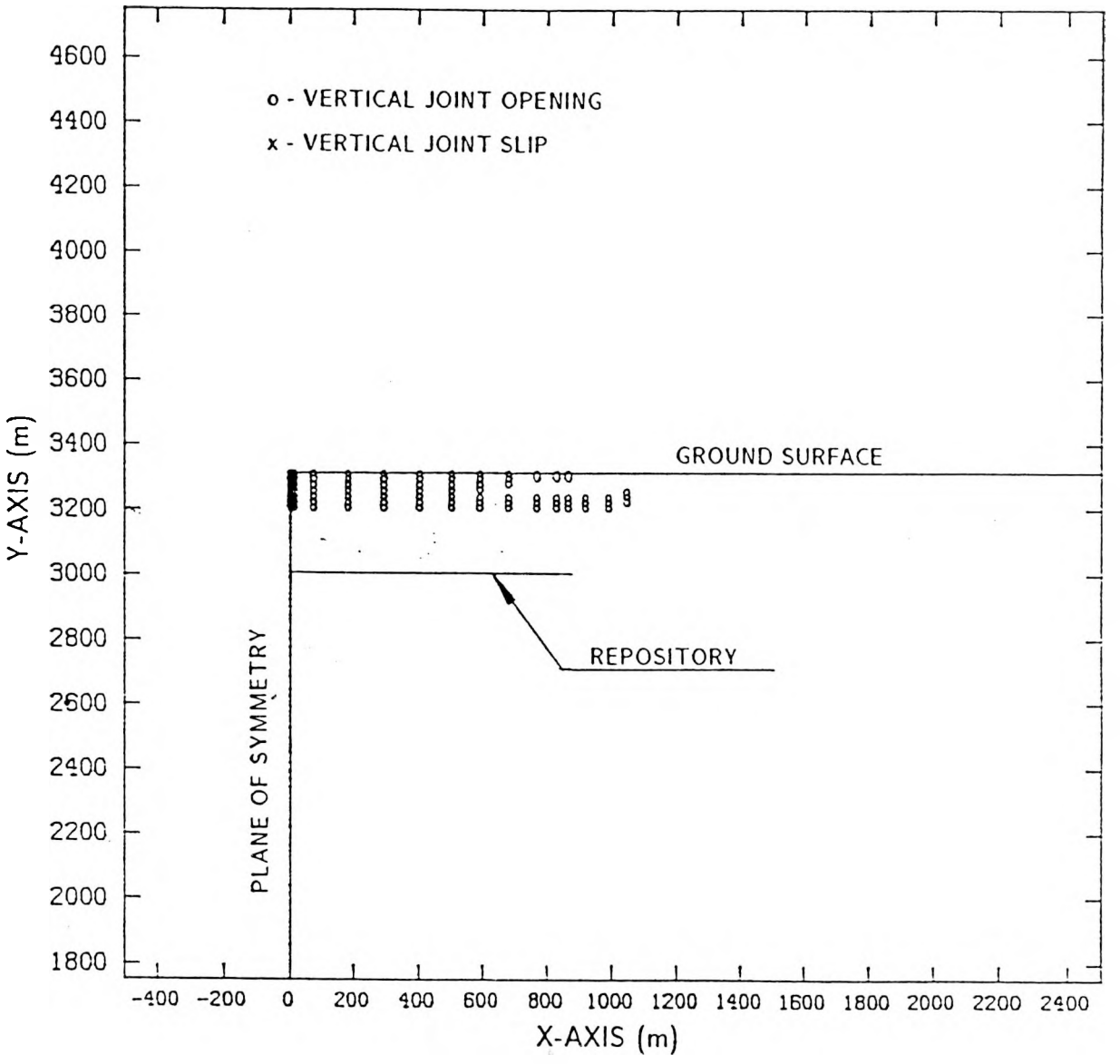

Figure A-34. Predicted Joint Activity at 2,000 Yr Using Mesh I.

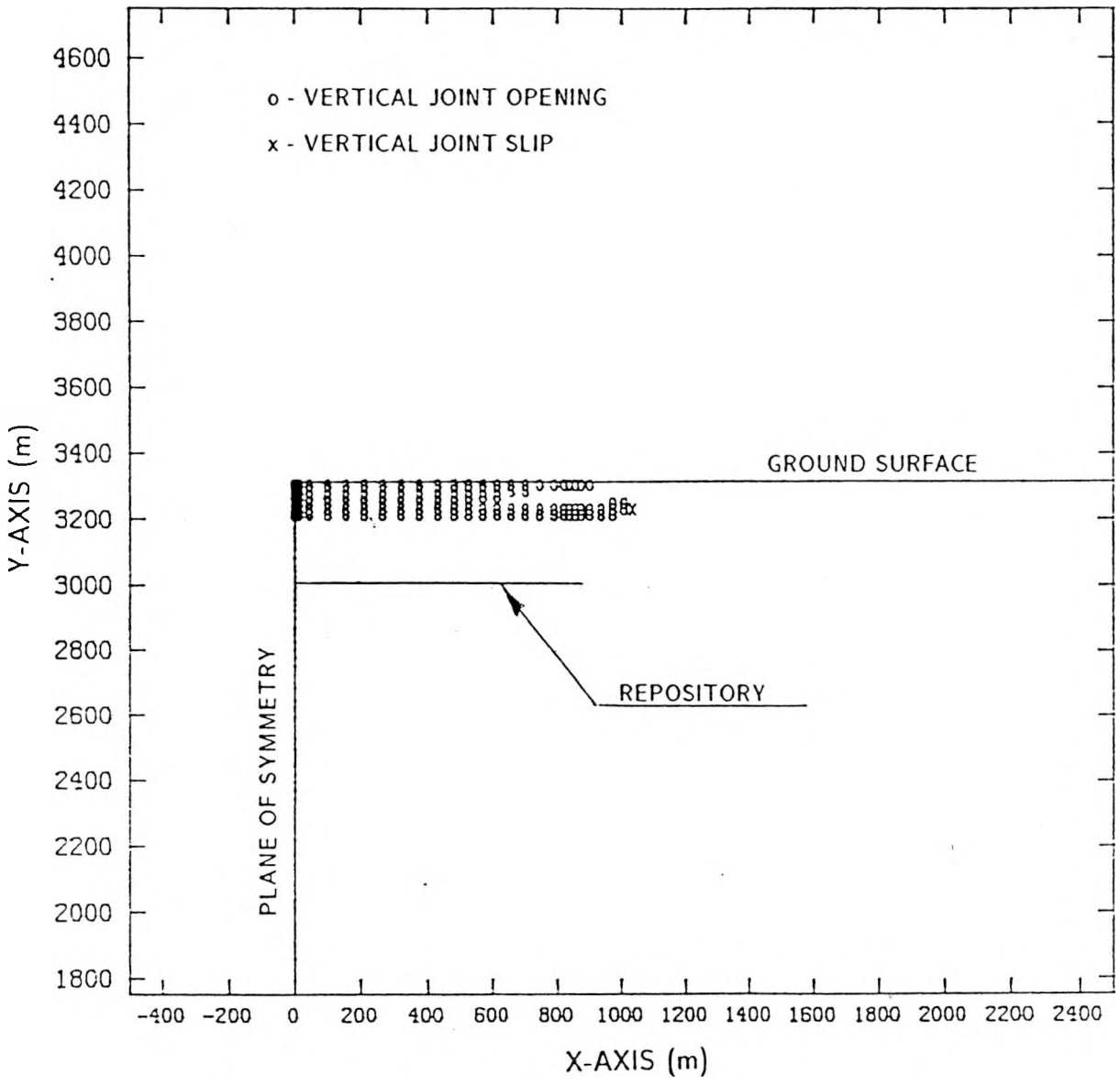

Figure A-35. Predicted Joint Activity at 2,000 Yr Using Mesh II.

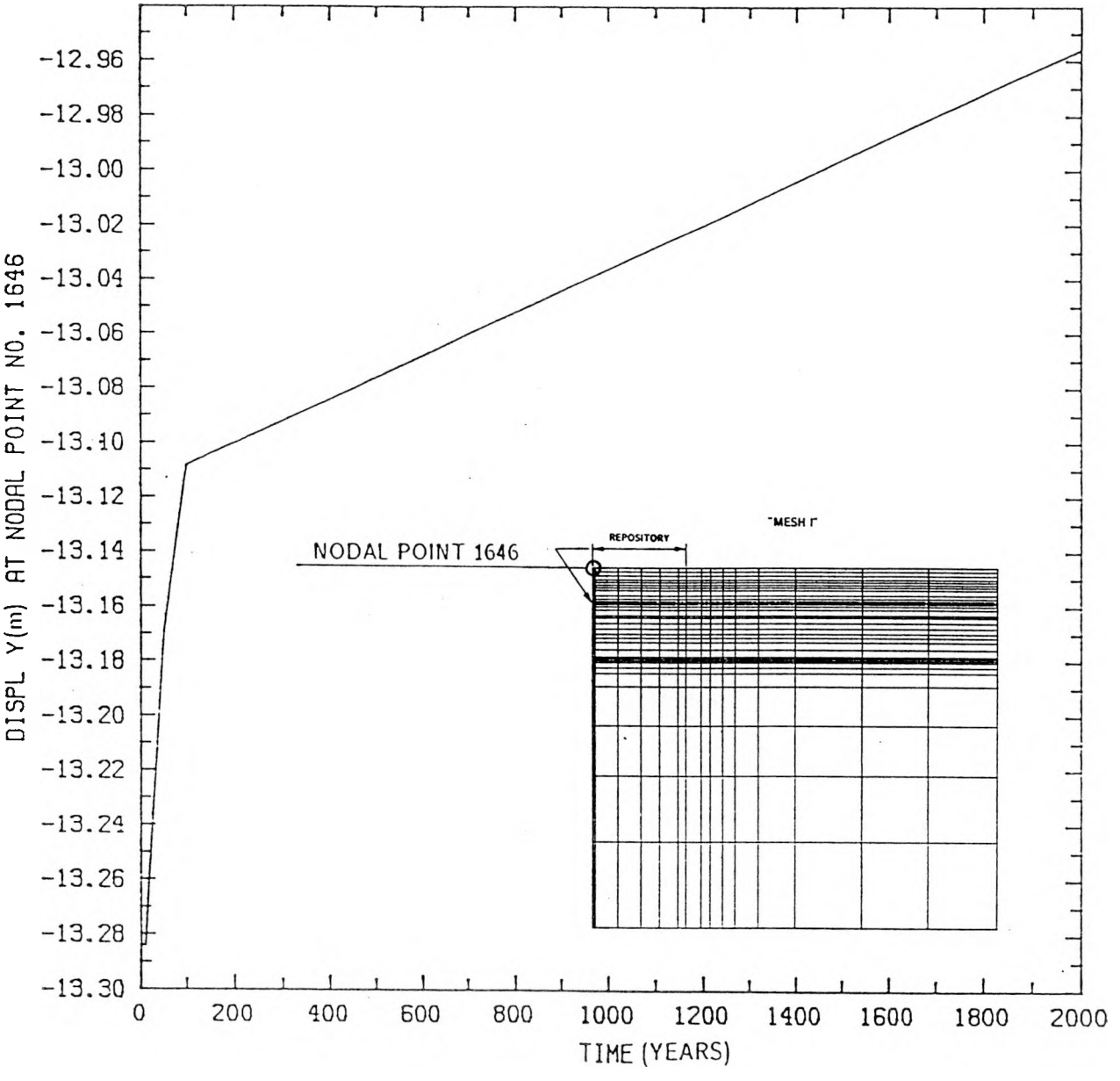

Figure A-36. Predicted Vertical Displacement as a Function of Time for Nodal Point 1646 of Mesh I.

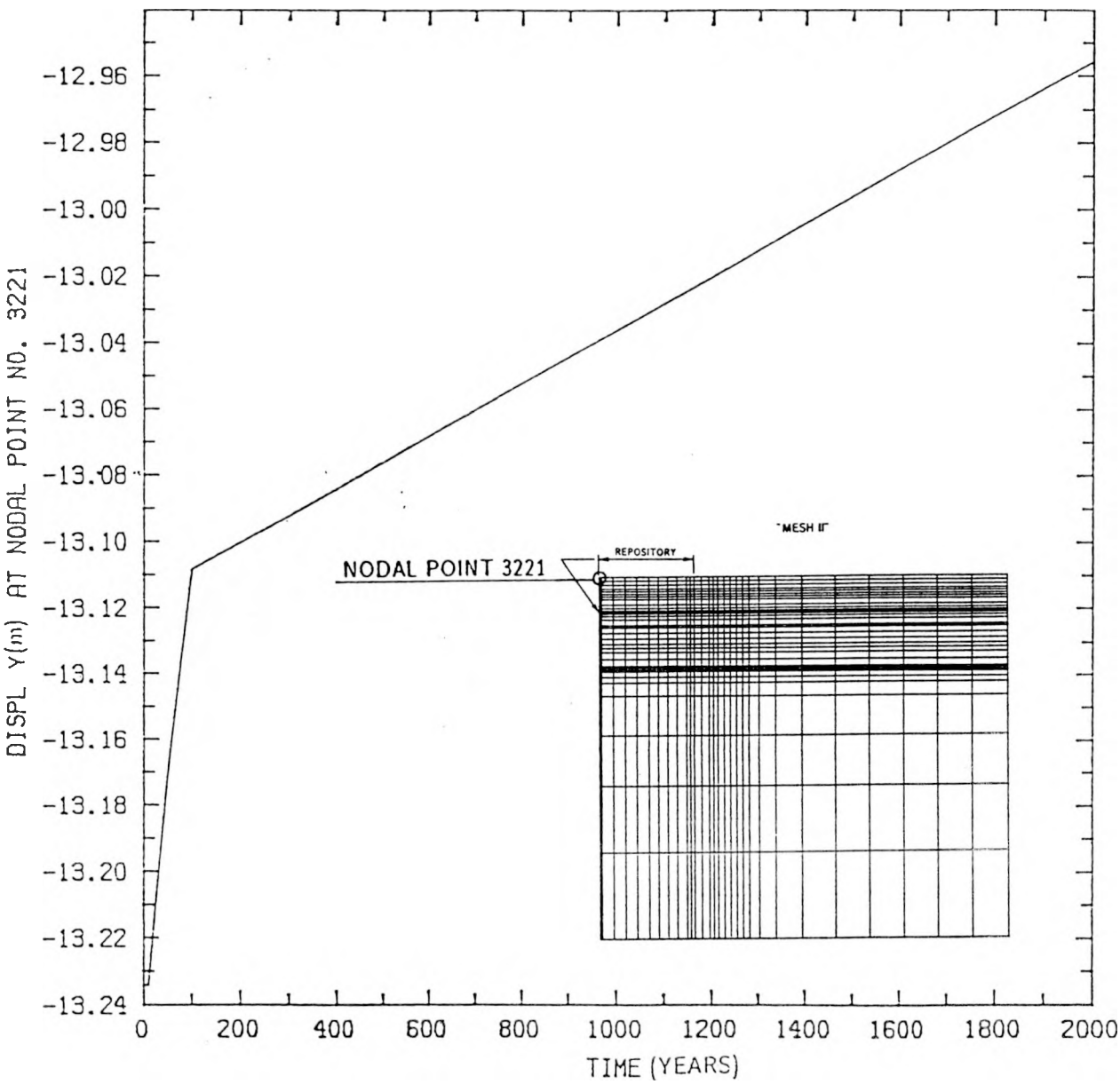

Figure A-37. Predicted Vertical Displacement as a Function of Time for Nodal Point 3221 of Mesh II.

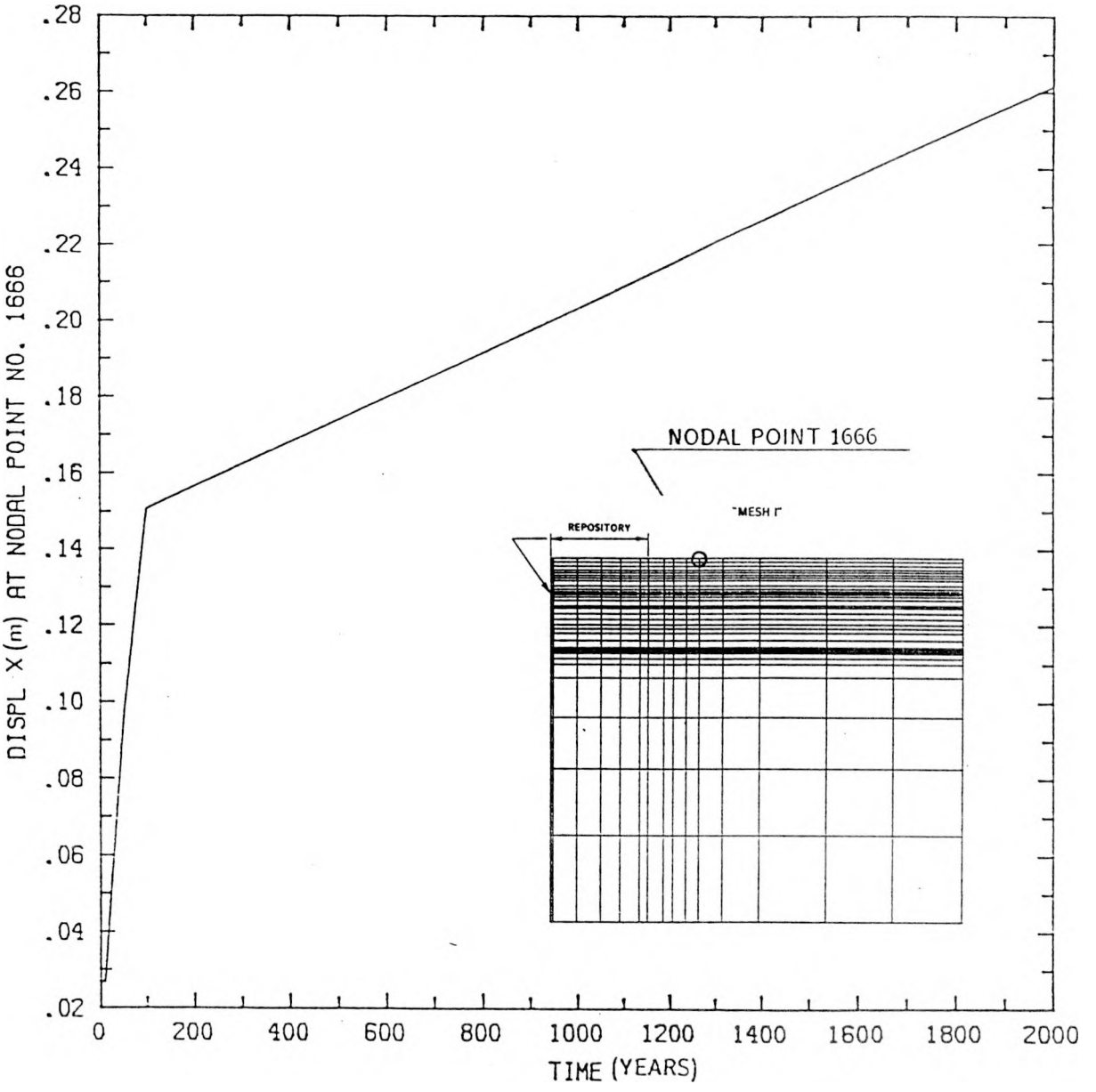

Figure A-38. Predicted Horizontal Displacement as a Function of Time for Nodal Point 1666 of Mesh I.

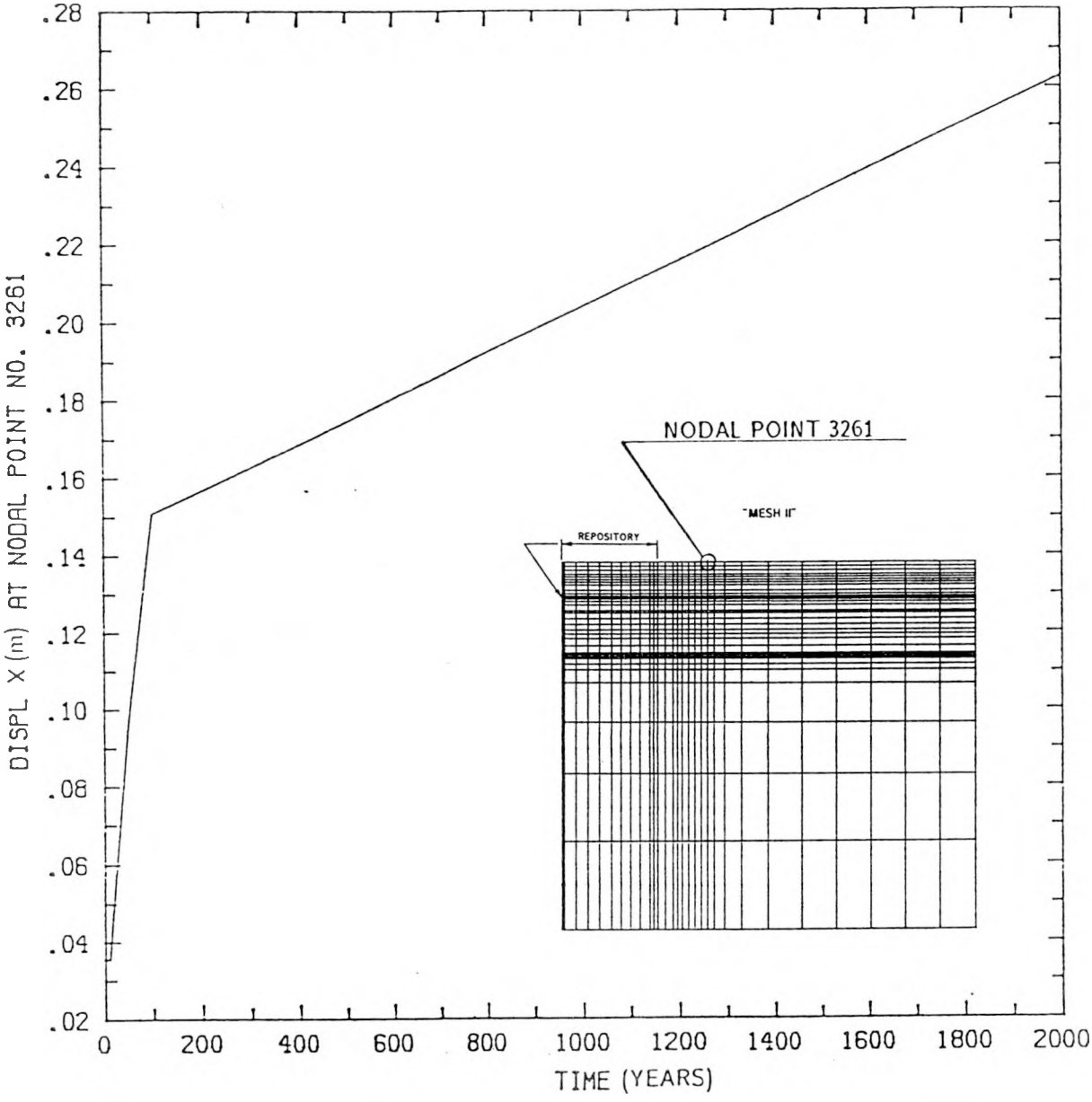

Figure A-39. Predicted Horizontal Displacement as a Function of Time for Nodal Point 3261 of Mesh II.

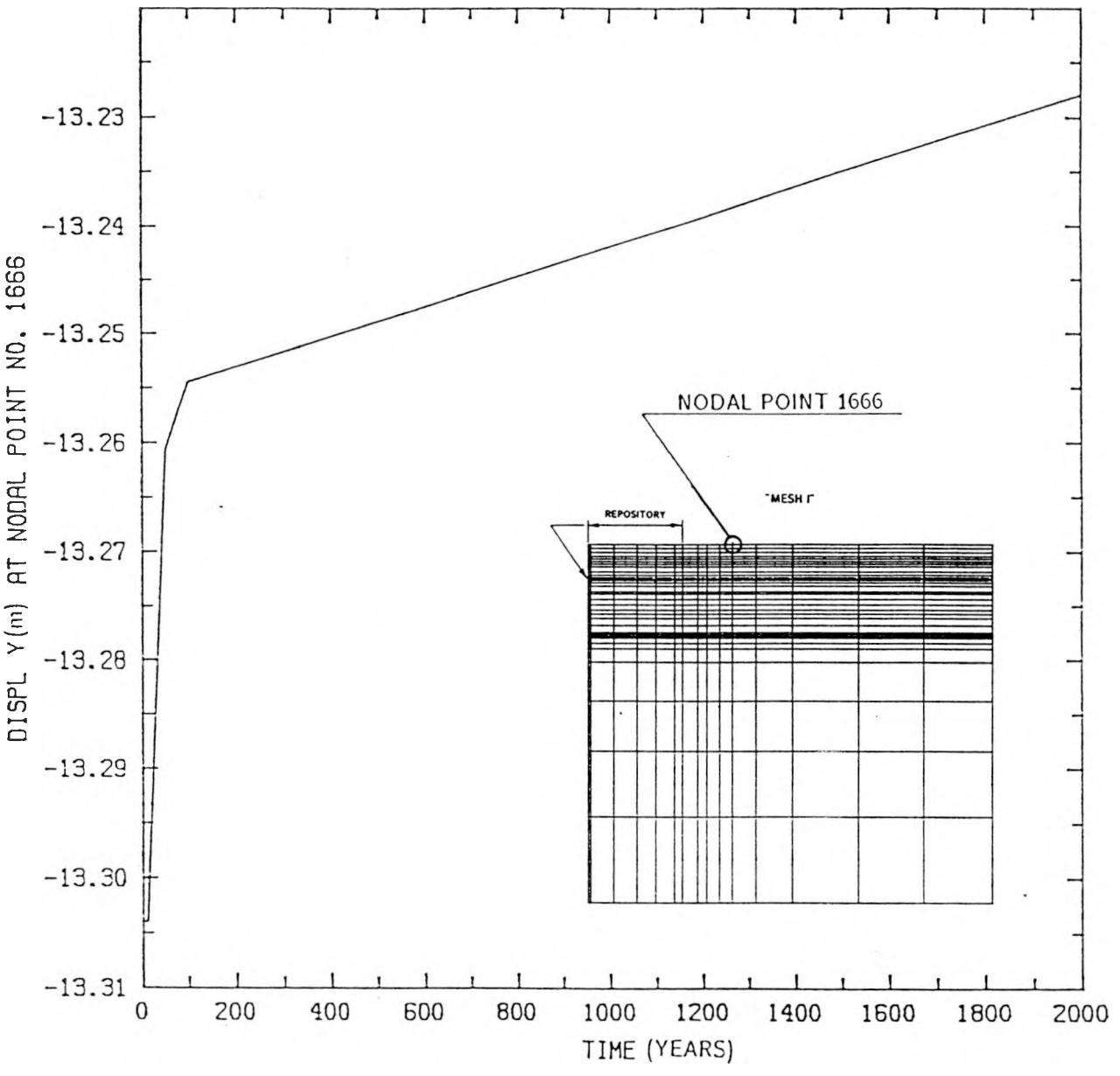

Figure A-40. Predicted Vertical Displacement as a Function of Time for Nodal Point 1666 of Mesh I.

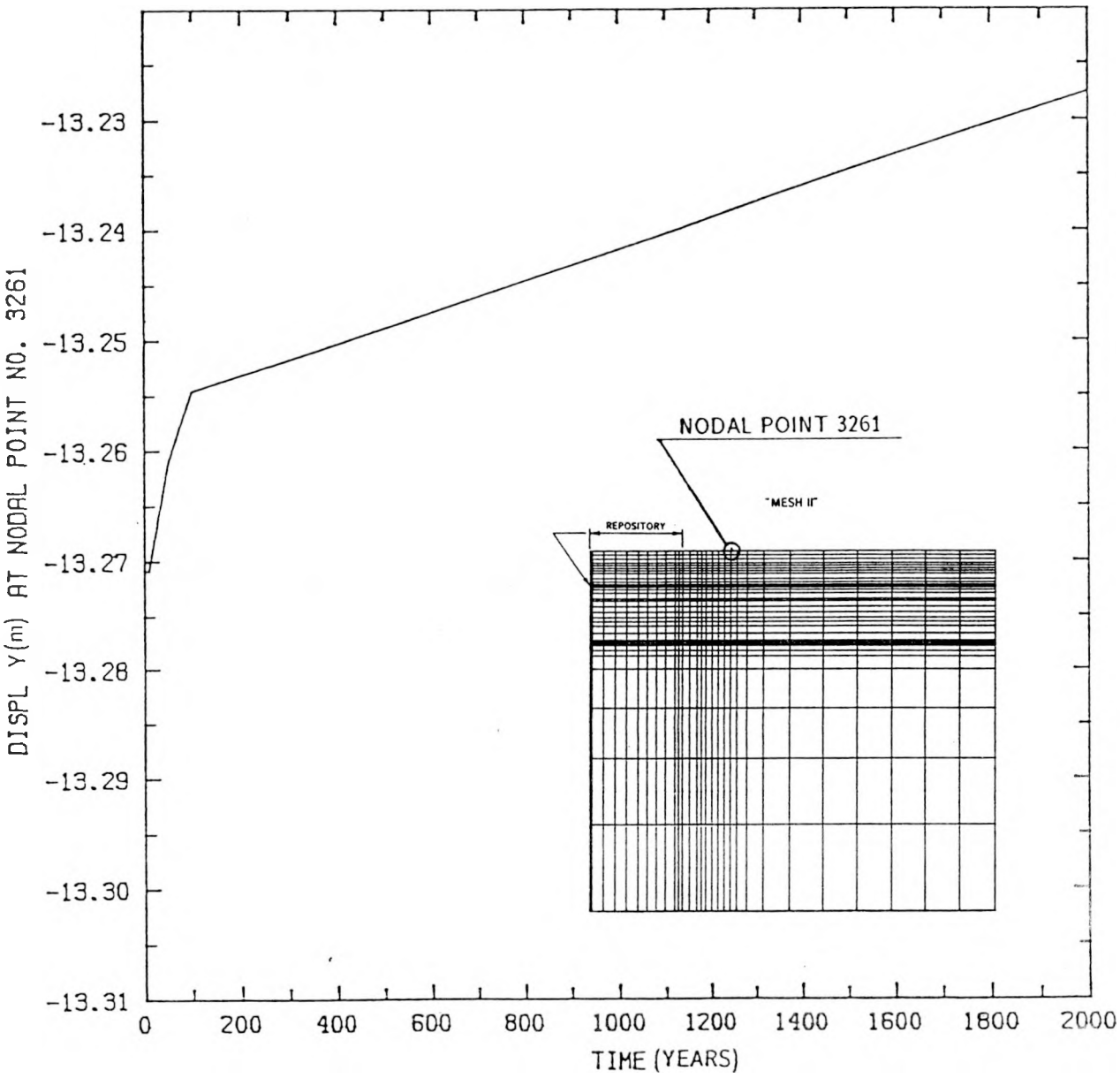

Figure A-41. Predicted Vertical Displacement as a Function of Time for Nodal Point 3261 of Mesh II.

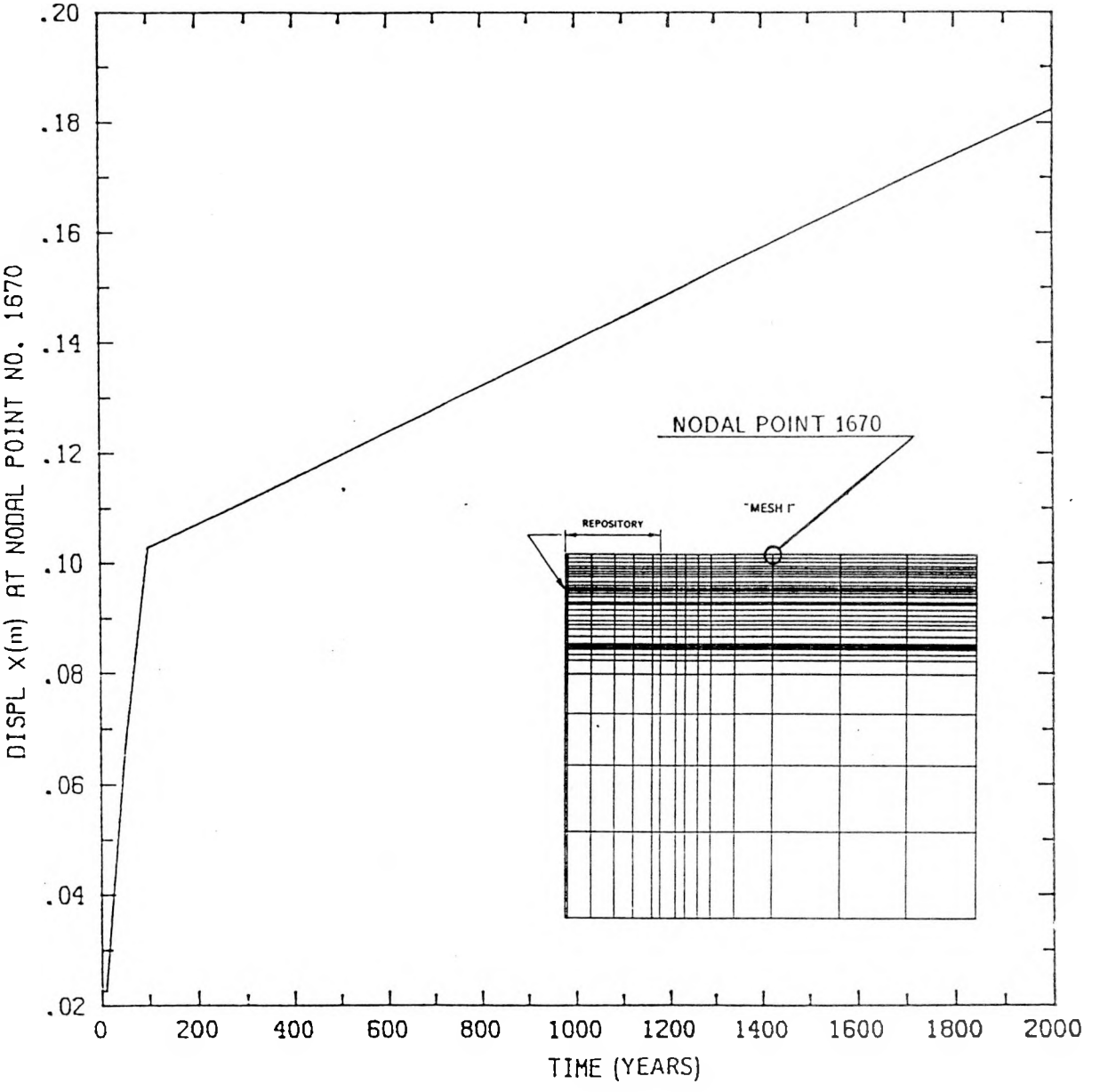

Figure A-42. Predicted Horizontal Displacement as a Function of Time for Nodal Point 1670 of Mesh I.

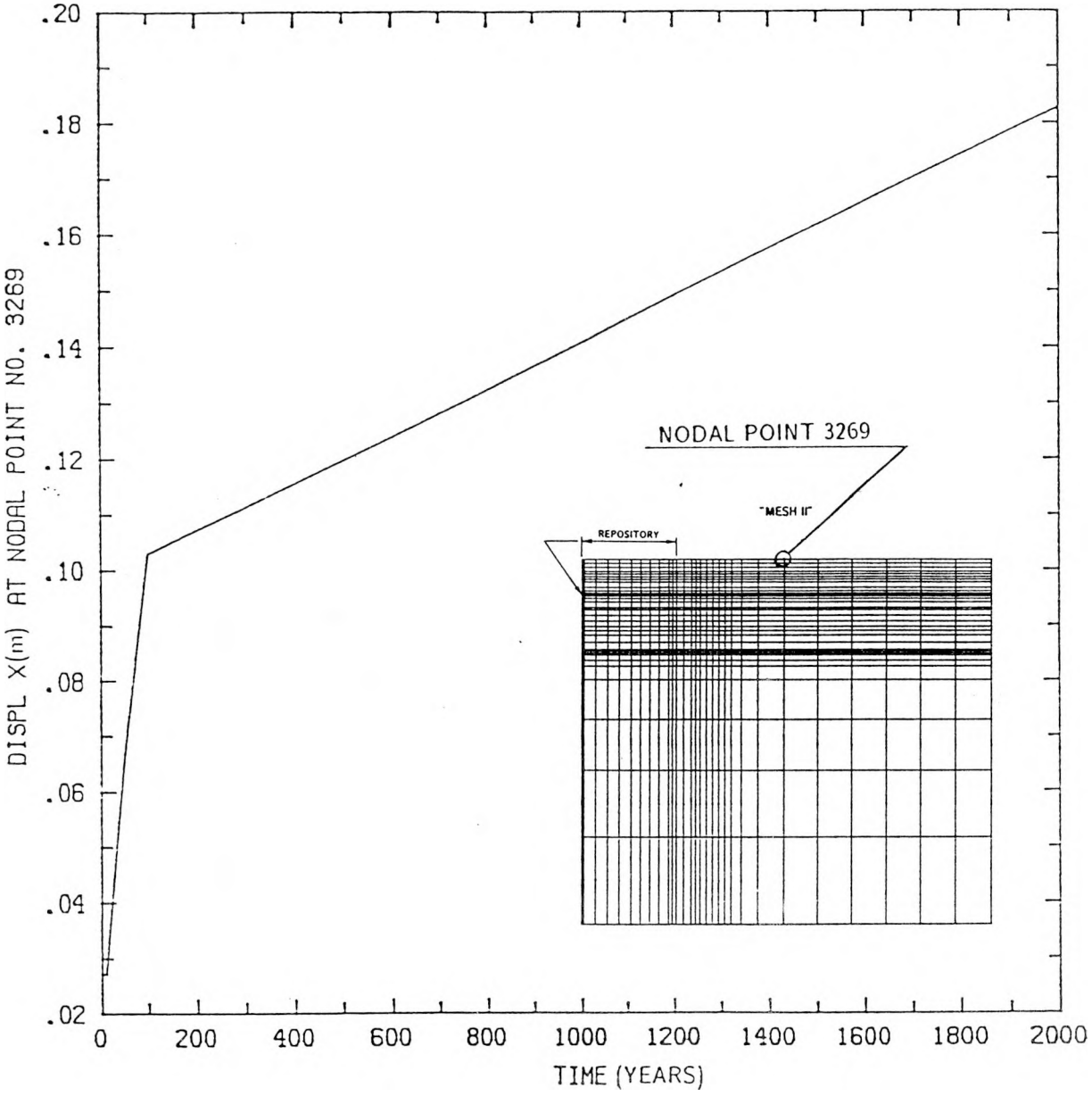

Figure A-43. Predicted Horizontal Displacement as a Function of Time for Nodal Point 3269 of Mesh II.

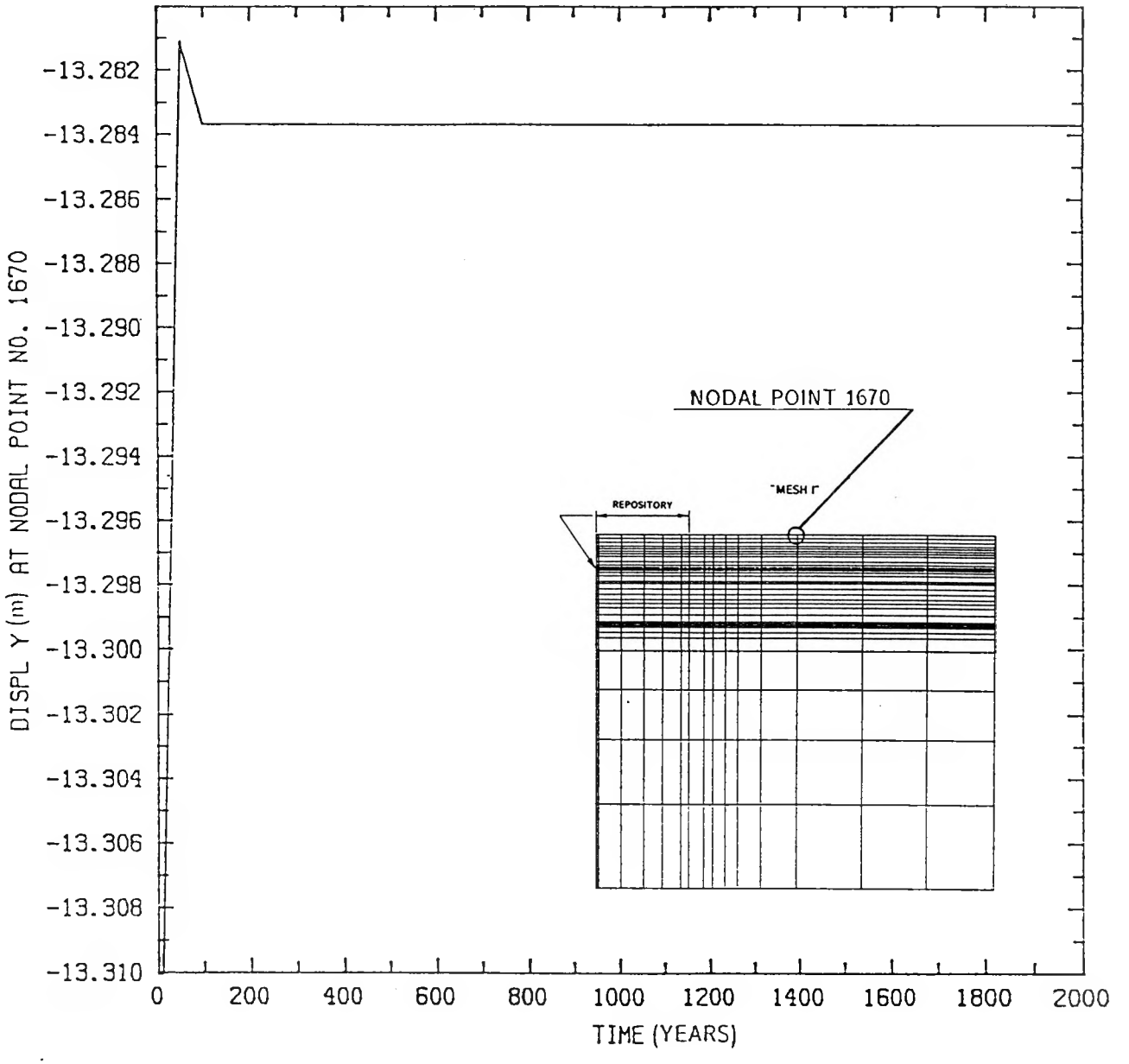

Figure A-44. Predicted Vertical Displacement as a Function of Time for Nodal Point 1670 of Mesh I.

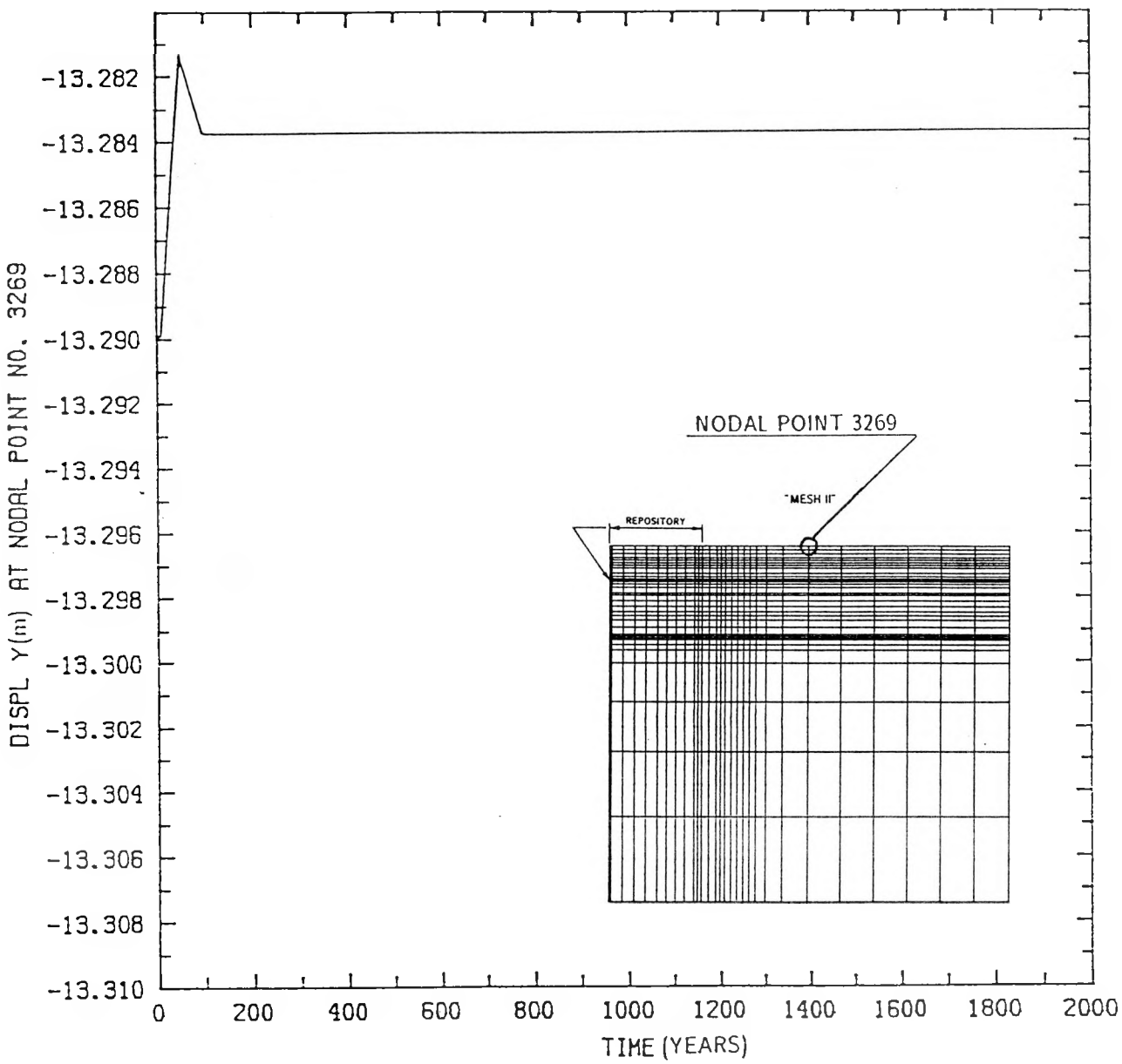

Figure A-45. Predicted Vertical Displacement as a Function of Time for Nodal Point 3269 of Mesh II.

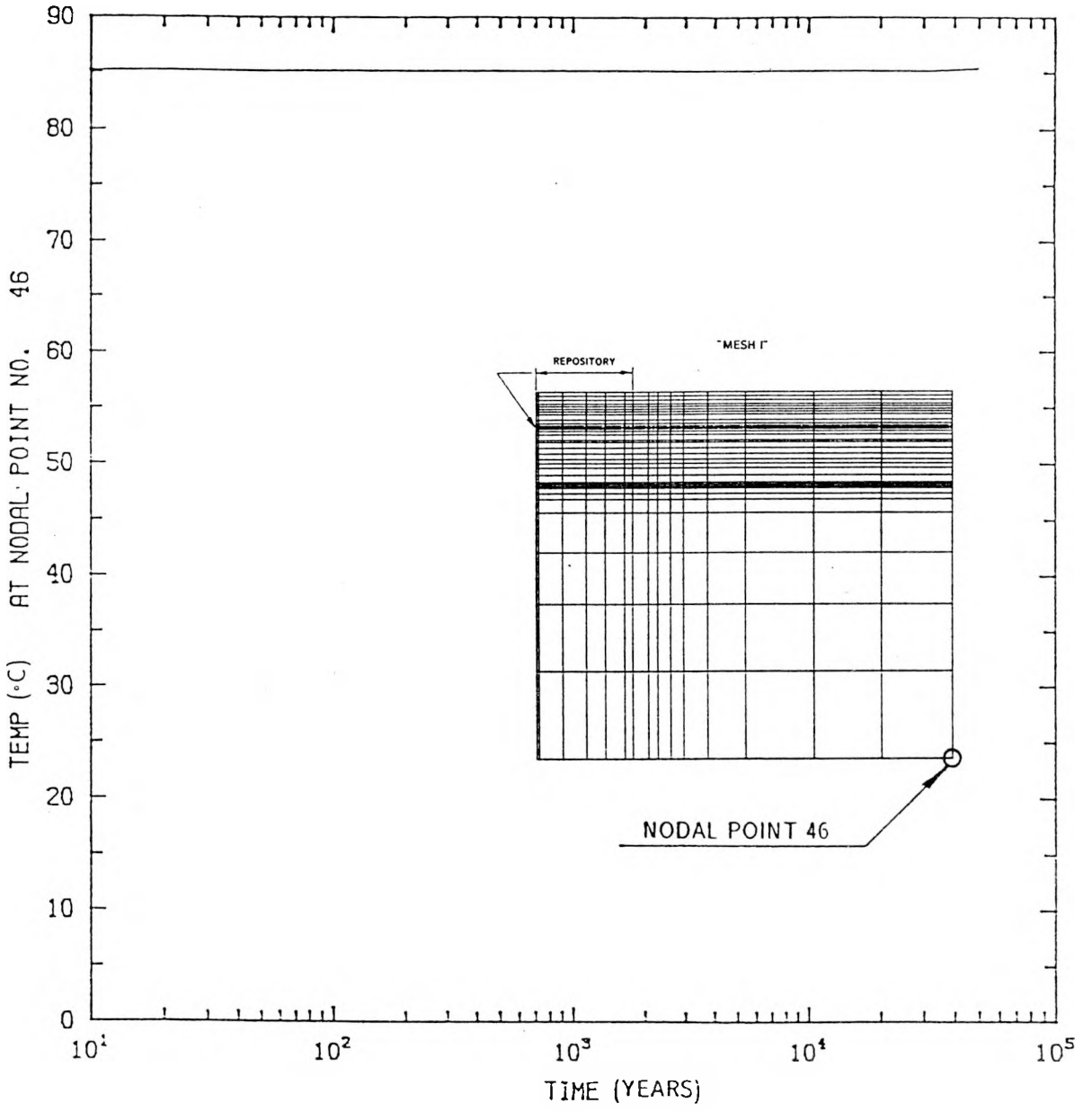

Figure A-46. Temperature History for Nodal Point 46 from Time of Waste Emplacement to 50,000 Yr of Waste Isolation.

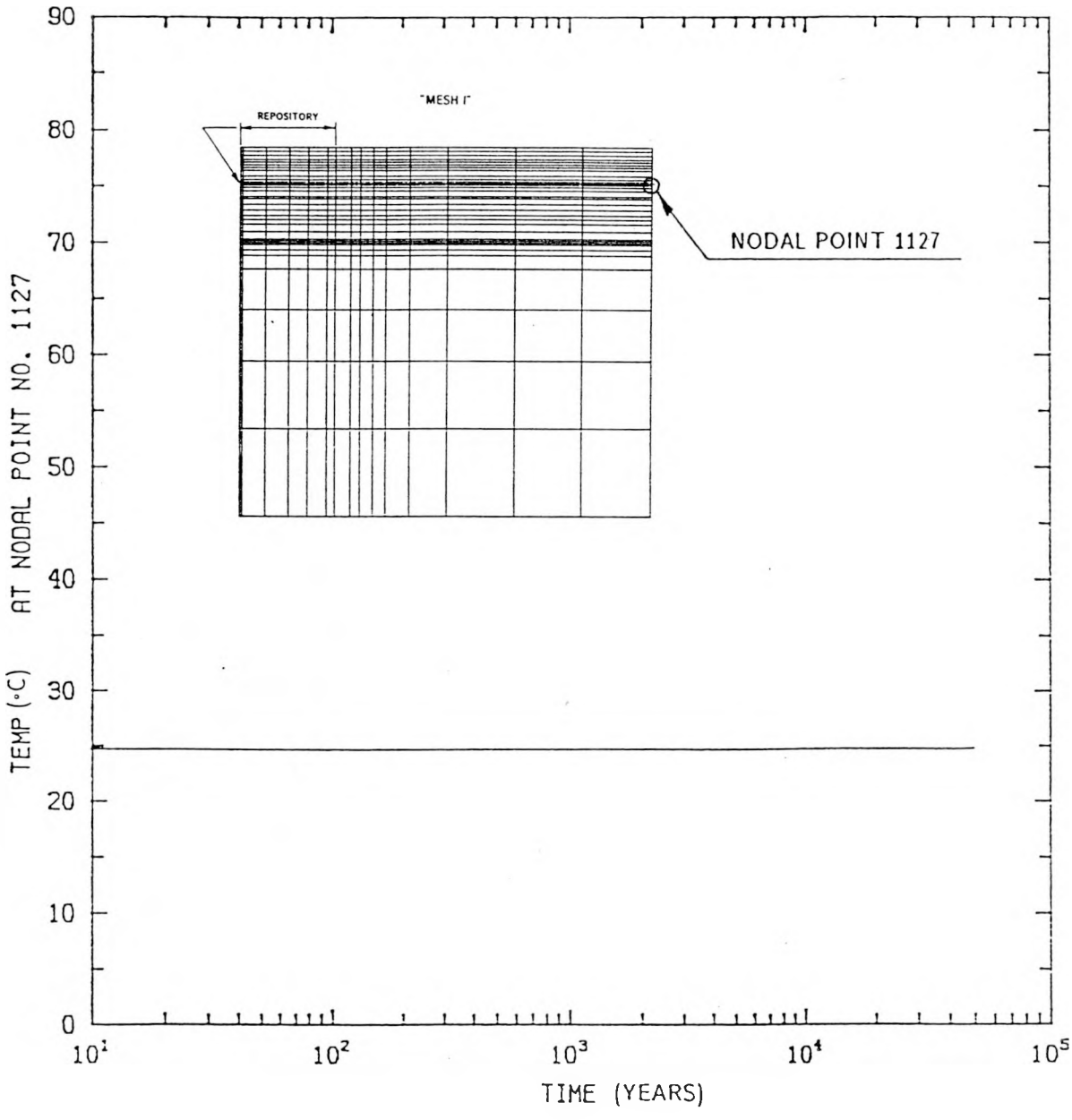

Figure A-47. Temperature History for Nodal Point 1127 from Time of Waste Emplacement to 50,000 Yr of Waste Isolation.

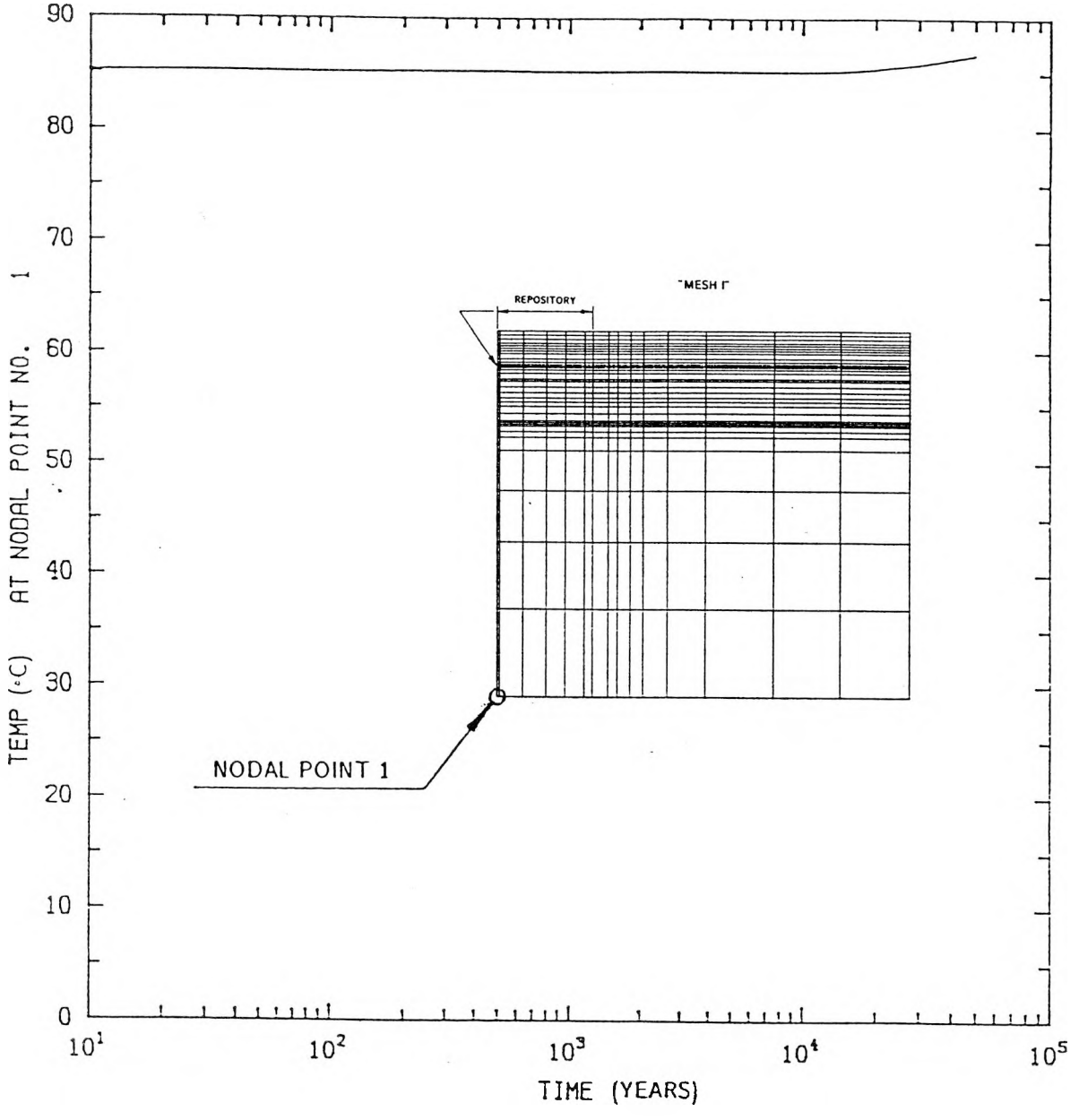

Figure A-48. Temperature History for Nodal Point 1 from Time of Waste Emplacement to 50,000 Yr of Waste Isolation.

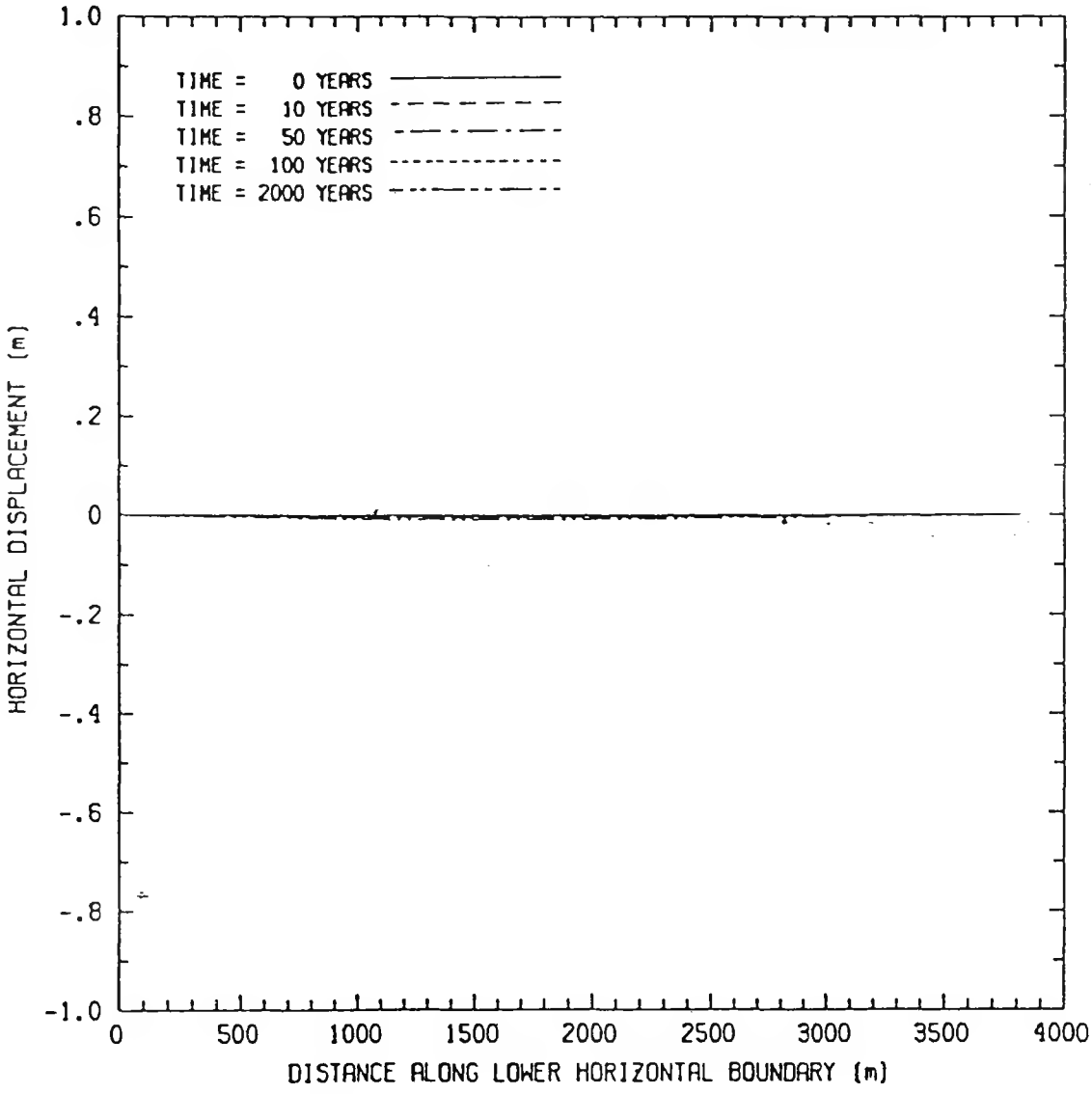

Figure A-49. Horizontal Displacement along the Lower Horizontal Boundary of the Mechanical Model from Time of Waste Emplacement to 2,000 Yr of Waste Isolation.

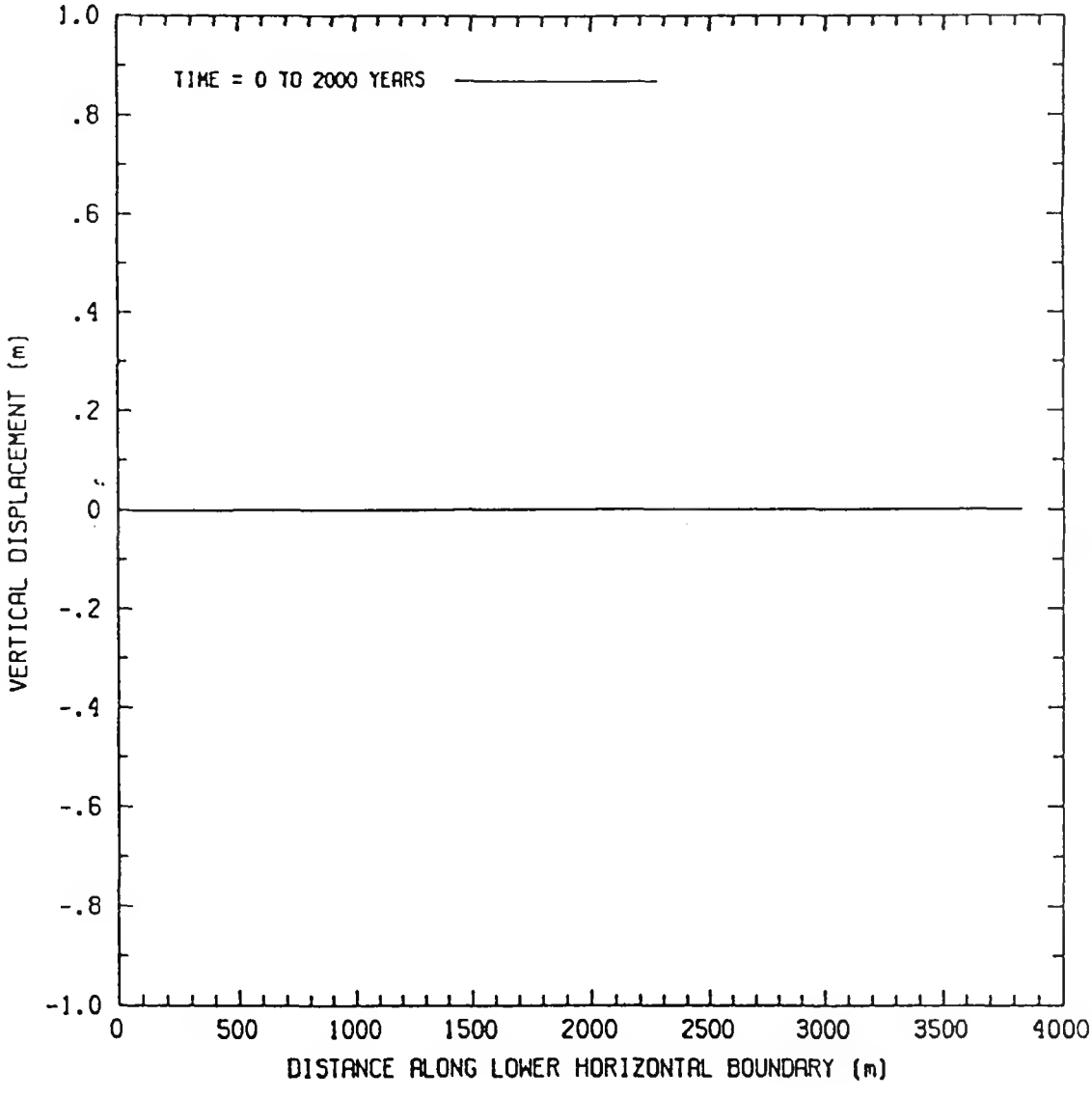

Figure A-50. Vertical Displacement along the Lower Horizontal Boundary of the Mechanical Model from Time of Waste Emplacement to 2,000 Yr of Waste Isolation.

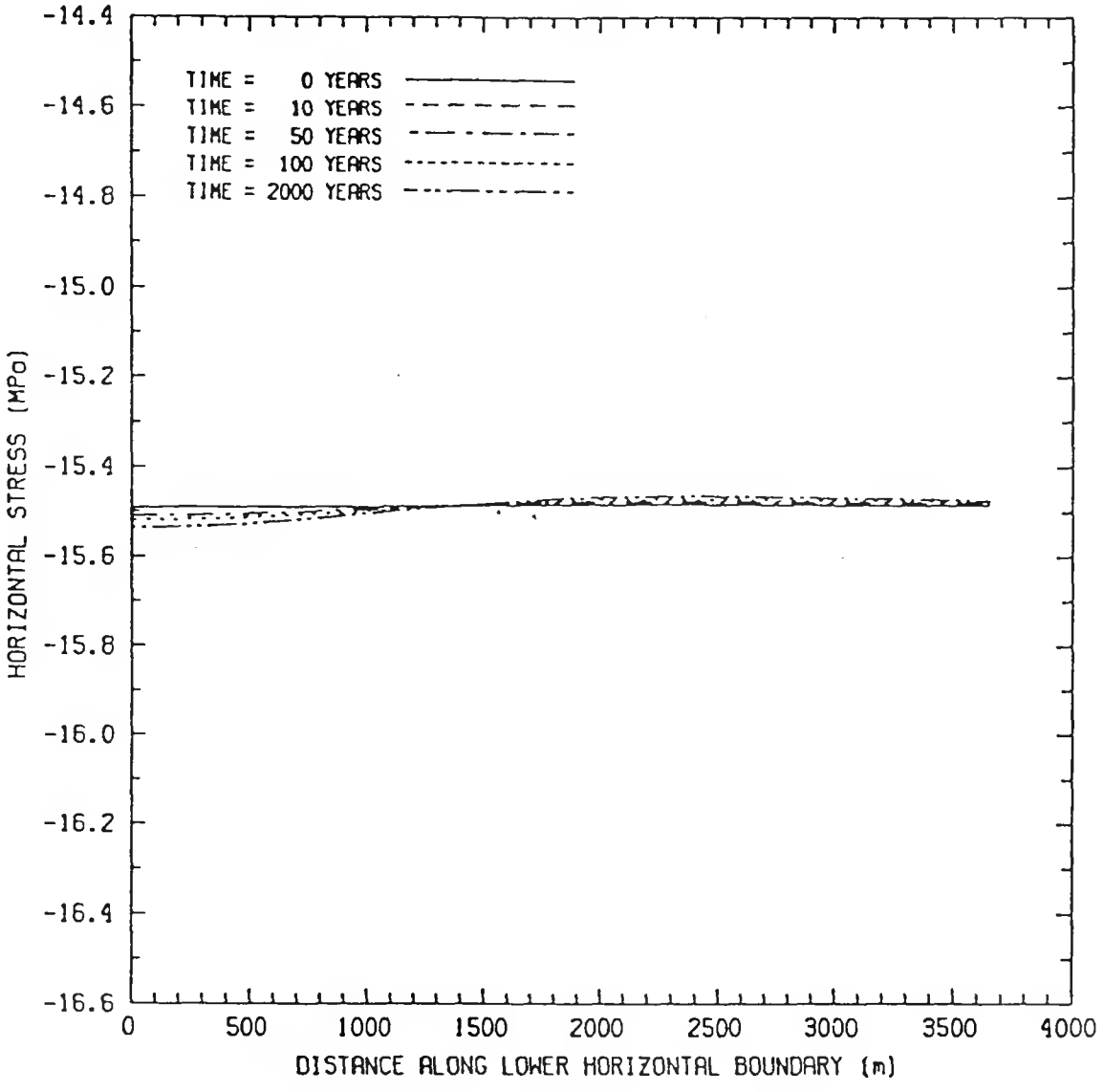

Figure A-51. Horizontal Stress along the Lower Horizontal Boundary of the Mechanical Model from Time of Waste Emplacement to 2,000 Yr of Waste Isolation.

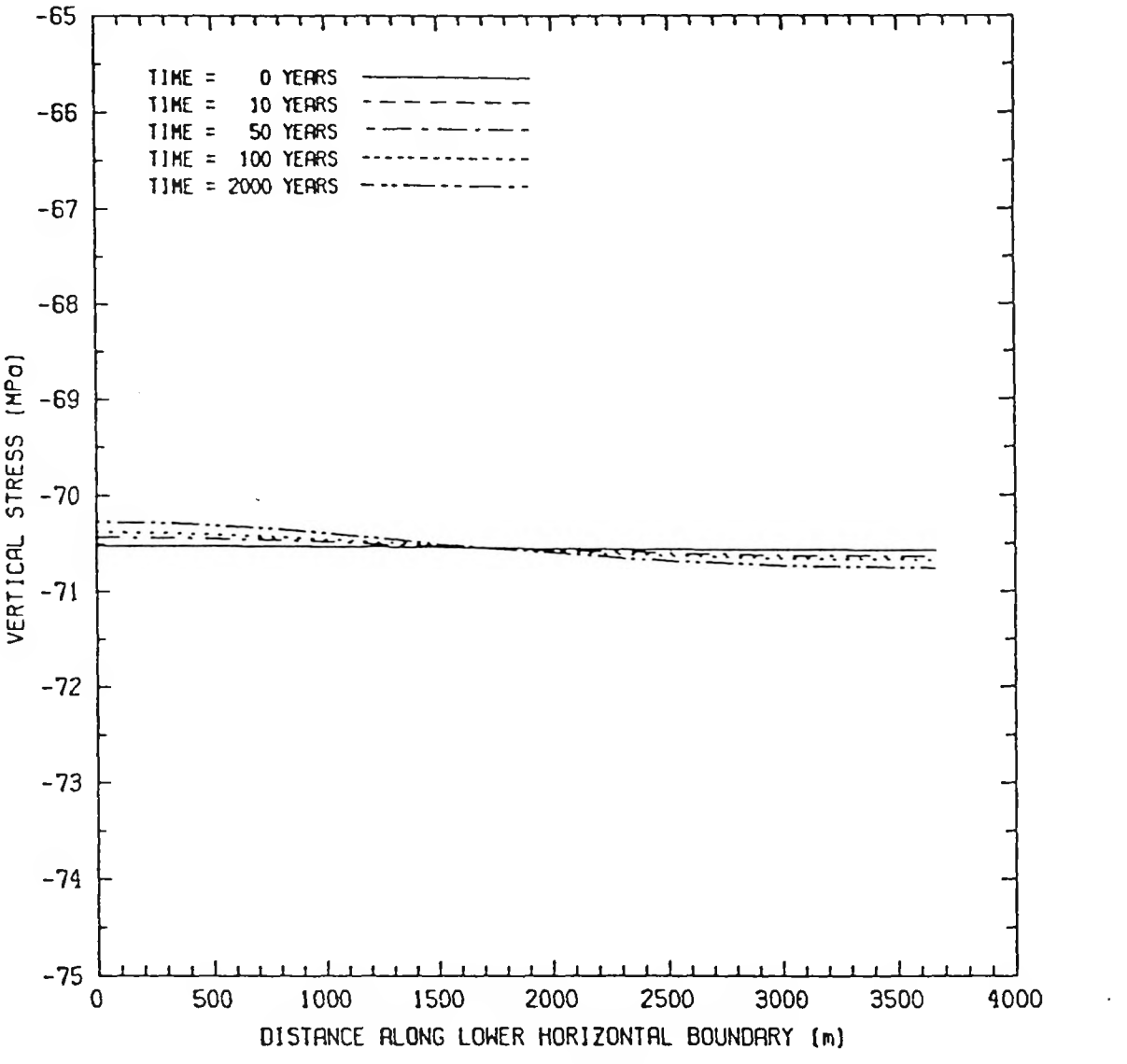

Figure A-52. Vertical Stress along the Lower Horizontal Boundary of the Mechanical Model from Time of Waste Emplacement to 2,000 Yr of Waste Isolation.

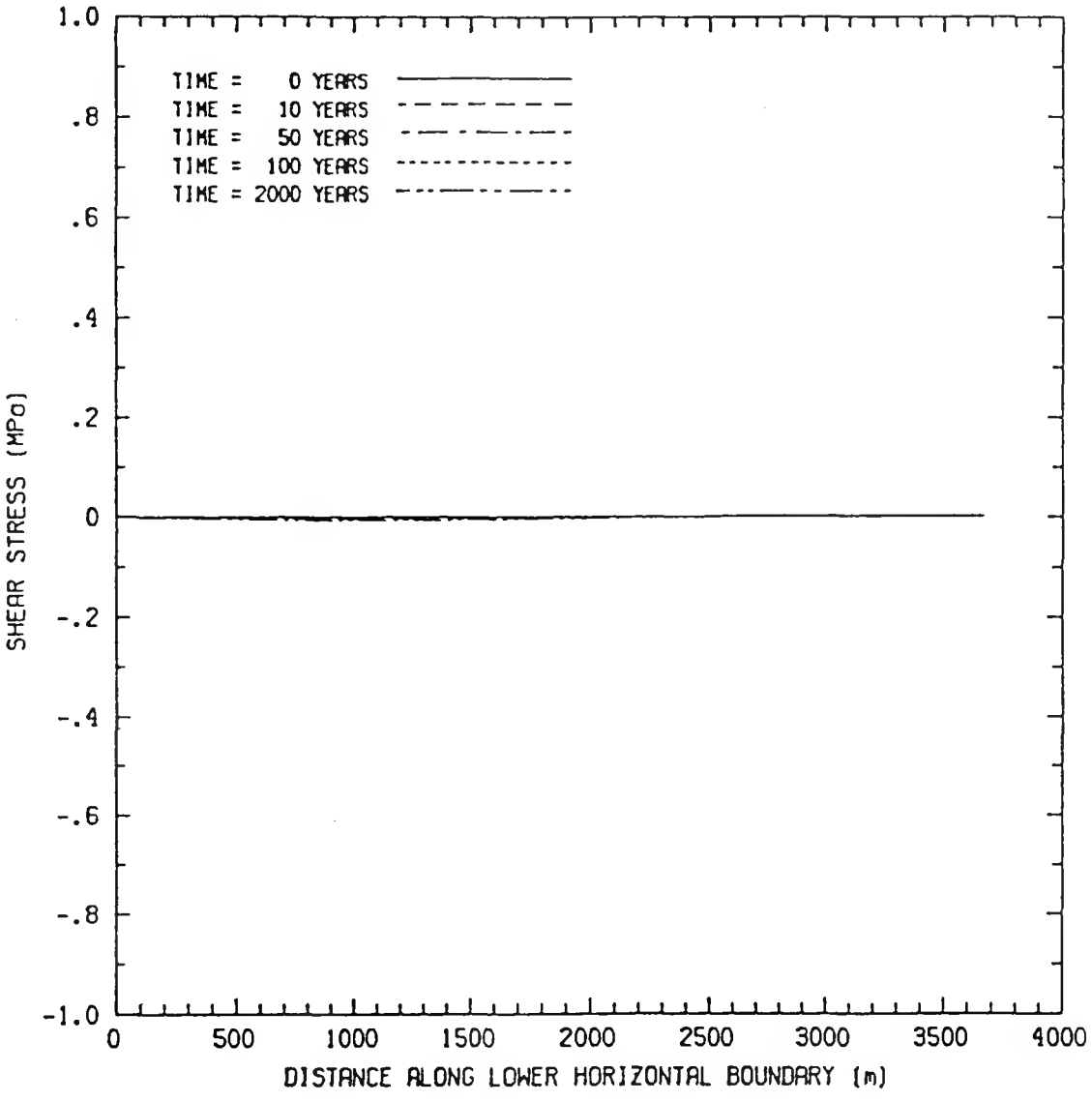

Figure A-53. Shear Stress along the Lower Horizontal Boundary of the Mechanical Model from Time of Waste Emplacement to 2,000 Yr of Waste Isolation.

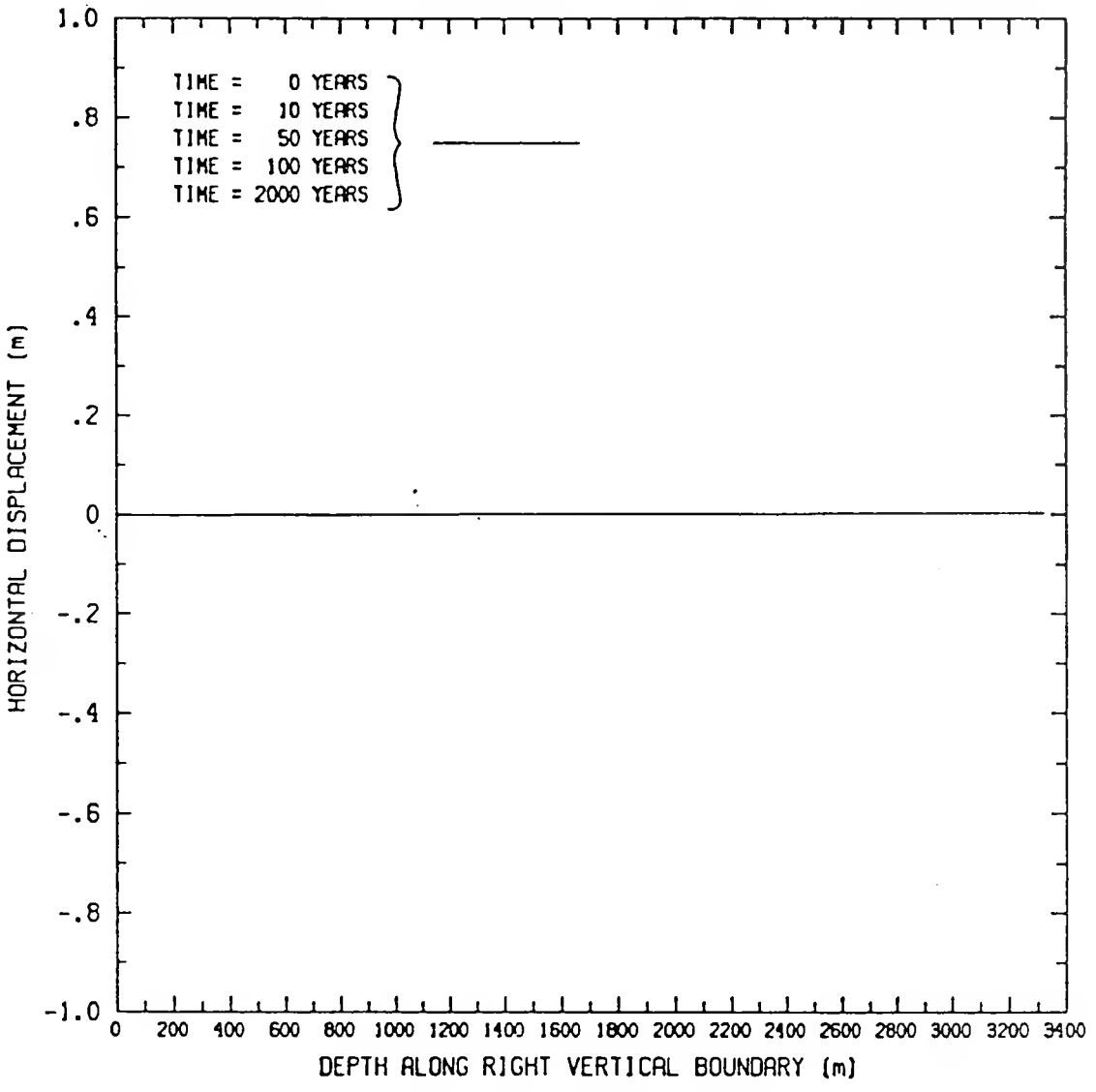

Figure A-54. Horizontal Displacement along the Right Vertical Boundary of the Mechanical Model from Time of Waste Emplacement to 2,000 Yr of Waste Isolation.

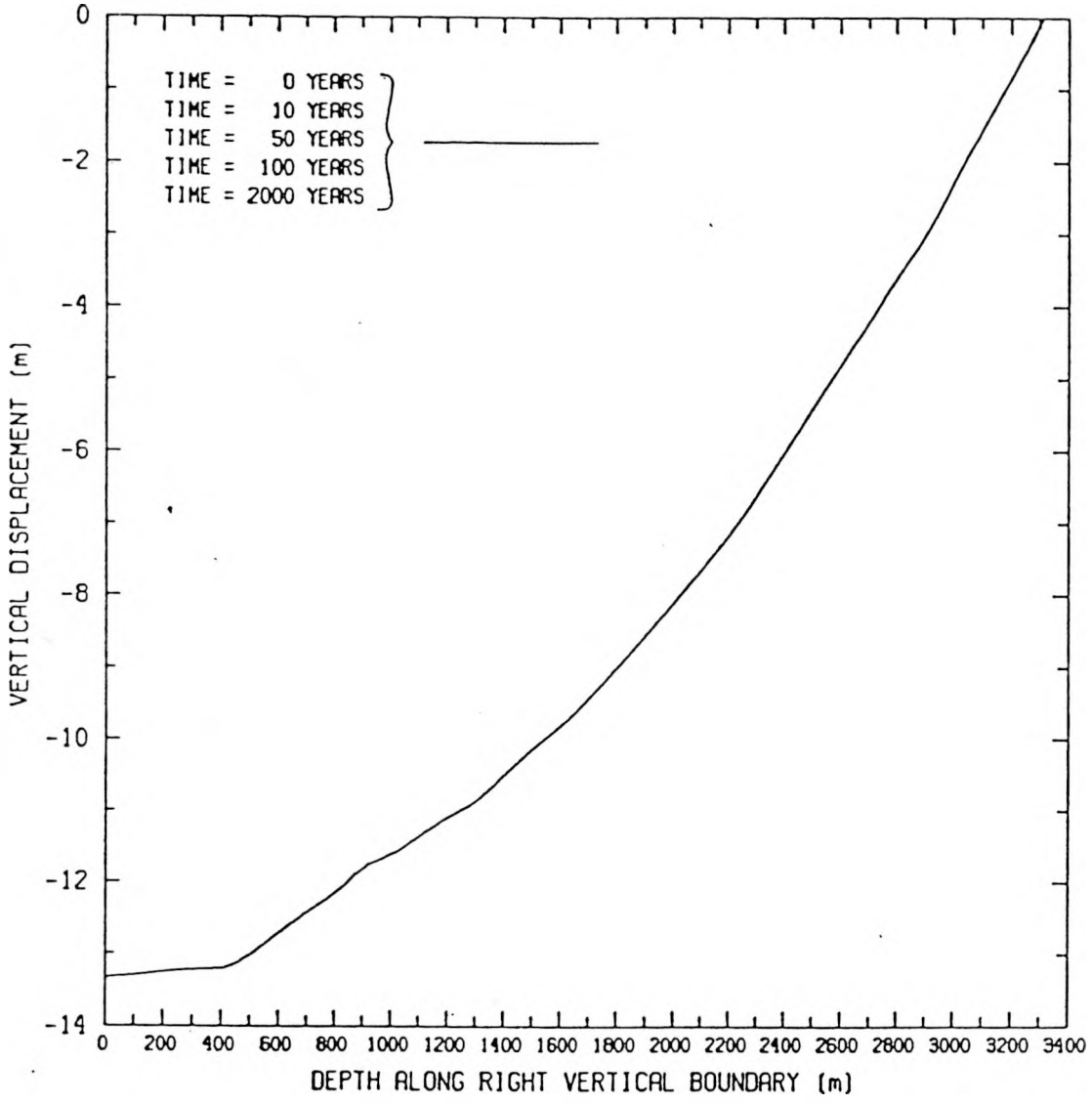

Figure A-55. Vertical Displacement along the Right Vertical Boundary of the Mechanical Model from Time of Waste Emplacement to 2,000 Yr of Waste Isolation.

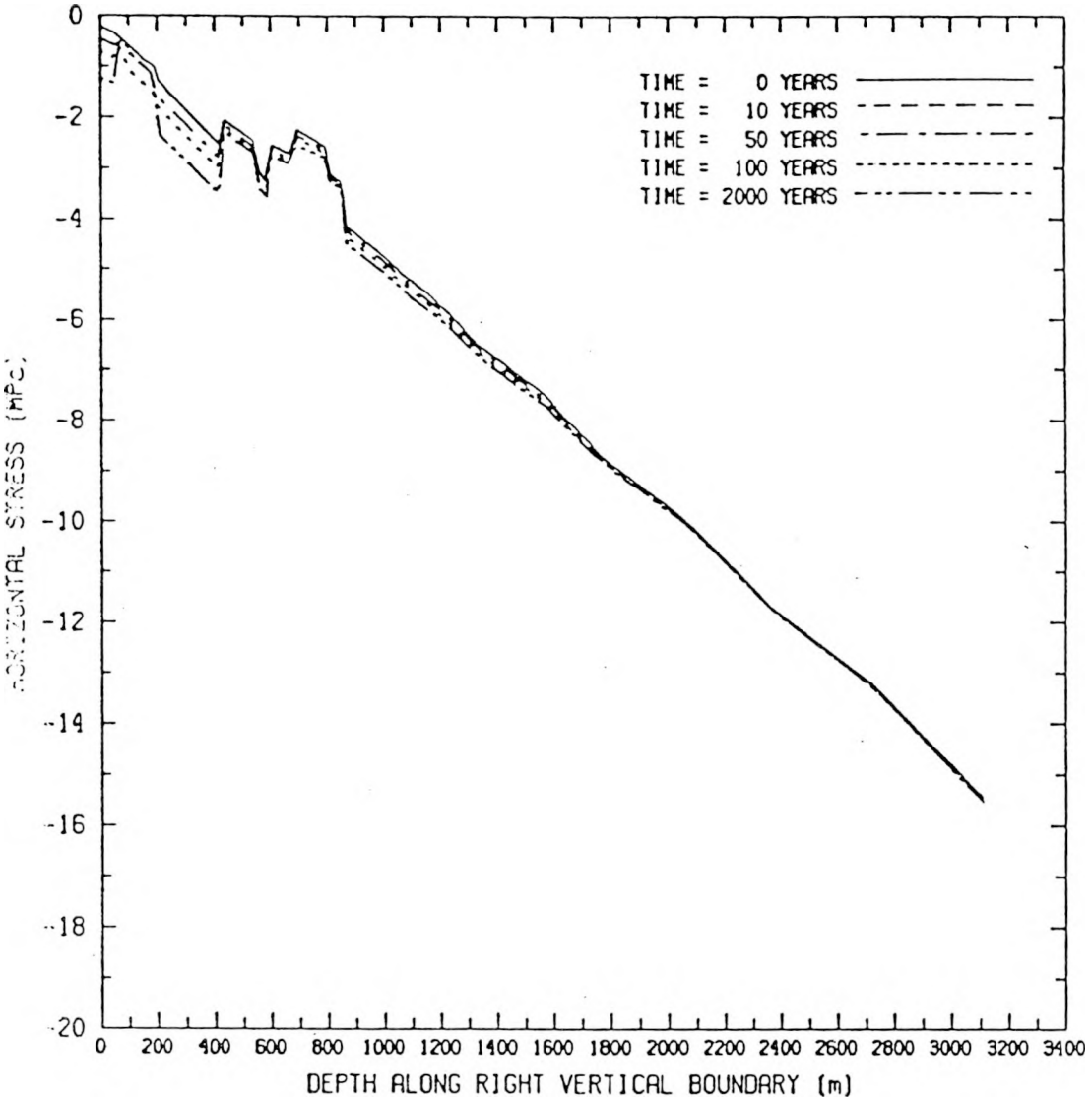

Figure A-56. Horizontal Stress along the Right Vertical Boundary of the Mechanical Model from Time of Waste Emplacement to 2,000 Yr of Waste Isolation.

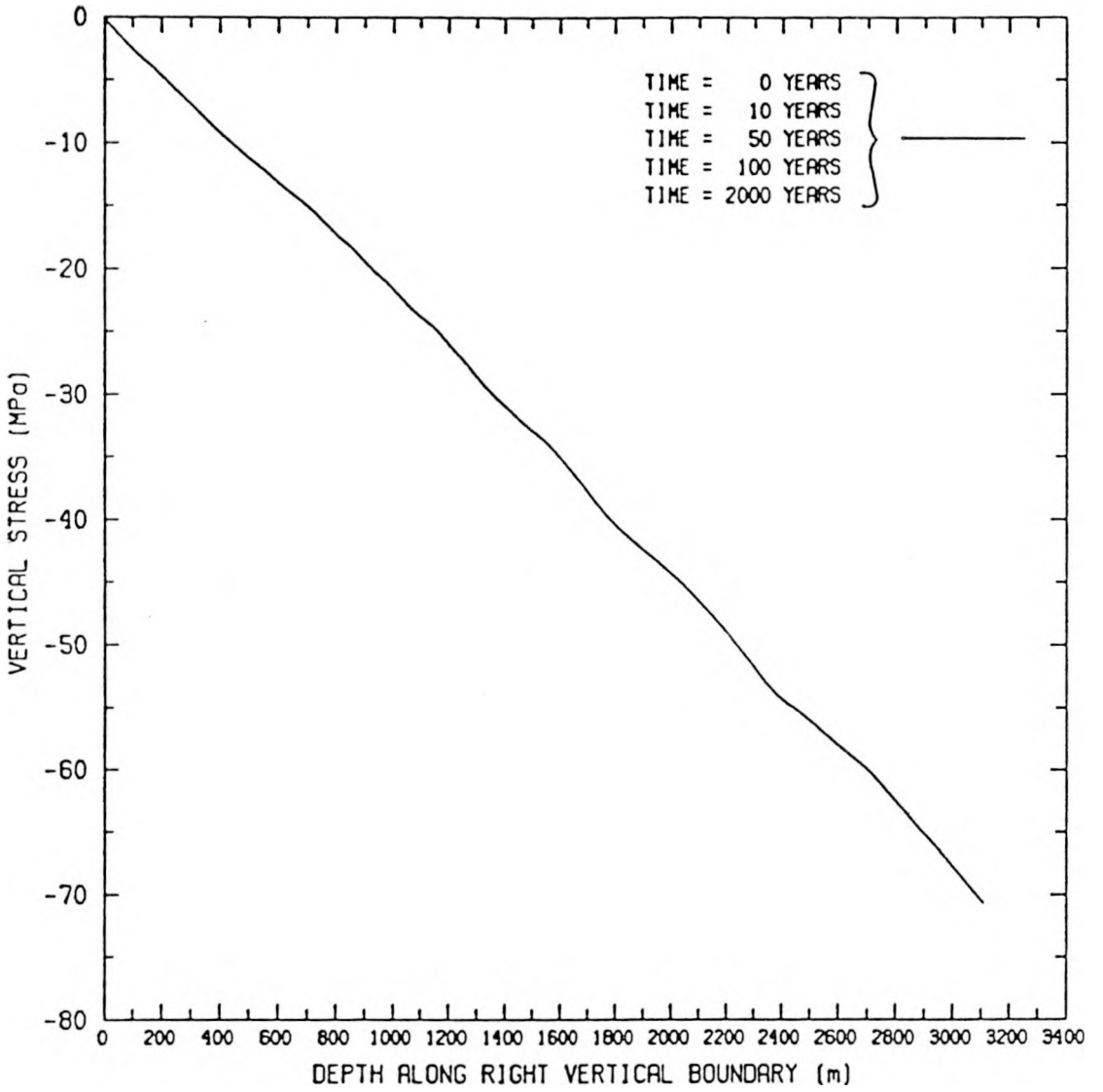

Figure A-57. Vertical Stress along the Right Vertical Boundary of the Mechanical Model from Time of Waste Emplacement to 2,000 Yr of Waste Isolation.

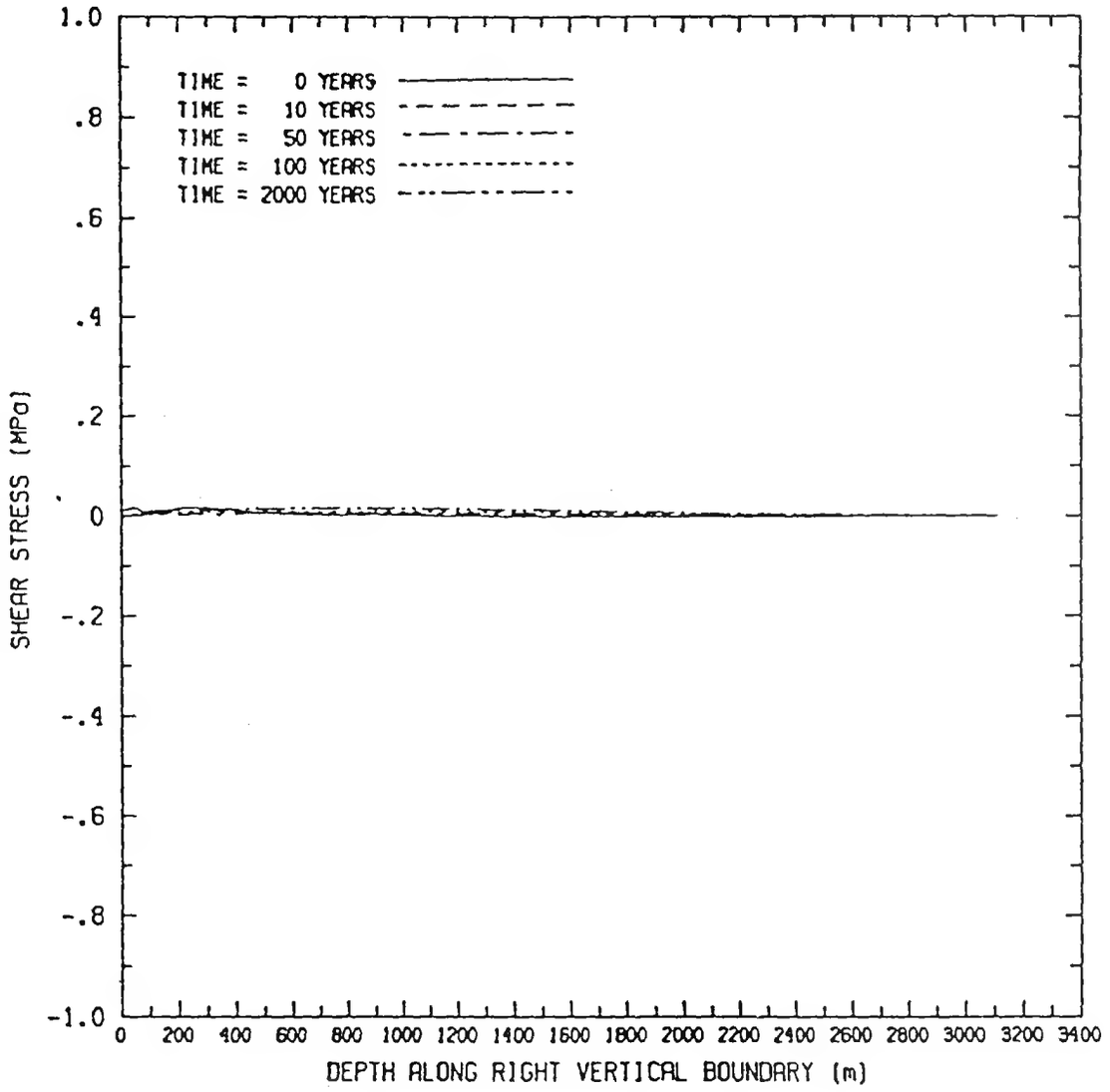

Figure A-58. Shear Stress along the Right Vertical Boundary of the Mechanical Model from Time of Waste Emplacement to 2,000 Yr of Waste Isolation.

APPENDIX A
REFERENCES

Brandshaug, T. and D. K. Svalstad, 1984. *Application of Far-Field Models to the Disposal of Nuclear Waste in Geologic Formations*, from Western States Mining Expo 84, Reno, Nevada, August. (NNA.890522.0226)

APPENDIX B

RELATIONSHIP OF DATA USED IN THIS ANALYSIS TO YMP SEPDB, DRMS, AND RIB

APPENDIX B
LIST OF TABLES

APPENDIX B
RELATIONSHIP OF DATA USED IN THIS ANALYSIS TO YMP SEPDB, DRMS, AND RIB

No data contained in this report is candidate information for the Site and Engineering Properties Data Base (SEPDB), the Data Records Management System (DRMS), and/or Reference Information Base (RIB).

The data used in this report was based on information available in 1984 and therefore it predates the first approved version of the RIB (Version 3.0). Much of the material property information was obtained from draft copies of portions of SNL [1987]. The air temperature value predated the consensus as to the proper value, so an estimate based on engineering judgment was used. The cross section used in this report CC' also predates the reference in the RIB (Version 3.0) on which other cross sections are based (Ortiz et al., 1985). However, it is based on the same surfaces that were used to generate the cross sections reported by Ortiz et al. [1985]. Thus, in principal, the only difference between the CC' cross section of this report and the LL' cross section in the RIB is that CC' is along a slightly different E-W line through the mountain. CC' is the cut used in the unit evaluation [Johnstone et al., 1984].

Comparisons between the material properties used in this study and the current RIB (Version 4.0) values are provided in Table B-1. If data were not available in Version 4.0, the remark "ND" was inserted to indicate "No data." This was true for the rock mass mechanical properties, for the joint properties, and for all units below CHn2z. A one-to-one correspondence also does not exist in the temperature ranges for the thermal properties. All comparisons should therefore be used only as a general indication of the differences. Version 4.0 of the RIB should be consulted for greater detail.

Table B-1. Comparison of Model Parameters and RIB Data

Property		Unit											
		TCw	PTn	TSw1	TSw2	TSw3	CHn1v	CHn1z	CHn2z	PPw	CFUn	BFw	CFMn1,2,3	TRw
Young's modulus, E (GPa)	Mod[a]	15.4	2.3	7.3	15.1	15.1	2.4	3.5	3.5	6.05	3.8	5.4	5.4	8.8
	RIB[b]	ND[c]	ND	ND	ND	ND	ND	ND	ND	ND	ND	ND	ND	ND
Poisson's ratio, ν	Mod	0.10	0.18	0.18	0.20	0.20	0.15	0.17	0.17	0.20	0.16	0.13	0.15	0.18
	RIB	ND	ND	ND	ND	ND	ND	ND	ND	ND	ND	ND	ND	ND
Specific weight, $\rho_{bs}g$ (MPa/m^3)	Mod	.022555	.018632	.022163	.022849	.022849	.017456	.018534	.018534	.021084	.019025	.021868	.020496	.022751
	RIB	.021574	.016102	.021045	.022526	.021545	.020721	.018495	.020299	ND	ND	ND	ND	ND
Uniaxial compressive strength, σ_0 (MPa)	Mod	77.3	11.1	33.4	75.4	75.4	8.4	13.5	13.5	25.3	15.5	20.8	22.3	35.9
	RIB	ND	ND	ND	ND	ND	ND	ND	ND	ND	ND	ND	ND	ND
Tensile strength, σ_T (MPa)	Mod	9.3	1.0	4.0	6.5	6.5	1.0	1.6	1.6	3.0	1.9	2.5	2.7	4.3
	RIB	ND	ND	ND	ND	ND	ND	ND	ND	ND	ND	ND	ND	ND
Coefficient of thermal expansion														
$\alpha_1 \times 10^{-6}$ (°C^{-1})	Mod	8.7	−70.0	10.7	10.7	10.7	−70.0	6.7	6.7	8.3	6.7	8.3	6.7	8.3
Temp. range (°C)		<100.	<100.	<200.	<200.	<200.	<100.	<100.	<100.	<100.	<100.	<100.	<100.	<100.
$\alpha_1 \times 10^{-6}$ (°C^{-1})	RIB	ND	ND	6.1	9.7	8.0	2.9	9.3	ND	ND	ND	ND	ND	ND
Temp. range (°C)		ND	ND	50–100	150–200	100–150	50–100	50–100	ND	ND	ND	ND	ND	ND
$\alpha_2 \times 10^{-6}$ (°C^{-1})	Mod	8.7	−11.5	31.8	31.8	31.8	−11.5	−52.0	−52.0	−12.0	−29.4	−12.0	−16.2	−12.0
Temp. range (°C)		100–125	100–125	200–350	200–350	200–350	100–125	100–150	100–150	100–125	100–150	100–125	100–150	100–125
$\alpha_2 \times 10^{-6}$ (°C^{-1})	RIB	ND	ND	ND	35.6	ND	−1.1	−15.7	ND	ND	ND	ND	ND	ND
Temp. range (°C)		ND	ND	ND	250 300	ND	100–150	100–150	ND	ND	ND	ND	ND	ND
$\alpha_3 \times 10^{-6}$ (°C^{-1})	Mod	8.7	−8.0	15.5	15.5	15.5	−8.0	−2.4	−2.4	10.9	4.4	10.9	1.5	10.9
Temp. range (°C)		>125.	>125.	350–400	350–400	350–400	>125.	>150.	>150.	>125.	>150.	>125.	>150.	>125.
$\alpha_3 \times 10^{-6}$ (°C^{-1})	RIB	ND	ND	ND	ND	ND	−1.1	ND	ND	ND	ND	ND	ND	ND
Temp. range (°C)		ND	ND	ND	ND	ND	100-150	ND	ND	ND	ND	ND	ND	ND

(Table is continued on following page)

Table B-1 (continued)

Property		Unit												
		TCw	PTn	TSw1	TSw2	TSw3	CHn1v	CHn1z	CHn2z	PPw	CFUn	BFw	CFMn1,2,3	TRw
Matrix cohesion, S_m (MPa)	Mod	22.4	4.6	11.5	22.1	22.1	3.3	5.1	5.1	8.7	5.7	7.2	7.8	11.5
	RIB	34.2	4.9	26.1	37.8	ND	35.8	11.6	ND	ND	ND	ND	ND	ND
Matrix angle of int. friction, Φ_m (deg)	Mod	29.7	11.2	20.9	29.2	29.2	13.4	15.8	15.8	21.1	17.8	21.6	20.5	24.8
	RIB	33.8	5.4	27.0	36.5	ND	35.0	12.7	ND	ND	ND	ND	ND	ND
Joint cohesion, S_j (MPa)	Mod	1.0	1.0	1.0	1.0	1.0	1.0	0.4	0.4	1.0	0.4	1.0	0.4	1.0
	RIB	ND	ND	ND	ND	ND	ND	ND	ND	ND	ND	ND	ND	ND
Joint angle of int. friction, Φ_j (deg)	Mod	38.7	38.7	38.7	38.7	38.7	38.7	28.8	28.8	38.7	28.8	38.7	28.8	38.7
	RIB	ND	ND	ND	ND	ND	ND	ND	ND	ND	ND	ND	ND	ND
Joint tensile strength (MPa)	Mod	0.1	0.1	0.1	0.1	0.1	0.1	0.0	0.0	0.1	0.0	0.1	0.0	0.1
	RIB	ND	ND	ND	ND	ND	ND	ND	ND	ND	ND	ND	ND	ND
Brittle/ductile trans. pressure, σ_n (MPa)	Mod	−92.7	−6.0	−25.0	−87.1	−87.1	−4.1	−17.6	−17.6	−18.5	−23.2	−15.3	−42.1	−31.0
	RIB	ND	ND	ND	ND	ND	ND	ND	ND	ND	ND	ND	ND	ND
Thermal conductivity,														
k_1 (T< 100°C) (Wet)	Mod	2.00	1.49	1.19	1.85	1.85	1.21	1.35	1.35	1.86	1.31	2.00	1.48	2.09
	RIB	1.51	1.61	1.51	1.91	1.30	1.20	1.27	1.56	ND	ND	ND	ND	ND
k_2 (100 ≤T≤ 125°C)	Mod	1.95	1.43	1.10	1.73	1.73	1.12	1.20	1.20	1.61	1.18	1.68	1.31	1.94
	RIB	ND	ND	ND	ND	ND	ND	ND	ND	ND	ND	ND	ND	ND
k_3 (T> 125°C) (Dry)	Mod	1.90	1.37	1.00	1.61	1.61	1.02	1.03	1.03	1.35	1.04	1.35	1.13	1.79
(W/mK)	RIB	1.42	1.45	1.42	1.84	1.29	0.85	0.54	0.54	ND	ND	ND	ND	ND

(Table is continued on following page)

Table B-1 (continued)

Property			Unit											
			TCw	PTn	TSw1	TSw2	TSw3	CHn1v	CHn1z	CHn2z	PPw	CFUn	BFw	CFMn1,2,3	TRw
Volumetric heat capacity,[d]															
ρC_{p1}	(T< 100°C)	Mod	0.070	0.078	0.061	0.069	0.069	0.078	0.077	0.077	0.077	0.077	0.085	0.082	0.082
	(T<95°C)	RIB	0.064	0.071	0.066	0.068	.065	0.081	0.085	0.081	ND	ND	ND	ND	ND
ρC_{p2}	(100≤T≤ 125°C)	Mod	0.838	0.321	0.386	0.308	0.308	0.880	0.520	0.520	0.605	0.478	0.737	0.425	0.599
	(95≤T<115°C)	RIB	0.297	0.929	0.389	0.332	0.143	1.121	1.063	0.727	ND	ND	ND	ND	ND
ρC_{p3}	(T> 125°C)	Mod	0.042	0.058	0.045	0.057	0.057	0.040	0.042	0.042	0.052	0.045	0.053	0.049	0.057
	(T≥115°C)	RIB	.066	.048	.064	.069	.081	.053	.050	.055	ND	ND	ND	ND	ND
($W \cdot yr/m^3K$)															
Wet bulk density,		Mod	2300.	1900.	2260.	2330.	2330.	1780.	1890.	1890.	2150.	1940.	2230.	2090.	2320.
ρ_{bs} (kg/m^3)		RIB	2200	1642	2146	2297	2197	2113	1886	2070	ND	ND	ND	ND	ND

[a]Mod = Model in this report (SAND85-7101).
[b]RIB = Version 4.0
[c]ND = No data.
[d]Averages of RIB values over the temperature range are reported.

APPENDIX B
REFERENCES

Johnstone, J. K., R. R. Peters, and P. R. Gnirk, 1984. *Unit Evaluation at Yucca Mountain, Nevada Test Site: Summary Report and Recommendation*, SAND83–0372, Sandia National Laboratories, Albuquerque, New Mexico. (NNA.870519.0052)

Ortiz, T. S., R. L. Williams, F. B. Nimick, B. C. Whittet, and D. L. South, 1985. *A Three Dimensional Model of Reference Thermal/Mechanical and Hydrological Stratigraphy at Yucca Mountain, Southern Nevada*, SAND84–1076, Sandia National Laboratories, Albuquerque, New Mexico. (NNA.890315.0013)

Sandia National Laboratories, 1987. SAND84–2641, *Site Characterization Plan Conceptual Design Report*, Volume 4, H. R. MacDougall, L. W. Scully, and J. R. Tillerson, compilers, Albuquerque, New Mexico. (NNI.880902.0014-.0019)

DISTRIBUTION LIST

1 John W. Bartlett, Director (RW-1)
Office of Civilian Radioactive
Waste Management
U.S. Department of Energy
Forrestal Bldg.
Washington, D.C. 20585

1 F. G. Peters, Deputy Director (RW-2)
Office of Civilian Radioactive
Waste Management
U.S. Department of Energy
Forrestal Bldg.
Washington, D.C. 20585

1 D. G. Horton (RW-3)
Office of Quality Assurance
Office of Civilian Radioactive
Waste Management
U.S. Department of Energy
Forrestal Bldg.
Washington, D.C. 20585

1 T. H. Isaacs (RW-4)
Office of Strategic Planning
and International Programs
Office of Civilian Radioactive
Waste Management
U.S. Department of Energy
Forrestal Bldg.
Washington, D.C. 20585

1 J. D. Saltzman (RW-5)
Office of External Relations
Office of Civilian Radioactive
Waste Management
U.S. Department of Energy
Forrestal Bldg.
Washington, D.C. 20585

1 Samuel Rousso (RW-10)
Office of Program and Resources
Management
Office of Civilian Radioactive
Waste Management
U.S. Department of Energy
Forrestal Bldg.
Washington, D.C. 20585

1 Carl P. Gertz (RW-20)
Office of Geologic Disposal
Office of Civilian Radioactive
Waste Management
U.S. Department of Energy
Forrestal Bldg.
Washington, D.C. 20585

1 D. E. Shelor (RW-30)
Office of Systems and Compliance
Office of Civilian Radioactive
Waste Management
U.S. Department of Energy
Forrestal Bldg.
Washington, D.C. 20585

1 L. H. Barrett (RW-40)
Office of Storage and Transportation
Office of Civilian Radioactive
Waste Management
U.S. Department of Energy
Forrestal Bldg.
Washington, D.C. 20585

1 F. G. Peters (RW-50)
Office of Contractor Business
Management
Office of Civilian Radioactive
Waste Management
U.S. Department of Energy
Forrestal Bldg.
Washington, D.C. 20585

1 J. C. Bresee (RW-10)
Office of Civilian Radioactive
Waste Management
U.S. Department of Energy
Forrestal Bldg.
Washington, D.C. 20585

1 S. J. Brocoum (RW-20)
Office of Civilian Radioactive
Waste Management
U.S. Department of Energy
Forrestal Building
Washington, D.C. 20585

1 Gerald Parker (RW-30)
Office of Civilian Radioactive
Waste Management
U.S. Department of Energy
Forrestal Bldg.
Washington, D.C. 20585

1 D. U. Deere, Chairman
Nuclear Waste Technical
Review Board
1100 Wilson Blvd. #910
Arlington, VA 22209-2297

5 Carl P. Gertz, Project Manager
Yucca Mountain Project Office
Nevada Operations Office
U.S. Department of Energy
Mail Stop 523
P.O. Box 98518
Las Vegas, NV 89193-8518

1 C. L. West, Director
Office of External Affairs
Nevada Operations Office
U.S. Department of Energy
P.O. Box 98518
Las Vegas, NV 89193-8518

12 Technical Information Office
Nevada Operations Office
U. S. Department of Energy
P.O. Box 98518
Las Vegas, NV 89193-8518

1 P. K. Fitzsimmons, Director
Health Physics & Environmental
Division
Nevada Operations Office
U.S. Department of Energy
P.O. Box 98518
Las Vegas, NV 89193-8518

1 Repository Licensing & Quality
Assurance Project Directorate
Division of Waste Management
U.S. Nuclear Regulatory Commission
Washington, D.C. 20555

1 Senior Project Manager for Yucca
Mountain Repository Project Branch
Division of Waste Management
U.S. Nuclear Regulatory Commission
Washington, D.C. 20555

1 NRC Document Control Desk
Division of Waste Management
U.S. Nuclear Regulatory Commission
Washington, D.C. 20555

1 P. T. Prestholt
NRC Site Representative
1050 East Flamingo Road
Suite 319
Las Vegas, NV 89119

1 E. P. Binnall
Field Systems Group Leader
Building 50B/4235
Lawrence Berkeley Laboratory
Berkeley, CA 94720

1 Center for Nuclear Waste
Regulatory Analyses
6220 Culebra Road
Drawer 28510
San Antonio, TX 78284

3 L. J. Jardine
Technical Project Officer for YMP
Lawrence Livermore National
Laboratory
Mail Stop L-204
P.O. Box 808
Livermore, CA 94550

4 R. J. Herbst
Technical Project Officer for YMP
Los Alamos National Laboratory
N-5, Mail Stop J521
P.O. Box 1663
Los Alamos, NM 87545

1 H. N. Kalia
Exploratory Shaft Test Manager
Los Alamos National Laboratory
Mail Stop 527
101 Convention Center Dr.
Suite 820
Las Vegas, NV 89109

1 J. F. Divine
Assistant Director for
Engineering Geology
U.S. Geological Survey
106 National Center
12201 Sunrise Valley Dr.
Reston, VA 22092

6 L. R. Hayes
Technical Project Officer for YMP
U.S. Geological Survey
P.O. Box 25046
421 Federal Center
Denver, CO 80225

1 D. Zesiger
U.S. Geological Survey
101 Convention Center Dr.
Suite 860 - MS509
Las Vegas, NV 89109

1 K. W. Causseaux
NHP Reports Chief
U.S. Geological Survey
P.O. Box 25046
421 Federal Center
Denver, CO 80225

1 R. V. Watkins, Chief
Project Planning and Management
U.S. Geological Survey
P.O. Box 25046
421 Federal Center
Denver, CO 80225

1 V. M. Glanzman
U.S. Geological Survey
P.O. Box 25046
913 Federal Center
Denver, CO 80225

1 J. H. Nelson
Technical Project Officer for
YMP
Science Applications International
Corp.
101 Convention Center Dr.
Suite 407
Las Vegas, NV 89109

2 SAIC-T&MSS Library
Science Applications International
Corp.
101 Convention Center Dr.
Suite 407
Las Vegas, NV 89109

1 Elaine Ezra
YMP GIS Project Manager
EG&G Energy Measurements, Inc.
Mail Stop D-12
P.O. Box 1912
Las Vegas, NV 89125

1 W. M. Hewitt, Program Manager
Roy F. Weston, Inc.
955 L'Enfant Plaza, Southwest
Suite 800
Washington, D.C. 20024

1 Technical Information Center
Roy F. Weston, Inc.
955 L'Enfant Plaza, Southwest
Suite 800
Washington, D.C. 20024

1 D. L. Fraser, General Manager
Reynolds Electrical & Engineering Co.
P.O. Box 98521
Mail Stop 555
Las Vegas, NV 89193-8521

1 Robert F. Pritchett
Technical Project Officer for YMP
Reynolds Electrical & Engineering Co.
Mail Stop 615
P.O. Box 98521
Las Vegas, NV 89193-8521

1 A. E. Gurrola
General Manager
Raytheon, Inc.
Mail Stop 580
P.O. Box 93838
Las Vegas, NV 89193-3838

1 James C. Calovini
Raytheon Services, Inc.
101 Convention Center Dr.
Suite P-280
Las Vegas, NV 89109

1 D. L. Lockwood, General Manager
Raytheon Services, Inc.
Mail Stop 514
P.O. Box 93265
Las Vegas, NV 89193-3265

1 Richard L. Bullock
Technical Project Officer for YMP
Raytheon Services, Inc.
101 Convention Center Dr.
Suite P250
Las Vegas, NV 89109

1 R. E. Lowder
Technical Project Officer for YMP
MAC Technical Services
Valley Bank Center
101 Convention Center Drive
Suite 1100
Las Vegas, NV 89109

1 D. J. Bales
Science and Technology Division
Office of Scientific and Technical Information
U.S. Department of Energy
P.O. Box 62
Oak Ridge, TN 37831

1 Carlos G. Bell, Jr.
Professor of Civil Engineering
Civil and Mechanical Engineering Department
University of Nevada, Las Vegas
4505 South Maryland Parkway
Las Vegas, NV 89154

1 C. F. Costa, Director
Nuclear Radiation Assessment Division
U.S. Environmental Protection Agency
Environmental Monitoring Systems Laboratory
P.O. Box 93478
Las Vegas, NV 89193-3478

1 ONWI Library
Battelle Columbus Laboratory
Office of Nuclear Waste Isolation
505 King Avenue
Columbus, OH 43201

1 T. Hay, Executive Assistant
Office of the Governor
State of Nevada
Capitol Complex
Carson City, NV 89710

3 R. R. Loux, Jr.
Executive Director
Nuclear Waste Project Office
State of Nevada
Evergreen Center, Suite 252
1802 North Carson Street
Carson City, NV 89710

1 C. H. Johnson
Technical Program Manager
Nuclear Waste Project Office
State of Nevada
Evergreen Center, Suite 252
1802 North Carson Street
Carson City, NV 89710

1 John Fordham
Water Resources Center
Desert Research Institute
P.O. Box 60220
Reno, NV 89506

1 Dr. Martin Mifflin
Desert Research Institute
Water Resources Center
2505 Chandler Avenue
Suite 1
Las Vegas, NV 89120

1 Eric Anderson
Mountain West Research-Southwest Inc.
2901 N. Central Ave. #1000
Phoenix, AZ 85012-2730

1 Department of Comprehensive Planning
Clark County
225 Bridger Avenue, 7th Floor
Las Vegas, NV 89155

1 Planning Department
Nye County
P.O. Box 153
Tonopah, NV 89049

1 Lincoln County Commission
Lincoln County
P.O. Box 90
Pioche, NV 89043

5 Judy Foremaster
City of Caliente
P.O. Box 158
Caliente, NV 89008

1 Economic Development Department
City of Las Vegas
400 East Stewart Avenue
Las Vegas, NV 89109

1 Community Planning & Development
City of North Las Vegas
P.O. Box 4086
North Las Vegas, NV 89030

1 City Manager
City of Henderson
Henderson, NV 89015

1 Director of Community Planning
City of Boulder City
P.O. Box 367
Boulder City, NV 89005

1 Commission of the European Communities
200 Rue de la Loi
B-1049 Brussels
Belgium

1	6300	T. O. Hunter, Actg.
1	6310	T. E. Blejwas, Actg.
1	6310A	F. W. Bingham
1	6311	A. L. Stevens
1	6312	F. W. Bingham, Actg.
1	6313	L. E. Shephard, Actg.
1	6314	L. S. Costin
1	6314	S. J. Bauer
1	6314	E. E. Ryder
1	6315	F. B. Nimick, Actg.
1	6316	R. P. Sandoval
1	6317	S. Sinnock
2	6318	L. J. Erickson for 100/121431/SAND85-7101/QA
1	6318	C. Crawford for for Accession No. Data Base
1	6319	R. R. Richards
20	6341	WMT Library
1	6410	D. J. McCloskey, Actg.
5	3141	S. A. Landenberger
3	3151	G. L. Esch
1	8523	Technical Library
8	3145	Document Processing for DOE/OSTI

1 Edgar Petrie
Yucca Mountain Site Characterization Project Office
U. S. Department of Energy
Nevada Operations Office
P.O. Box 98608
Las Vegas, NV 89193-8608

1 Michael Cloninger
Yucca Mountain Site Characterization Project Office
U. S. Department of Energy
Nevada Operations Office
P.O. Box 98608
Las Vegas, NV 89193-8608

1 Robert Waters
Yucca Mountain Site Characterization Project Office
U. S. Department of Energy
Nevada Operations Office
P.O. Box 98608
Las Vegas, NV 89193-8608

1 Jon White
Yucca Mountain Site Characterization Project Office
U. S. Department of Energy
Nevada Operations Office
P.O. Box 98608
Las Vegas, NV 89193-8608

1 James Replogle
Raytheon Services of Nevada
101 Convention Center Drive
Suite P-250
Las Vegas, NV 89109

1 Steve Smith
Science Applications International Corporation
101 Convention Center Drive
Suite 407
Las Vegas, NV 89109

The number in the lower right-hand corner is an accession number used for Office of Civilian Radioactive Waste Management purposes only. It should not be used when ordering this publication.